Republic of Iraq
Ministry of Higher Education
& Scientific Research
University of Babylon
College of Education for Pure Sciences
Department of Physics

Cold Plasma Optical Treatment of Nano_Al_2O_3 Doped Polymeric blend

A Thesis

Submitted to The Council of The College of Education
For Pure Sciences, University of Babylon in Partial
Fulfillment of Requirements for The Degree
of Master in Education / Physics

By

Fatima Mohammed Nayef
B.Sc. in physics
University of Babylon (2018)

Supervised by

Prof. Dr. Bahaa Hussein Salih Rabee

2023 A.D **1445 A.H**

بِسْمِ اللَّهِ الرَّحْمَٰنِ الرَّحِيمِ

(أَمَّنْ هُوَ قَانِتٌ آنَاءَ اللَّيْلِ سَاجِدًا وَقَائِمًا يَحْذَرُ الْآخِرَةَ وَيَرْجُو رَحْمَةَ رَبِّهِ قُلْ هَلْ يَسْتَوِي الَّذِينَ يَعْلَمُونَ وَالَّذِينَ لَا يَعْلَمُونَ إِنَّمَا يَتَذَكَّرُ أُولُو الْأَلْبَابِ)

صدق الله العلي العظيم

(سورة الزمر - الآية ﴿9﴾)

Dedication

To Whom I carry your name with pride, I miss you since childhood, Whom my heart is shivering for remembrance (my father)..

To my angel in life, to the meaning of love and the meaning of compassion and the smile in my life, to the mystery of existence of the secret of my success, to whom her prayer and affection surgical balm, to all the lad (my mother)..

To the star who wake all the nights for My relief

" My husband "..

To the blooming flowers in my life

" My brothers & my sisters "..

To my soul mate.. My sons

"Shams & Ali & Laya"..

Ftatima . . .

Acknowledgments

Praise be to Allah Lord of the world, and best prayers and peace upon him best messenger Mohammed, his pure descendants, and his noble companions.

Then, I would like to express my deep gratitude and appreciation to my supervisors, **Dr. Bahaa Hussein Rabee** for their guidance, suggestions, and encouragement throughout the research work, without him, this thesis would have been impossible.

I would like to thank the staff of the department of Physics in College of Education for Pure Sciences in the University of Babylon for their kind attention and assistances.

Finally, I would like to thank all members of my family for their help and encouragements and everyone who helped me during

the preparation of this thesis.

Ftatima ...

Abstract

In this study, the (Poly-methyl-methacrylate-Polystyrene/Aluminum oxide) nanocomposites has been prepared by using casting method with variant content of (Al_2O_3) nanoparticles (2, 4, 6 and 8) wt.%. The structural, morphological optical and AC electrical properties of (PMMA-PS/Al_2O_3) nanocomposites films have been investigated. The structural properties include optical microscope (OM), Fourier transformation infrared ray (FTIR) and scanning electron microscope (FESEM). The optical microscope images show that Al_2O_3 nanoparticles form a continuous network inside the polymers when the ratio of (8)wt.%. FTIR spectra show a shift in some bands and change in the intensities of other bands comparing with pure (PMMA-PS/Al_2O_3) films, this indicates there is no interaction between the polymers and the added nanoparticles. FESEM measurements reveal the surface morphology of the (PMMA-PS/Al_2O_3) nanocomposites films, which are homogeneous and coherent with aggregates or chunks scattered at random on the top surface. The variation in the morphology after exposed Ar plasma is the outcome of the impression progression encouraged by argon plasma species on the (PMMA-PS) surface. The optical properties before and after exposed Ar plasma exhibited that the absorbance, absorption coefficient, refractive index, extinction coefficient, dielectric constant (real and imaginary) and optical conductivity of (PMMA-PS/Al_2O_3) nanocomposites increased with the increasing of the concentrations of the Al_2O_3 nanoparticles. The transmittance and the energy gap for indirect transition (allowed, forbidden) decreased with the increasing of the concentrations of Al_2O_3 nanoparticles The dielectric properties explain that the dielectric constant and dielectric loss for (PMMA-PS/Al_2O_3) nanocomposites films are increased with the increasing of Al_2O_3 nanoparticles concentration and decreasing with the increase of frequency of the applied electric field while the A.C electrical conductivity increased with the

increasing of nanoparticles concentration and frequency of the applied electric field before and after exposed Ar plasma. The dielectric constant, dielectric loss and A.C electrical conductivity after irradiation have high values compared before irradiation which attributed to the increased charge carriers and the occurrence of some bonds breaking. The (PMMA-PS/Al_2O_3) nanocomposites films were tested as antibacterial for against gram-positive (Staphylococcus aureus) and gram-negative (Escherichia coli). The result obtained the inhibition zone diameter increases with the increase in Al_2O_3 nanoparticles concentrations.

List of Contents

List of Figures

List of Tables

List of Symbols

Symbol	Physical Meanings
n	Refractive index
k	Extinction coefficient
A	Absorption
I_o	Incident intensity of light
I_A	Absorbed intensity of light
T	Transmittance
I_T	Intensity of transmitted
k	Wave vector
α	Absorption coefficient
h	Planck constant
υ	Photon frequency
$E_g^{opt.}$	Optical energy gap
r	Value determines the type of electronic transitions
E_{ph}	Energy phonon
c	Velocity of light
λ	Wavelength of light
R	Reflectance
d	Thickness
N	Complex refractive index
ε'	Dielectric constant
ε	Complex dielectric constant
$ε_1$	Real dielectric constant

ε_2	Imaginary dielectric constant
σ_{op}	Optical Conductivity
σ	Electrical conductivity
P	Polarization
E	Electrical field intensity
D	Electrical displacement
ε_o	Vacuum permittivity
P_e	Electronic polarization
P_i	Ionic polarization
P_d	Rotational polarization
P_o	Space charge polarization
V_m	Maximum voltage
I	Current
i	Imaginary number
ω	Angular frequency
C	Capacitance
f	Frequency
ε''	Dielectric loss
C_P	Parallel capacitance
C_o	Vacuum capacitor
$\sigma_{A.C}$	A.C electrical conductivity

List of Abbreviations

Abbreviations	Physical meaning
ATH	Aluminium tetrahidra
TiO_2	Titanium Dioxide
PVA	Polyvinyl alcohol
CMC	Carboxy methyl cellulose
XPs	X_ray photo electron spectroscopy
SFE	Surface free energy
DC	Direct current
N_2	Nitrogen gas
Ar	Argon
ZoO	Zinc Oxide
XRD	X-ray-diffraction
EDX	Energy dispersive spectroscopy
GPTMS	(3-Glycidy loxypropyl) trimethoxysilane
a_IGZO TFTs	Amorphous lndium Gallium Zin Oxide thin film transistors
IGZO TFTs	lndium Gallium Zin Oxide thin film transistors
PMMA	Polymethylmethacrylate
Ps	Polystyrene
Al_2O_3	Aluminum Oxide
NPs	Nanoparticle
OM	Optical microscope
FESEM	Field Emission Scanning Electron Microscope
FTIR	Fourier Transformation Infrared Region
UV	Ultraviolet
C.B	Conduction Band
V.B	Valence Band
AC	Alternative current

Chapter One

Introduction and Literature Review

1.1 Introduction

Nanotechnology is a new science which evolved as it was observed that materials displayed significantly different properties at nanometer sizes as compared to the properties of the same material at bigger particle sizes. The term "nanotechnology" was first coined by Norio Taniguchi in 1974, in Japan, as follows: "Nanotechnology mainly consists of the processing of separation, consolidation and deformation of materials by one atom or one molecule [1].

Nanotechnology is an emerging interdisciplinary technology that has been booming in many areas during the recent decade, including materials science, mechanics, electronics, optics, medicine, plastics, energy and aerospace. The reasons of the enthusiasm arising from the "nanosciences" are numerous. Among them, the very large surface to volume ratio exhibited by many nanoscaled materials opened novel possibilities in surface-based science, such as heterogeneous catalysis [2].

Furthermore, it was discovered that properties of the materials change as their size approaches the nanoscale, in other words, as the fraction of specific atoms at the surface of a material becomes significant. For example, inert materials such as platinum become catalysts, semiconductors like silicon become conductor, etc [2].

The applications of nanotechnology has only been increasing in the recent years, the highest potential application is in the field of materials, followed by electronics and medicine. Some of the potential applications of nanotechnology are as follows [3]:

- Ultra-light weight, high strength, precision formed materials
- Nano-composite polymers and thin protective coatings for structural and electronic applications
- Filters for cost-effective desalinization of water
- Barriers for thermal and optical application

- Miniaturized computers, non-volatile memory
- Low voltage and high-brightness displays
- Miniature thin film photovoltaic solar cells for cost effective power generation for applications ranging from laptop to automobiles.
- Faster, smaller and more efficient semiconductors and micro-processors.
- Highly effective drug compounds and perfectly targeted drug delivery.
- Micro sensors and diagnostics for more effective treatment
- Antibacterial dressings and coatings.

1.2 Introduction of Plasma

In order to introduce plasma, it is often stated that plasma is the fourth state of matter in the sequence: solid, liquid, gas, and plasma. The state of matter changes from solid to liquid to gas to plasma by increasing the temperature of the material under consideration. When gas atoms are subjected to energy (thermal, electrical or light) they become ions by releasing some of their electrons. Collisions between electrons and molecules and bond breaks in molecules create radicals. Energy will also create excited species that will generate photons. This is how plasma is created with a unique mixture of electrons, ions, radicals, photons and neutral atoms and molecules [4].

Based on the relative temperatures of electrons, ions and neutrals, plasmas are classified as thermal “equilibrium” and non-thermal “non-equilibrium”. Due to the light mass of the electrons present in the plasma, these electrons are instantly accelerated by the electric field to higher velocities than the heavier ions in the time available between collisions. When the collision occurs only a small fraction of the electron energy is lost. This is why the electron temperature in the plasma is initially higher than that of heavy particles. The resulting plasma is a non-thermal or cold plasma in which the electron temperature (≈ 10000 °C) is much higher than the gas

temperature (< 200 °C). However, if the pressure is so high that the charged particles do not move very far before the next collision or the electrical field is very low, the energy of the electrons may tend towards that of the heavy particles. In this case, the resulting plasma is a thermal or hot plasma [5].

Plasmas used in "plasma technology" are usually cold plasmas in the sense that only a small fraction of the gas molecules are ionized which can provide electrons and ions at the right energy without excessive heat enabling the use of plasma on heat-sensitive materials such as polymers. The most commonly used method for generating and sustaining a low-temperature plasma for technological and technical applications is applying an electric field to a pure or mixed gas [6].

1.3 Nanomaterials

Nanomaterials: are materials with dimensions below 100nm and they have at least one unique properties that is different than the bulk material and the characteristics can be applied in different fields such as nanoelectronics, pharmaceutical and cosmetic. Several methods have been studied in fabricating these nanostructures, which include laser ablation, chemical vapor deposition (CVD) [7] , and template-directed growth [8].

Nanomaterials can be classified by different approaches such as; according to the X ,Y and Z dimension, according to their shape and according their composition. The more widely used classification is the order of dimension into 0D. (quantum dot), 1D. (nanotube, nanowire and nanorod), 2D. (nanofilm), and 3D. dimensions such as bulk material composited by nanoparticles[9]. Be one of the ends of the tube is often open and one closed in the form of a hemisphere, as might be the wall of the tube individual atoms and is called in this case the nanotubes and single-wall single wall nanotube (SWNT), or two or more named multi-wall tubes multi wall nanotube (MWNT) The tube diameter ranges from less than one nm to 100 nm (smaller than

the width head of hair by 50000 times), and has a length of up to 100 micrometers to form the nanowire .Of several forms of nanotubes may be straight, spiral, zigzag, or conical bamboo and so on .The properties of these tubes are unusual in terms of strength and hardness and electrical conductivity, and others [10].

1.4 Polymer Structure

A polymer consists of large organic molecules (macromolecules) of repeating small structural units (monomers) connected together in a process called polymerization ,each molecule is composed of thousands of atoms connected by covalent chemical bonds. Molecules in a polymer attract each other by forces that depend on the type of the polymer [11,12]. Polymers can be classified into two groups according to the effect of temperature on them. They are:

1.4.1 Thermoplastic polymers: The properties of these polymers are changed by the effect of temperature. When the temperature increases, they become flexible and sticky; by lowering the temperature, these polymers return to their original solid state. This is because the molecules in a thermoplastic polymer are connected by relatively weak intermolecular forces (Van der Waals forces). When heated, these molecules can slide over each other as in Polystyrene, Polyethylene, Polypropylene, and Polyvinyl chloride, Poly vinyl alcohol [13].This figure explains atomic configuration of thermoplastic polymers.

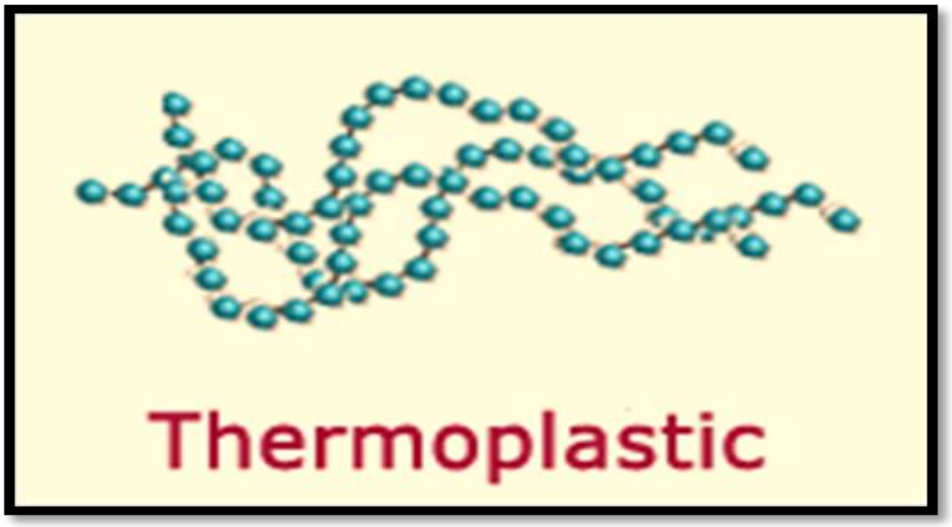

Figure (1.1): Series configuration of thermoplastic polymers [13]

.

1.4.2 Thermoset Polymers: These polymers are chemically changed when heated. Thermosets are usually three-dimensional networked polymers in which there is a high degree of cross-linking between polymer chains. After being heated, these polymers become insoluble, non-conductive of heat and electricity, and hard because molecules of these polymers are connected by strong covalent chemical bonds. Phenol formaldehyde resin and urea-formaldehyde resin are examples of this type of polymers [11,14,15,16,17]. This figure explains atomic configuration of thermoset Polymers.

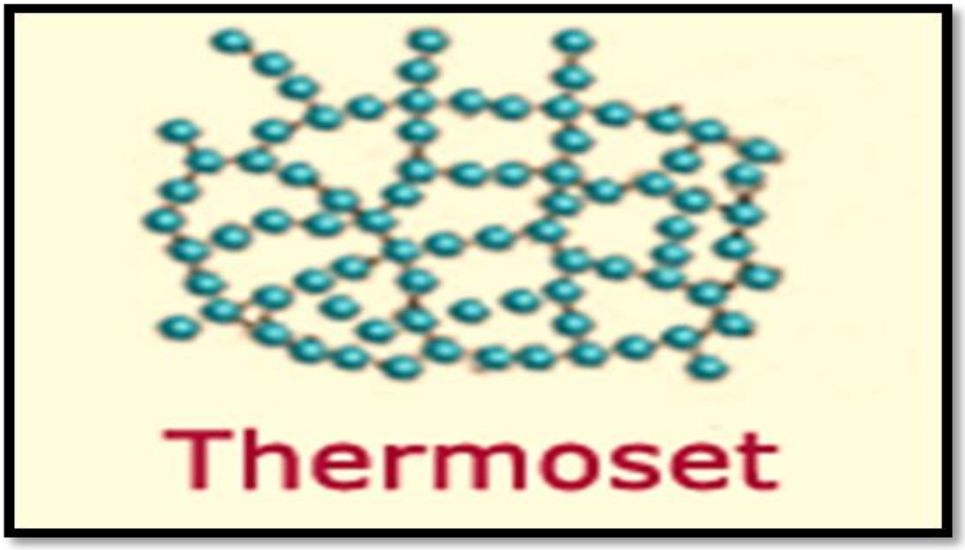

Figure (1.2): Series configuration of thermoset Polymers [13].

1.5 Nanocomposites

Nanocomposites can be defined as a composite material in which at least one of the phases (mostly the filler) shows dimensions in the nanometer range. As the fillers size reaches the nanometer level, the interactions at the interfaces become considerably large with respect to the size of the inclusion and thus the final properties show significant changes [18]. A nanocomposite, like a traditional composite has two parts, filler and the matrix. A traditional composite typically uses a fiber such as carbon fiber or fiberglass as the filler, in a nanocomposite the filler is a nanomaterial. Some examples of nanomaterial are carbon nanofiber, and nanoparticles such as gold, silver, diamond, copper and silicon. Of particular interest are nanocomposites because of their high strength and stiffness composites they produce at relatively low concentrations [19, 20].

1.6 Materials used in the study

1.6.1 Poly methyl-methacrylate (PMMA)

Poly-methyl-methacrylate (PMMA) has been used for vertebra– plasty, the percutaneous augmentation of vertebral bodies, since the late 1980s (Galibert et al.,1987) and is today the most commonly used augmentation material [21]. The used matrix material is Poly methyl-methacrylate (PMMA) as a polymer waveguide has attracted much attention for use as optical components and in optoelectronic devices due to its low cost and volume productivity. Poly-methyl-methacrylate is an important and interesting polymer because of attractive physical and optical properties decisive about its broad application. This is the thermoplastic material with the good tensile strength and hardness, high rigidity, transparency, good insulation properties and thermal stability dependent on tactility. Poly-methyl-methacrylate has some disadvantages such as brittleness and low chemical resistance which can be eliminated by chemical or physical modification [22]. Poly-methyl methacrylate is one of the earliest and best known polymers. Poly-methylmethacrylate was seen as a replacement for glass in a variety of applications and is currently used extensively in glazing applications. The material is one of the hardest polymers, and is rigid, glass-clear with glossy finish and good weather resistance. Poly-methylmethacrylate is naturally transparent and colorless. The transmission for visible light is very high. Polymeric composites of Poly-methylmethacrylate are known for their importance in technical applications [23]. Studies of doping transition metal halides into Poly-methylmethacrylate are important for determining and controlling the operational characteristic of the different Poly-methylmethacrylate composites. The addition of transition metal halides to the Poly-methylmethacrylate network will cause a remarkable change

in their properties. Figure (1.3) explain the chemical structure of PMMA [24]. Table (1-1) shows some physical properties of PMMa[24].

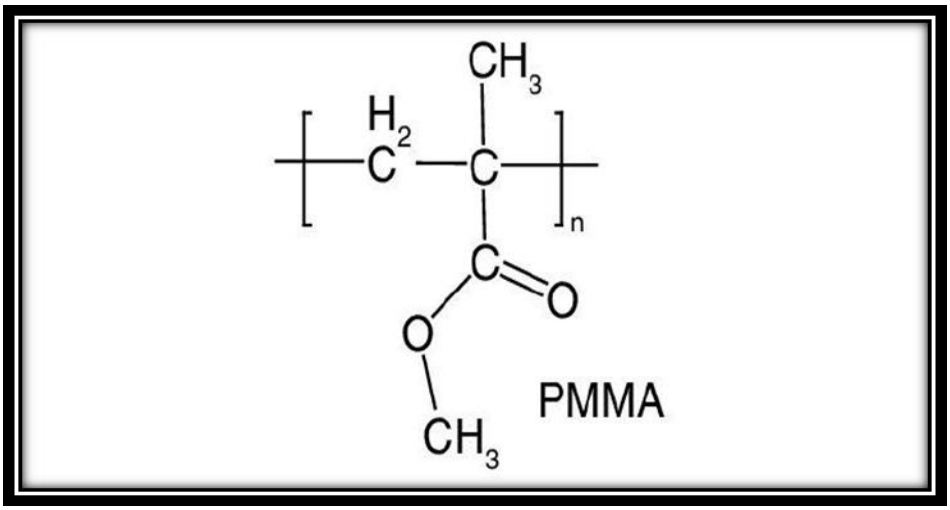

Figure (1.3): A chemical structure of the repeating unit of PMMA polymer [24].

Table (1.1): The most important physical properties of PMMA polymer [25].

Property	Description
Chemical formula	$CH_2=C(CH_3)COOH_3$
Density	1.2 g/cm^3
Melting point	140°C
Boiling point	200°C
Solubility in water	Insoluble
Molecular weight	120000
Energy gap	3.9 eV
Solubility	Soluble in benzene, carbon disulfide, chloroform
Glass Transition Temperature Tg (K)	106 °C

1.6.2 Polystyrene (PS)

Polystyrene (PS) is a flexible plastic that is commonly used in several aspects of human life and industry due to its low cost, light weight, ease of fabrication, flexibility, thermal efficiency, durability, and moisture resistance. However, polystyrene is exceptionally stable and difficult to degrade in the surroundings after disposal [26]. It is produced by the polymerization of styrene and is the most widely used plastic. At room temperature, the thermoplastic polymer is a solid but when heated above 100 °C it flows. It becomes rigid again when it cools down. Polystyrene is insoluble in water. Polystyrene is compound that is non-biodegradable with a couple of exceptions. It is easily dissolved by many aromatic hydrocarbon solvents and chlorinated solvents. It is widely used in the food-service industry as rigid trays, containers, disposable eating plates, bowls, etc [27]. Figure(1.4) explain the chemical properties of PS [26].Tables(1-2)show the Properties of PS [27].

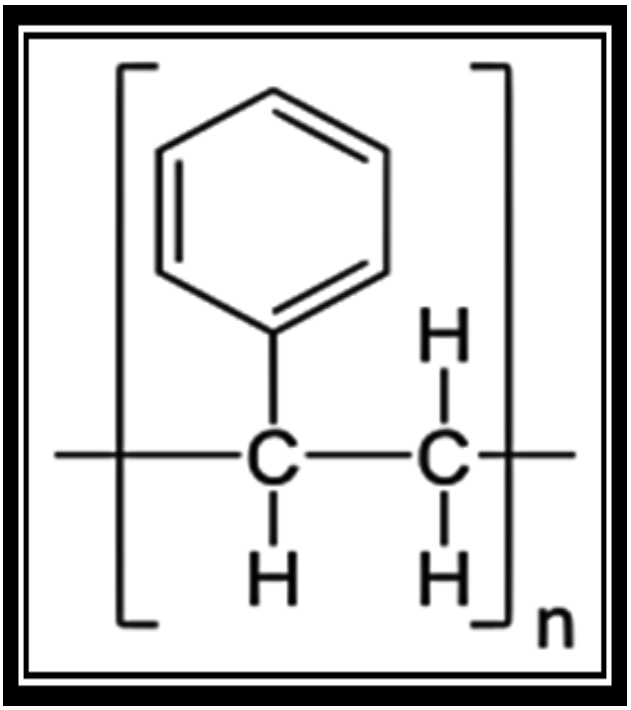

Figure (1.4): A chemical structure of PS [27].

Table (1.2): The most important physical properties of PS polymer [27].

Property	Description
Chemical formula	(C8H8)n
Density	0.96–1.05 g/cm3
Melting point	~ 240 °C
Boiling point	430 °C
Solubility in water	Insoluble
Solubility	Soluble in benzene, carbon disulfide, chloroform
Molecular weight	150000 g/mol
Energy gap	4.5 eV
Glass Transition Temperature (T_g)	100 °C

1.6.3 Aluminum Oxide Nanoparticle (Al_2O_3 NPs)

Aluminum oxide is a chemical made up of two aluminum atoms and three oxygen atoms linked in a hexagonal close-packed crystal structure. Alumina is the popular term for the chemical, and due to its availability, it has a variety of uses in the industry [28]. Alumina is derived from bauxite and recycled alumina. Alumina is derived from the aluminum-rich mineral bauxite. Top bauxite producers are Australia, China, Jamaica, and Brazil. When mixed with transition metals, the result is a stunning crystal. Due to its properties of light absorption and reflection in the visible range. Aluminum oxide is made by recycling raw aluminum. The characteristics and functions of virgin aluminum and recycled aluminum are nearly identical. Alumina is a frequent element in sunscreen and can also be found in cosmetics like nail polish, blush, and lipstick, as well as in glass formulations as a catalyst and in sandpaper as an abrasive. Aluminum oxide is also an electrical insulator [29]. Alumina properties are shown in Table (1-3) [29].

Table (1.3): The most important physical properties of Al_2O_3 nanoparticle [29].

Property	Description
Chemical formula	Al_2O_3
Molar mass	101.960 $g \cdot mol^{-1}$
Appearance	white solid
Odor	odorless
Density	3.987g/cm^3
Melting point	2,072 °C
Boiling point	2,977 °C
Solubility in water	insoluble
Refractive index (*n*)	1.62

1.7 Literature Review

In (2014), C. Mandolfino, *et. al.* [30] prepared the effect of cold plasma treatment on polyethylene and polypropylene substrates, a large number of samples were exposed to radio frequency (RF) low pressure plasma, using mainly air as working gas. In particular, the optimization of three plasma process parameters, exposure time, voltage and working gas, were studied performing roughness measurement, contact angle evaluation and lap-shear tests. The experimental results show that the optimized plasma process may remarkably change the surface morphology, increasing wettability properties of the surfaces and shear strength of the bonded joints. These good properties remain almost unchanged even after some days of storage in the laboratory.

In (2015) L. M. Wallenhorst *et aL.* [31] studied the characteristics of aluminium trihydrate (ATH) filled poly (methyl methacrylate) (PMMa) composite (PMMa/ATH) coatings realised by plasma deposition at atmospheric pressure. For this purpose, PMMa/ATH powder was fed to a plasma jet where the process and carrier gas was compressed air. The deposited coatings were investigated by X-ray photoelectron spectroscopy and water contact angle measurements. Further, the raw

material was characterised before deposition. It was found that, with respect to the raw material, aluminium was uncovered in the course of the plasma deposition process which can be explained by plasmainduced etching of the PMMA matrix. As a result, the wettability of plasma-deposited PMMa/ATH was significantly increased.

In (2016), A. M. Shehap *et. al*. [32] studied polyvinyl alcohol (PVA) doped with titanium dioxide nanoparticles at different weight percentage (1.25, 2.5, 5, 7.5, 10 TiO2/PVA) were prepared using the sonification and casting techniques. The structural properties of those samples were examined by XRD, FTIR, and UV-Visible. The XRD pattern revealed that the amorphous domain in PVA polymer matrix increased with raising the TiO_2 content. The complexation of the dopant with the polymer was examined by FTIR studies. The absorption spectra of UV-Visible light showed irregular changes of the absorption for high doping samples in UV range (7.5, 10 TiO_2 /PVA). Absorbance, transmittance and reflectance spectra were used for the determination of the optical constants. The results indicated that the optical band gap decreases with increasing TiO_2 content, while the refractive index increased to high value for the composites of high dopant.

In (2017), R. G. Kadhim *et al*. [33], prepared (Poly vinyl alcohol (PVA) - Carboxymethyl Cellulose (CMC)–Copper Oxide (CuO)) Nanocomposites by solution casting method. The AC electrical and optical properties were examined. From the AC electrical properties, the dielectric constant, dielectric loss and AC. Electrical conductivity of (PVA-CMC) blend increase with the increasing of the copper oxide nanoparticles concentrations at 100HZ. Whereas dielectric constant and dielectric loss decrease with increased frequency but AC. Electrical conductivity increases with increased frequency. The optical measurements are showed the absorbance of (PVA-CMC-Copper Oxide) nanocomposites are

increased with increase of the concentrations of copper oxide nanoparticles. The indirect energy gap (E_g) of (PVA-CMC) blend decreases with the increase of the concentrations of copper oxide nanoparticles. All the optical constants as absorption coefficient, extinction coefficient, and refractive index, real and imaginary dielectric constants of nanocomposites are variation with the increase of the weight percentages of copper oxide nanoparticles. Surface resistance of (PVA-CMC-Copper Oxide) nanocomposites variation with increase relative humidity.

In (2018), M. Vovk *et. al.* [34], studied Air plasma treatments of aluminium trihydrate filled poly(methyl methacrylate) polymer (PMMa) composites were carried out in a dielectric barrier discharge. X-ray photoelectron spectroscopy (XPS) and attenuated total reflection – infrared spectroscopy have been employed to analyse the changes in chemical composition. Confocal laser-scanning microscopy and atomic force microscopy yielded the impact on surface structure and morphology. The plasma treatments resulted mainly in an etching of the matrix polymer and a minor chemical modification. An apparent contradiction of XPS, ATR and SFE results was attributed to a repolymerization and re-deposition of the etched PMMa material as debris back onto the surface.

In (2019), N. M. El-Sayed [35] studied the optical and electrical properties of Polymethylmethacrylate (PMMA) films have been investigated under the effect of direct current (DC) glow discharge plasma. PMMa films have been prepared and treated with low-pressure DC glow discharge plasma at different plasma conditions; mainly various working gas and plasma treatment times. The optical and electrical properties of the treated PMMa samples were measured and compared to the untreated one. Nitrogen, argon, and nitrogen-argon mixture have been used as working gases. Plasma parameters, such as the electron density, the ion density, and electron temperature, were measured, at the position of the PMMa films, using

Langmuir probe. The results reveal that, the optical properties of PMMA were found to be more sensitive to N_2 - plasma treatment than Ar and N_2 -Ar gas mixture. The optical energy gap showed a decreasing behavior with increasing the treatment time of N_2 plasma, however, the band tail width and the electrical resistivity increased.

In (2020), Y. Al-Mahweet [36] studied physicochemical properties of prepared ZnO/Polystyrene nanocomposite: structure, mechanical and optical. Nanocomposites of polystyrene nano sphere (PS) with different loading of nano zinc oxide (ZnO) were prepared by two different methods, blend and in situ method. The prepared films of the synthesized nanocomposites materials were characterized by energy dispersive investigation (EDX), X-ray diffraction (XRD) and the morphology of ZnO/PS nanocomposite were investigated by transmission electron microscope (TEM). The effect of ZnO nanoparticles on linear optical properties was studied in the PS lattice. The obtained results indicate that, the refractive index has been increased while the energy gap decreased with increasing ZnO nanoparticles

In (2021), J. Meza-Arroyo *et al*,[37] studied the effects of ultra-dry-air plasma surface treatments on the properties of Al_2O_3-GPTMS-PMMa hybrid dielectric layers for applications to high-performance a-IGZO TFTs. The hybrid layers were deposited by an easy dip coating sol-gel process at low temperature and then treated with dry-air plasma at 1, 2 and 3 consecutive cycles. Their properties were analyzed as a function of the number of plasma cycles and contrasted with those of the untreated ones. The results show that the plasma treatments increase the surface energy and wettability of the hybrid films. There is also a reduction of the OH groups and oxygen vacancies in the hybrid network improving the dielectric properties.

In (2022), Q. A. Alsulami, and A. Rajeh [38] The casting method was employed for the preparation of polymer blend films doped with TiO_2 (0.5, 1, 1.5, and 2.3 wt%). According to the XRD results. The samples of PANI/PMMa-TiO_2 nanocomposite are amorphous nature. The FTIR technique is used to reveal the

nanocomposites' vibrational bands as well as the intermolecular bonding between the blend and the TiO2 NPs. Absorption spectra, reflectance, transmission spectra, extinction coefficient, refractive index, real and imaginary parts of the dielectric constant, third-order susceptibility (χ3), and optical band gaps are among the optical constants studied. As preselected TiO2 NPs are put into thin films (doping ≤1.5 wt%), the optical band gap values (Eg) of the fabricated nanocomposite films decreased.

In (2023), A. Hashim *et. al.* [39] studied polystyrene (PS)-cerium oxide (CeO_2)-silicon carbide (SiC) nanostructures prepared by the casting method. The structural, optical and electrical characteristics of PS/CeO_2/SiC nanostructures have been investigated. The results indicated that the absorbance (A) was increased about 46.1% at UV-spectra (λ = 300 nm) and 59.1% at visible- spectra (λ = 500 nm). The energy gap of PS was decreased from 4 eV to 2.8 eV when the ratio of CeO_2/SiC nanostructures reached (4.8 wt.%) which made it suitable for several optics and nanoelectronics fields. The optical parameters of PS matrix were enhanced with an increase in the CeO_2/SiC NPs content. Results of the AC electrical properties showed that the dielectric constant (ε') and AC electrical conductivity (σ_{AC}) were improved about 35% and 66.1% with rise in the CeO_2/SiC nanostructures content at (f = 1 kHz).

1.8 The Aim of the Study

The aim of this study can be noted as:

1- The effect of Al_2O_3 nanoparticle on some physical properties of polymer blend.

2- Effect of the cold plasma on the optical and electrical properties before and after exposed of the (PMMA-PS/Al_2O_3) nanocomposites films.

3- The possibility of synthesized (PMMA-PS/Al_2O_3) nanocomposites films as antibacterial coating materials.

Chapter Two

Theoretical Part

2.1 Introduction

This chapter includes a general description of a theoretical part of the studies, as well as physical concepts, scientific clarifications, relationships, and rules utilized to understand the findings.

2.2 The Optical Properties

Optical properties can be defined as the interaction between electromagnetic radiation or light with matter that includes absorption, reflection in addition to polarization, etc.[40]. The study of the optical properties of films is of great importance in finding the optical constants through which it is possible Identifying the value of the optical energy gap, as well as we can know the other constants of absorption and transmittance and their coefficients, as well as the damping coefficient and the real and imaginary dielectric coefficients[41].

2.2.1 Absorbance (A) and Transmittance (T) and Reflection

a. Absorbance(A): the absorbance defines as the ratio between the intensity of the absorbed radiation by the membrane (I_A) to the original intensity of the radiation incident on it (I_o) and the absorbance is a unit-free quantity. It is given by the following relationship[42]:

$$A = I_A / I_o \quad (2.1)$$

b. Transmittance(T): it is defined as the ratio between the intensity of the radiation passing through the membrane (I_T) and the original intensity of the radiation incident on it (I_o) , which is also a quantity devoid of units, and is given by the following relationship[43]:

$$T = I_T / I_o \quad (2.2)$$

c. Reflection (R): the reflectivity (R) is defined as the ratio between the intensity of the radiation reflected from the membrane in a particular direction to the original intensity of the radiation incident on it, and it is given in the following equation[44]:

$$R = I_R / I_o \quad (2.3)$$

Also, the value of the reflectivity can be found from the knowledge of the spectral absorption and permeability by adopting the law of energy conservation, In the following relationship[45]:

$$A + R + T = 1 \quad (2.4)$$

2.2.2 The electronic transitions

Electronic transmission is divided into two types [46, 47]:

1. Direct Transition

This transition occurs in semiconductors when the bottom of the conduction band (C.B.) is exactly over the top of the valence band (V.B.), that meaning they have the same wave vector value (**$\Delta k = 0$**). The conservation of energy and momentum was needed for this transition form. There are two types forms of direct transitions

a. Direct Allowed Transition

As shown in Figure (2.1,a), this transition occurs between the top points in the (V.B.) and the bottom points in the (C.B.).

b. Direct Forbidden Transition

This transition happens between near top points of (V.B.) and near points in the bottom of (C.B.), as shown in figure (2.1, b).

2. Indirect Transition

In these transition types the bottom of conductivity band is not over the top of valence band. The electron transits from (V.B.) to (C.B.) not perpendicularly, they in different regions of **(K)** space ($\Delta \mathbf{K} \neq \mathbf{0}$). This type of transition occurs with the help of a particle known as a "Phonon". there are two types of indirect transitions:

a. Allowed Indirect Transition

As shown in (2.1) these transitions happen between the top of (V.B.) and the bottom of (C.B.) in a different region of (**K-space**).

b. Forbidden Indirect Transition

As shown in figure (2.1) in (d), these transitions occurred between near points in the top of (V.B.) and near points in the bottom of (C.B.). The (Taos's equation) is used to calculate the optical energy gap value of the allowed and forbidden indirect transition.

$$\alpha h\boldsymbol{\nu} = B_o (h\boldsymbol{\nu} - E_g \pm E_{Phonon})^r \qquad (2.5)$$

Where E_{Phonon} means the energy of phonon, (-) when phonon absorption and (+) means when phonon emission, E_g means energy gap, h means blank constant, r means the exponential constant; its value depends on the type of transition, r=2 for the allowed indirect transition, meanwhile r=3 for the forbidden indirect transition.

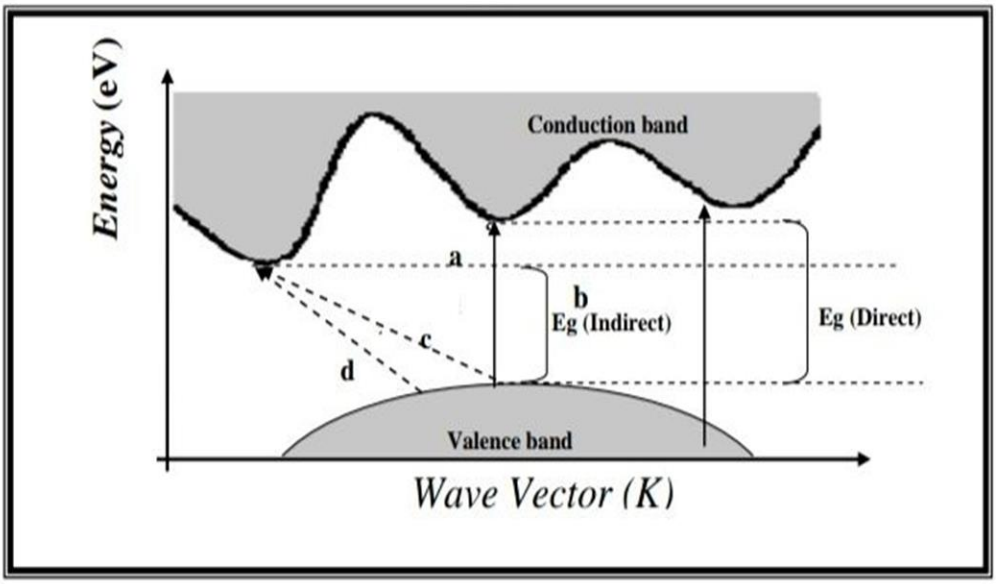

Figure (2.1): Types of electronic transfers [46,47]

(a) Allowed direct transition (b) Forbidden direct transfers

(c) Allowed indirect transition (d) Forbidden indirect transfers

2.2.3 Optical Constants

1. Optical absorption coefficient (α)

It is the decrease in the radiation energy incident on the material and it depends on the energy of the incident rays and the nature of material that falls on it; and it is measured in cm^{-1} unit. If the energy of the photons (hυ) is equal to the energy gap (E_g), then the photons are absorbed to generate a pair (electron-gap) as shown in (a) from figure (2.2). But if the energy of the photons (hυ) is greater than the energy gap (E_g), then it can be a transition process occurs in the semiconductor and produces an excitation of the electron from the valence band to the conduction band. While the extra energy is dissipated to be in the form of heat, as shown in (b) from figure (2.2). Both (a) and (b) are referred to as self-transition, or packet to packet transition,

But if the energy of the photons (hυ) is less than the energy gap (E_g), the absorption will only take place in the presence of localized energy levels in the blocked gap that are caused by chemical impurities and physical defects, as shown in (c) from figure (2.2). This process is called non self-transfer [48, 49].

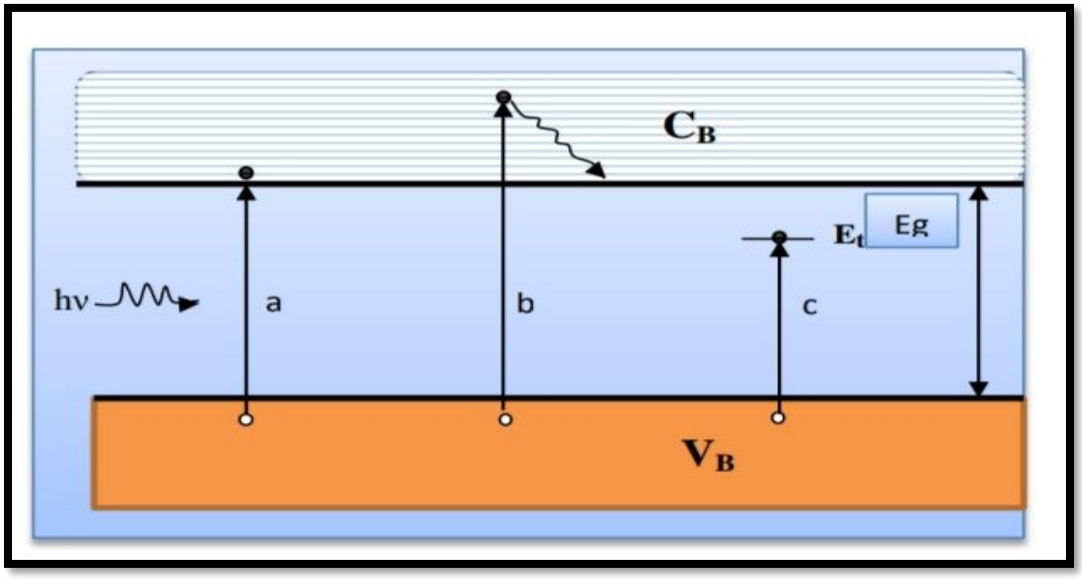

Figure (2.2): Self and non-self-transitions of semiconductors [48].

The absorption coefficient can calculate of the relationship called (Per-Lambert's relationship) [49]:

$$I = I_o e^{-\alpha t} \quad (2.6)$$

Where (I_o) and (I) are the intensity incident ray before and after it passes through the material; respectively, (α) is a absorption coefficient, and (t) thickness of film. After reworking the equation (2.6) above we get[49]:

$$\alpha = 2.303\ A/t \quad (2.7)$$

where A: absorbance and t : thickness

2. Extinction Coefficient (k)

It is defined as the amount of attenuation in the intensity of electromagnetic radiation as a result of the interaction of electromagnetic rays and particles of the thin film material, the damping coefficient can be calculated through the following equation, which is related with the absorption coefficient[43]:

$$k = \alpha\lambda / 4\pi \quad (2.8)$$

Where λ (cm) is the wavelength of the incident radiation and α (cm^{-1}) absorption coefficient.

3. Refractive lndex (n)

The index of refraction of a material is the ratio of the velocity of the light in vacuum to that of the specimen:

$$n = c / v \quad (2.9)$$

where (n) refractive index, (c) the velocity of light in a vacuum, and (v) the velocity of light in any material medium[50].Refractive index can be expressed by the following equation[51]:

$$n = [4R/(R-1)^2 - k^2]^{1/2} + (R+1)/(R-1) \quad (2.10)$$

Where (n) the refractive index, (R) the reflection, and (k) extinction coefficient.

4. Dielectric Constant ($\mathcal{E}$)

Represents the ability of a substance to be polarized, when the interaction between light and the charges of the medium occurs the resulting polarization of the charges of this medium is described by the nodal dielectric constant (ε) that defined by the following equation[52]:

$$\mathcal{E} = \mathcal{E}_1 - i\mathcal{E}_2 \quad (2.11)$$

Where $\mathcal{E}$: complex dielectric constant, $\mathcal{E}_1$:the real part of the dielectric constant, and $\mathcal{E}_2$: the imaginary part of the dielectric determined constant. The real and imaginary part of dielectric constant can be by using equations[53]:

$$\mathcal{E}_1 = n^2 - k^2 \quad (2.12)$$

$$\mathcal{E}_2 = 2nk \quad (2.13)$$

2.3.4 Optical Conductivity

Is the phenomenon of an increase in the number of charge carriers (electrons or holes) as a result of a light beam incident on a semiconductor. The optical conductivity can be calculated from the equation[54]:

$$\sigma_{op} = \alpha \frac{nc}{4\pi} \quad (2.14)$$

Where (σ_{op}) the optical conductivity, (α) is the absorption coefficient, (n) the refractive index, (c) the velocity of light.

2.3 Electrical Properties

Polymers are generally insulators, but they are also not completely free of conduction mechanisms. Conduction often occurs due to impurities that include concentrations of charge carriers[55]. Insulators can be used to store electrical energy in the form of charge separation when the electron distributions around the constituent atoms or molecules are polarized by an external electric field[56].

2.3.1 The A.C Electrical Conductivity

The electric field frequency in the A.C conductivity would be variable during[15]. Dielectric materials can be used to store electrical energy by separating the charge by applying an external electric field. So, when applied a low-frequency electric field on the insulator the permanent or induced dipoles keep pace with the

direction of the applied electric field, that is, the material becomes polarized[14]. The complex permittivity of a material (ε*) can be written as[56]:

$$\mathcal{E}^* = \mathcal{E}_a - j\,\mathcal{E}_b \qquad (2.15)$$

where $\mathcal{E}_a$ and $\mathcal{E}_b$ are value real and the imaginary parts of complex permittivity and Permittivity and j imaginary number equal √-1. The real part is determined by[56]:

$$\mathcal{E}_a = \mathcal{E}_o\ \mathcal{E}' \qquad (2.16)$$

The magnitudes of $\mathcal{E}_a$ and $\mathcal{E}_b$ depend on the angular frequency (ω) of applied the electric field. Magnitude of $\mathcal{E}_a$ (or the dielectric constant $\mathcal{E}'$) indicates the ability of material to store energy from applied electric field[72]. The equation can be used to measure the capacitance of a capacitor made up of two parallel plates[57]:

$$C = \mathcal{E}'\ \mathcal{E}_o\ A/t \qquad (2.17)$$

Where $\mathcal{E}'$ is the constant of dielectric, t is the sample thickness and $\mathcal{E}_o$ is Permittivity in vacuum. Dielectric constant is given by the relation[58] :

$$\mathcal{E}' = C_P / C_o \qquad (2.18)$$

Where: C_P is capacitance in parallel and C_o this is vacuum capacitor[74]. The dielectric of loss ($\mathcal{E}''$) is given by[59] :

$$\mathcal{E}'' = \mathcal{E}'\ D \qquad (2.19)$$

Where D is dispersion factor, and this measures the lost electrical energy in the sample from the applied field which is transformed to thermal energy in the sample. The dissipated power in the insulator is represented by the existence of alternating potential as a function of the alternating conductivity is given by [60]:

$$\sigma_{A.C} = \omega\ \mathcal{E}_o\ \mathcal{E}'' \qquad (2.20)$$

where ω is an angular frequency ($\omega = 2\pi f$).

2.4 Anti-bacterial Application

Antibiotics have been the preferred treatment method for bacterial infections due to their cost-effectiveness and robust results. In reality, antibiotic overuse has recently resulted in the development of superbugs that are resistant to practically all antibiotics[61]. Because of the emergence and spread of drug resistance in bacterial pathogens, antibiotics often lose their effectiveness over time. The so-called "antibiotic resistance crisis" by drug-resistant bacteria result in additional medical costs of up to billions of dollars annually [62]. Faced with this increasingly severe situation, discovering new antibacterial agents and therapeutic strategies is urgently necessary. Nanoparticles provide a universal platform for therapeutic applications based on their own unique physical and chemical properties and provide treatment for drug-resistant bacteria[63].

2.5 Plasma Interaction with matter

From a scientific point of view, matter in the known universe is often classified in terms of four states: solid, liquid, gaseous, and plasma. The basic distinction among solids, liquids, and gases lies in the difference between the strength of the bonds that hold their constituent particles together. These binding forces are relatively strong in a solid, weak in a liquid, and essentially almost absent in the gaseous state. Whether a given substance is found in one of these states depends on the random kinetic energy (thermal energy) of its atoms or molecules, i.e., on its temperature. The equilibrium between this particle thermal energy and the interparticle binding forces determines the state [64].

By heating a solid or liquid substance, the atoms or molecules acquire more thermal kinetic energy until they are able to overcome the binding potential energy. This leads to phase transitions, which occur at a constant temperature for a given pressure.

The amount of energy required for the phase transition is called the latent heat. If sufficient energy is provided, a molecular gas will gradually dissociate into an atomic gas as a result of collisions between those particles whose thermal kinetic energy exceeds the molecular binding energy [65]. At sufficiently elevated temperatures an increasing fraction of the atoms will possess enough kinetic energy to overcome, by collisions, the binding energy of the outermost orbital electrons, and an ionized gas or plasma results. However, this transition from a gas to a plasma is not a phase transition in the thermodynamic sense, since it occurs gradually with increasing temperature [66].

Chapter Three

Experimental Part

3.1 Introduction

In any experimental work, there are a specific mechanism for manner of working, devices to examine the samples and an exact theorem to explain the results. In this chapter we will illustrate in details the materials used and the preparation process with devices that used in this work to find out the structural, optical, and electrical properties.

3.2 Materials

The used materials in this study are:

3.2.1 Matrix Material

1. Poly methacrylate (PMMA): The polymer was used as granular form and was obtained from Apha Co, India (120000 M.W) with high purity (99.99 %).

2. Polystyrene (PS): The polymer was used as granular form and was obtained from Apha Co, India (150000 M.W) with high purity (99.99 %).

3.2.2 Additive Nanomaterial

1. Aluminum oxide nanoparticle (Al_2O_3 NPs): It was obtained as powder from (Nano shel USA) company with grain size (20nm) and high purity (99.9%) .

3.3 The Preparation of (PMMA-PS/Al_2O_3) Nanocomposites Films

Poly methyl methacrylate (PMMA)- Polystyrene (PS) doped with Aluminum oxide nanoparticle (Al_2O_3 NPs) has been prepared by casting method. The blend film (70%PMMA-30%PS) was prepared by dissolving of 1 gm in chloroform (30 ml). The fabricated of nanocomposite by adding of the Al_2O_3 NPs to solution (PMMA-PS) with content 2, 4, 6 and 8 wt. % are shown in table (3-1) and casting on glass betri dish. Then, the nanocomposite prepared were exposed to the Ar plasma. Finally, the samples are ready for the structural, optical, electrical (before

and after exposed to the Ar plasma) and then apply as the antibacterial as shown in Figure (3.1). The thickness of the produced films was about 0.11 mm.

Table (3.1): Weight percentages for nanocomposites (PMMA-PS/Al_2O_3)

PMMA (wt.%)	**PS (wt.%)**	**Al_2O_3 (wt.%)**
70	30	0
69	29	2
68	28	4
67	27	6
66	26	8

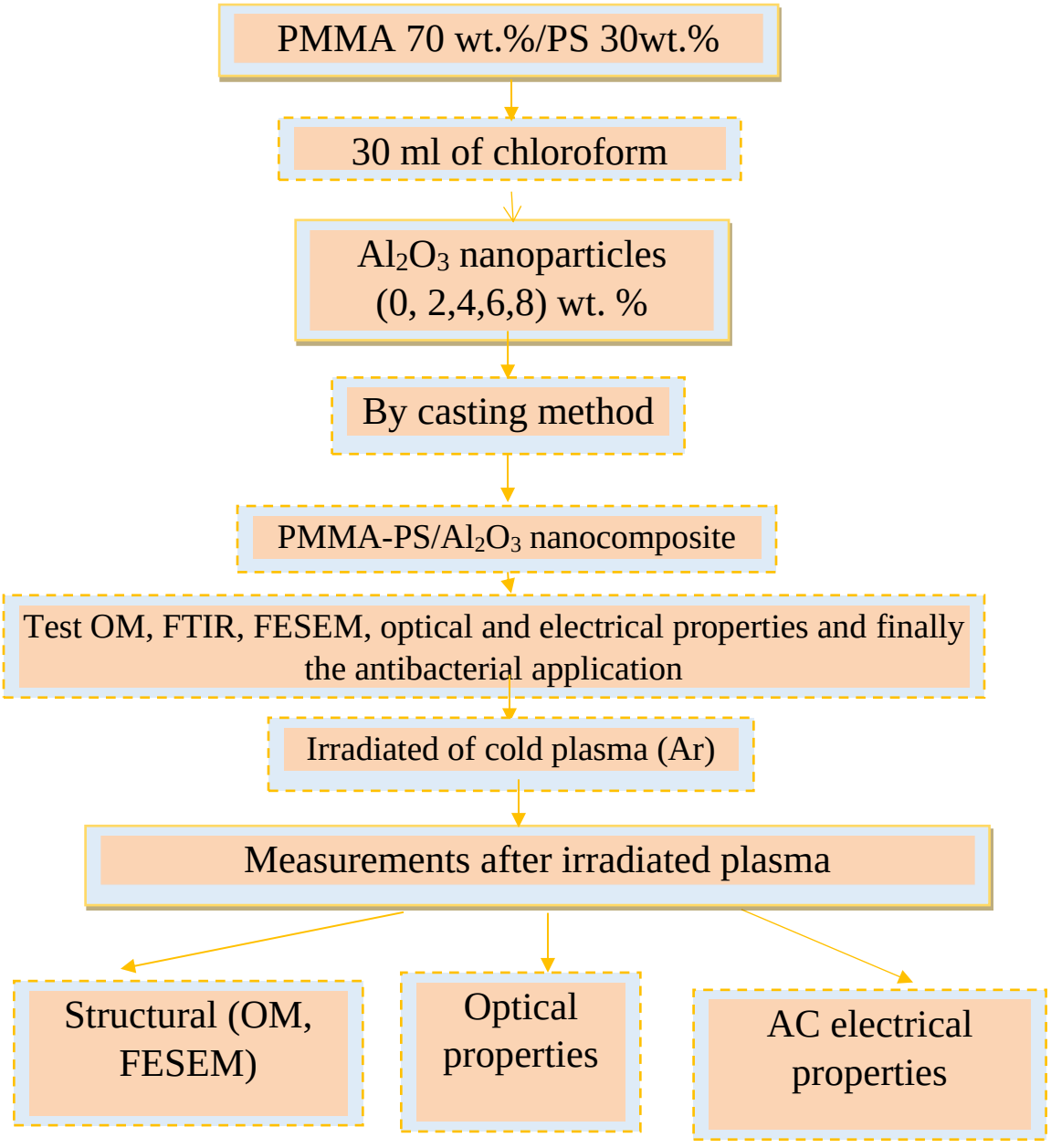

Figure (3.1): The schematic of experimental work.

3.4 Measurements of Structural Properties

3.4.1 Optical Microscope

The optical microscope supplied by Olympus name (Toup View) model (Nikon-73346) as shown in figure (3.2) and fitted with a light intensity automatic operated camera is used to analyze the sample of (PMMA-PS/Al_2O_3) Nano composites films. This calculation was carried out Department of Physics, University of Babylon/College of Education for Pure Sciences, under magnification(10x).

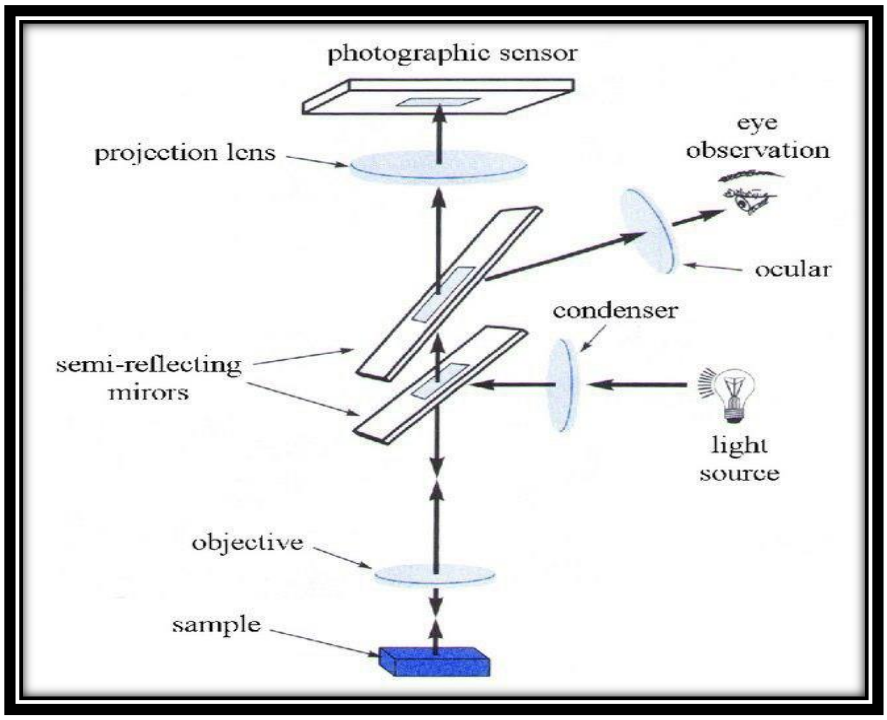

Figure (3.2): Optical Microscope.

3.4.2 FTIR Spectral Characterization

FTIR spectra were recorded by FTIR (Bruker company, German origin, type vertex -70). FTIR was implemented in the University of Babylon /College of Education for Pure Sciences/Department of Physics. In this study, the considered wave number range is (500-4000) cm^{-1}, as shown in figure (3.3)

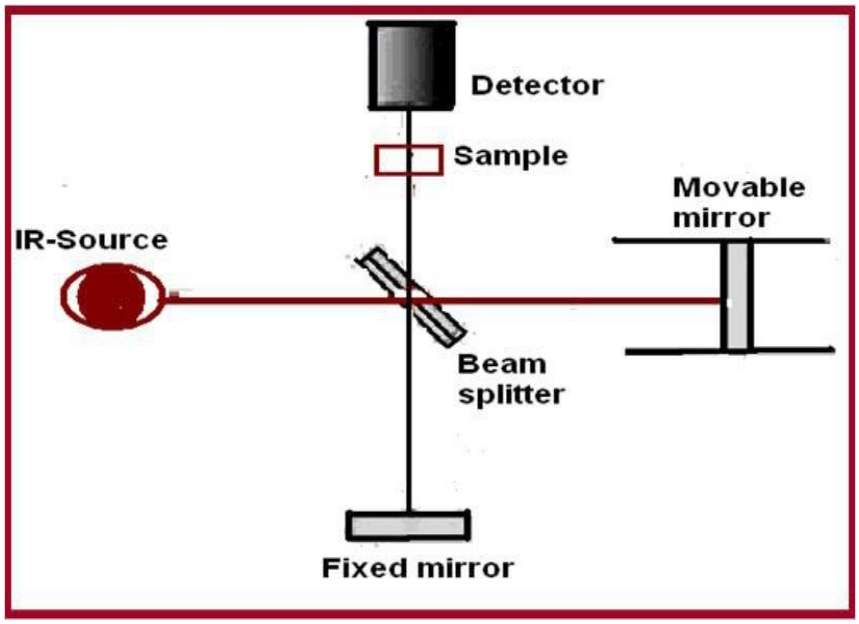

Figure (3.3) : Fourier transform infrared (FTIR) spectroscopy device .

3.4.3 Field Emission Scanning Electron Microscope (FESEM)

Field Emission Scanning Electron Microscope (FESEM) is an electron microscope that images the sample surface by scanning it with a high -energy beam of electrons in a raster scan pattern. The specimens for an FESEM testing must be electrically conductive, at least at the surface, and electrically grounded to prevent the accumulation of electrostatic charge at the surface. Small part of ($1cm^2$) was taken from the sample to examine it by SEM. In this work low vacuum scanning electron microscope was used. The surface morphology of (PMMa-PS/Al_2O_3) nanocomposites films was observed using Tescan mira3 FE- SEM microscope. is equipped with dual Bruker XFlash EDS detectors and Bruker Flash HD EBSD (Czech Tescan Instrument Co.) for analytical studies at the University of Tehran as shown in figure (3.4). The advantage was observed using this technique (Low vacuum SE detecto) is beam deceleration technology (BDT) for high resolution imaging and high surface sensitivity at very low kv and variable pressure operation, fully integrated active anti-vibration system.

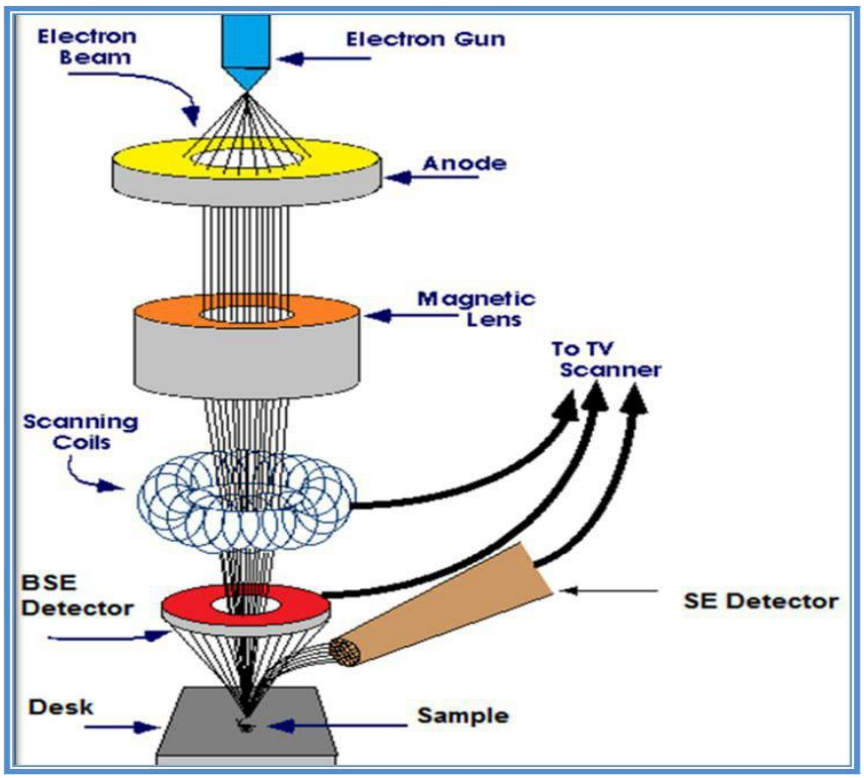

Figure (3.4): Image of system of FE-SEM device.

3.5 Optical Properties Measurements

At the University of Babylon, Department of Physics, College of Education for Pure Sciences, the absorption spectrum of (PMMA-PS/Al_2O_3) nano composites films was measured with a double beam spectrophotometer (Shimadzu model UV-1800 Ao (JAPAN)) in the wavelength range (190-1100) nm. As shown in figure (3.5). It found at room temperature; the absorption spectrum was recorded. The optical constants, absorption coefficient, extinction coefficient, refractive index, and energy gaps are all examples of parameters were calculated using a computer program.

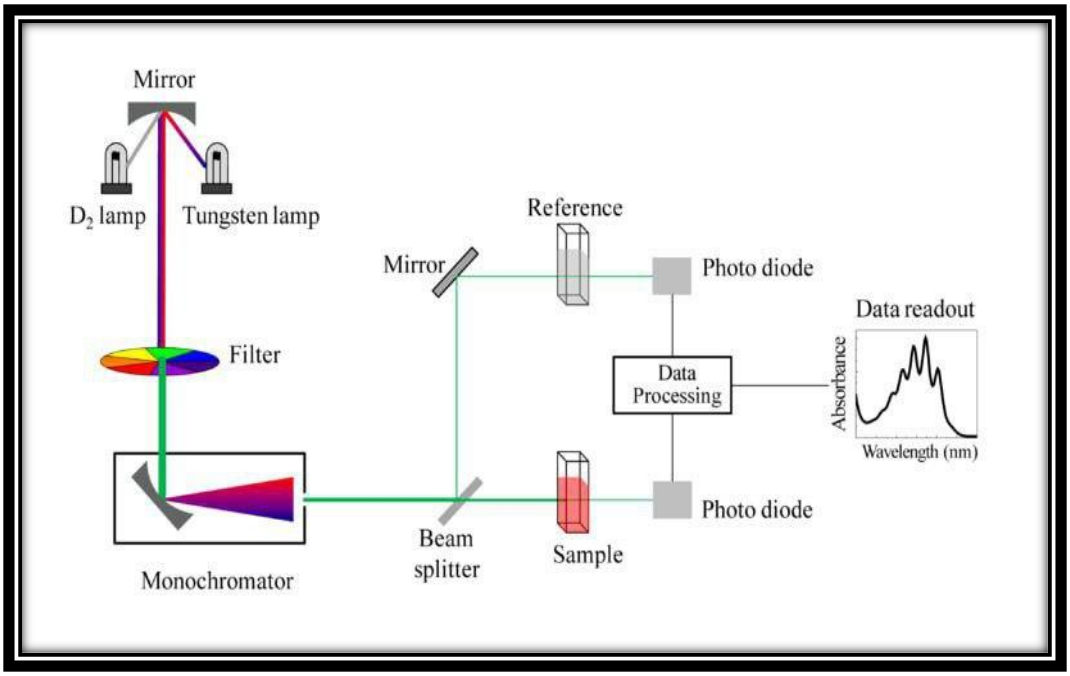

Figure (3.5): Image of UV spectrophotometer (photometer).

3.6 A.C. Electrical Properties Measurement

LCR meter style (HIOKI 3532-50 LCR Hi TESTER (Japan) is used to measure A.C. electrical conductivity at the University of Babylon/College of Education for Pure Sciences/Physics Department figure (3.6) shows a diagram for the A.C electrical measurement system. Only (1cm) from each one of the samples has been taken and put between two electrodes and by different frequencies from (100Hz-5MHz) at room temperature. The capacity and dissipated factor have been recorded for all 43 the samples. Dielectric constant, dielectric loss and conductivity have been calculated from this data.

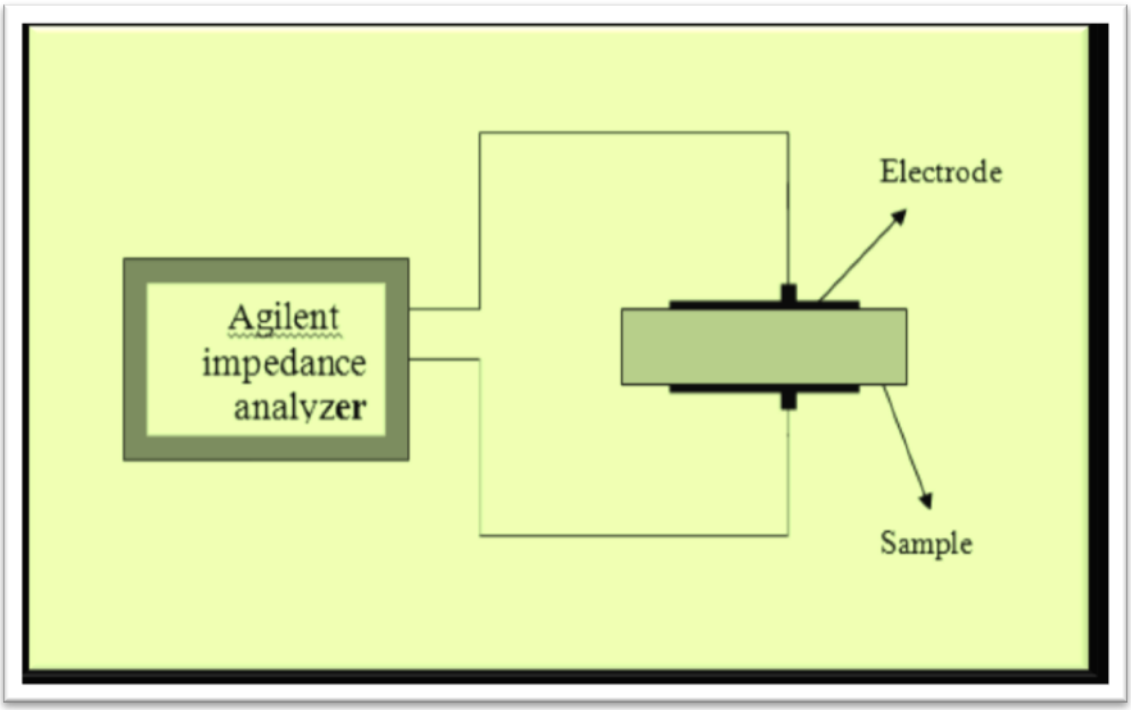

Figure (3.6): Diagram for system of A.C electrical measurement system

3.7 Application of (PMMA-PS/Al_2O_3) Nanocomposites Films

Antibacterial activity of the (PMMA-PS/Al_2O_3) nanocomposites films tested samples were determined using a disc diffusion method. The antibacterial activities were done by using gram positive organisms (Staphylococcus aureus) and gram-negative organisms, Escherichia coli, Bacteria (Staphylococcus aureus and Escherichia (coli) were cultured in Muller-Hinton agar. The disks of the (PMMA-PS/Al_2O_3) nanocomposites films were placed over the media and incubated at 37°C for 24 hours. The inhibition zone diameter was measured.

3.8 Irradiation plasma

After prepared of (PMMA-PS/Al_2O_3) nanocomposite films, the cold plasma (Ar gas) irradiated with voltage 4.8 KV , current 0.2 A, pressure 5 mbar and the diameter of the tube for generating the plasma is 5 mm are shown in figure (3.8). This calculation was carried out Department of Physics, University of Babylon/College of Education for Pure Sciences, which consists of the following specifications:

-Tube end 3 mm

-Between the electrodes 1,5 cm

-Electrode thickness 1 mm

-Electrodes width 1 cm

-Frequency 5.6 Hz

-Inner tube diameter 5mm

-Outer tube diameter 3mm

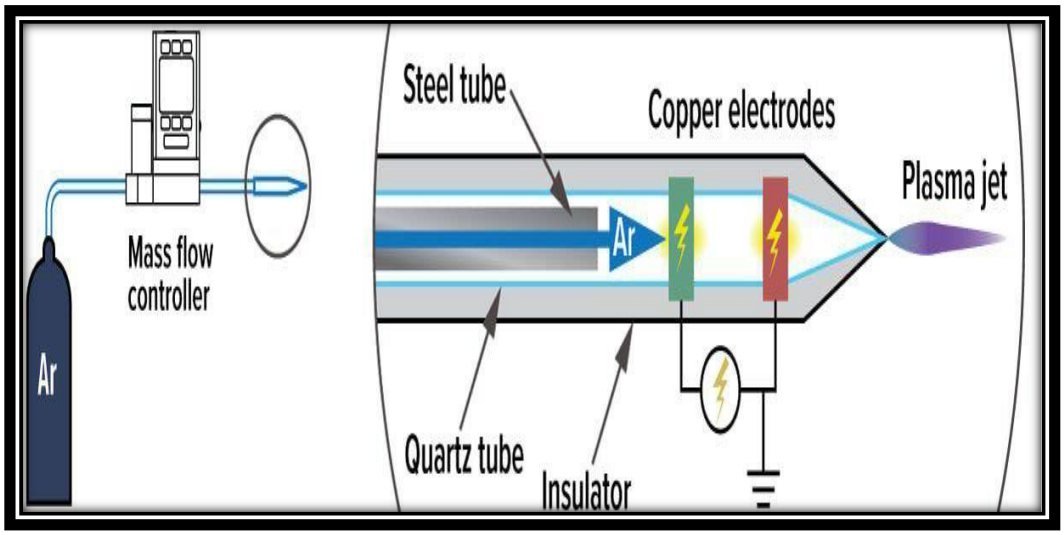

Figure (3.8): Cold plasma irradiation

Chapter Four

Results, Discussion and Conclusions

4.1 Introduction

This chapter includes the results and its discussion of the structural, optical and (A.C) electrical measurements for (PMMA-PS/Al_2O_3) nanocomposites films. It also discusses the effect of different concentrations additive nanoparticles (Al_2O_3) in the optical microscope, Fourier transform infrared rays (FTIR), Field Emission Scanning Electron microscope (FE-SEM) before and after exposed of argon plasma and antibacterial activity applications of (PMMA-PS/Al_2O_3) nanocomposites films are also discussed.

4.2 The Structural Properties

4.2.1 The Optical Microscope Measurements

Figures (4.1)(4.2) shows photomicrograph of the pure (PMMA/PS) blend and vary ratio of Aluminum oxide nanoparticle (Al_2O_3 NPs) before and after exposed Ar plasma respectively. From these figures (4.1A) (4.2A), the surface of (PMMA-PS) composite homogenous and uniform distribution which indicate a successful this method. In image B, C, D and E in figure (4.1), we note that at low ratio of the Al_2O_3 NPs collective as groups. When the concentration of Al_2O_3 NPs is increase, the nanoparticles create a continuous network inside the (PMMA-PS) nanocomposites films at 8 % , while in figure (4.2), at low concentrations of Al_2O_3 NPs, it can be noted that the formation of small pits on the surface of the nanocomposite as a result of exposure to Argon plasma gas and when were reach a concentration of 8 wt.% Al_2O_3 NPs, it notes that these pits increase due to the increase in the interaction of the plasma with the surface of the sample.

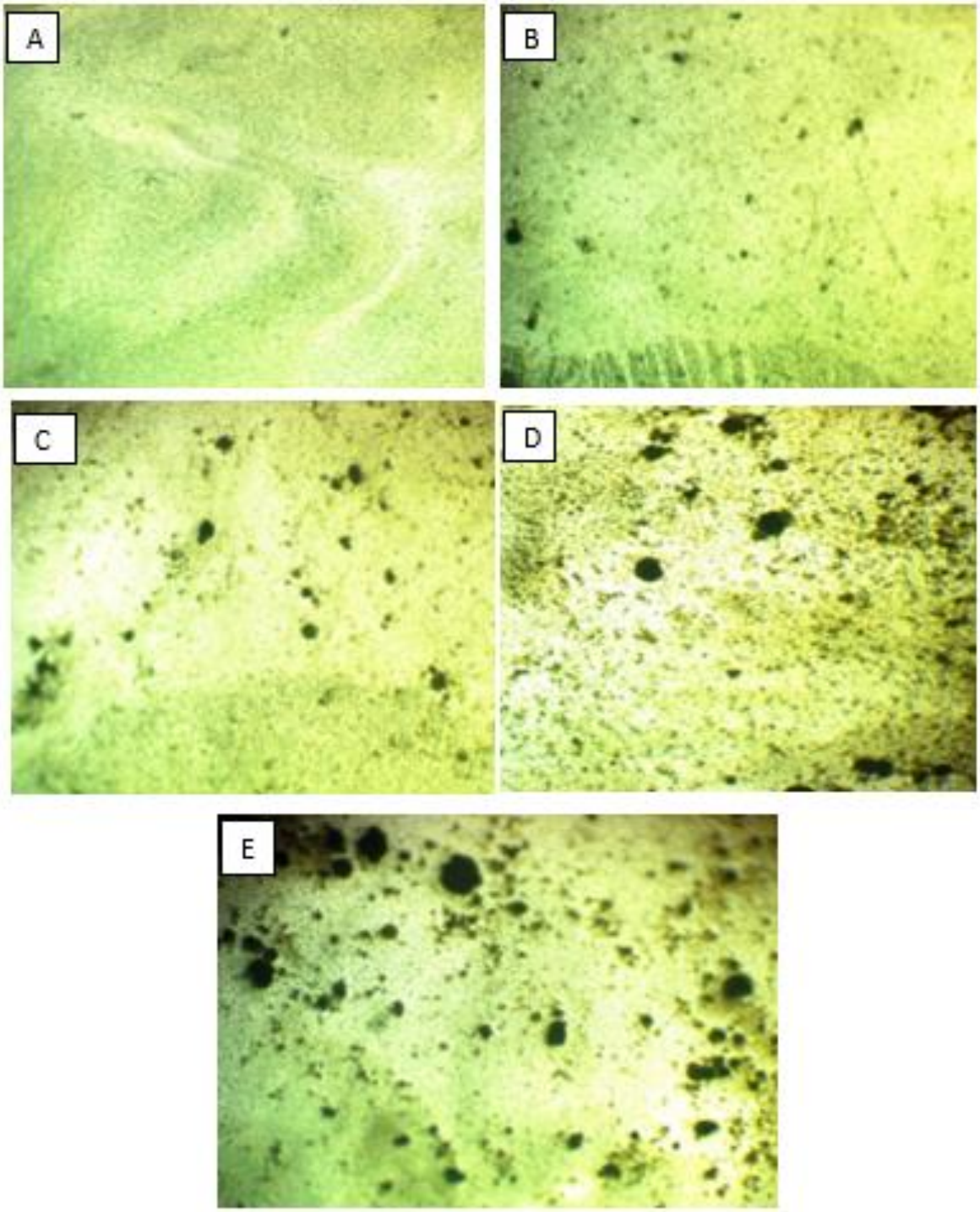

Figure (4.1): Photomicrographs (x10) for (PMMa-PS/Al_2O_3) nanocomposites films: (A) for pure (B) for 2 wt.% Al_2O_3 NPs, (C) for 4 wt.% Al_2O_3 NPs, (D) for 6 wt.% Al_2O_3 NPs and (E) for 8 wt.% Al_2O_3NPs.

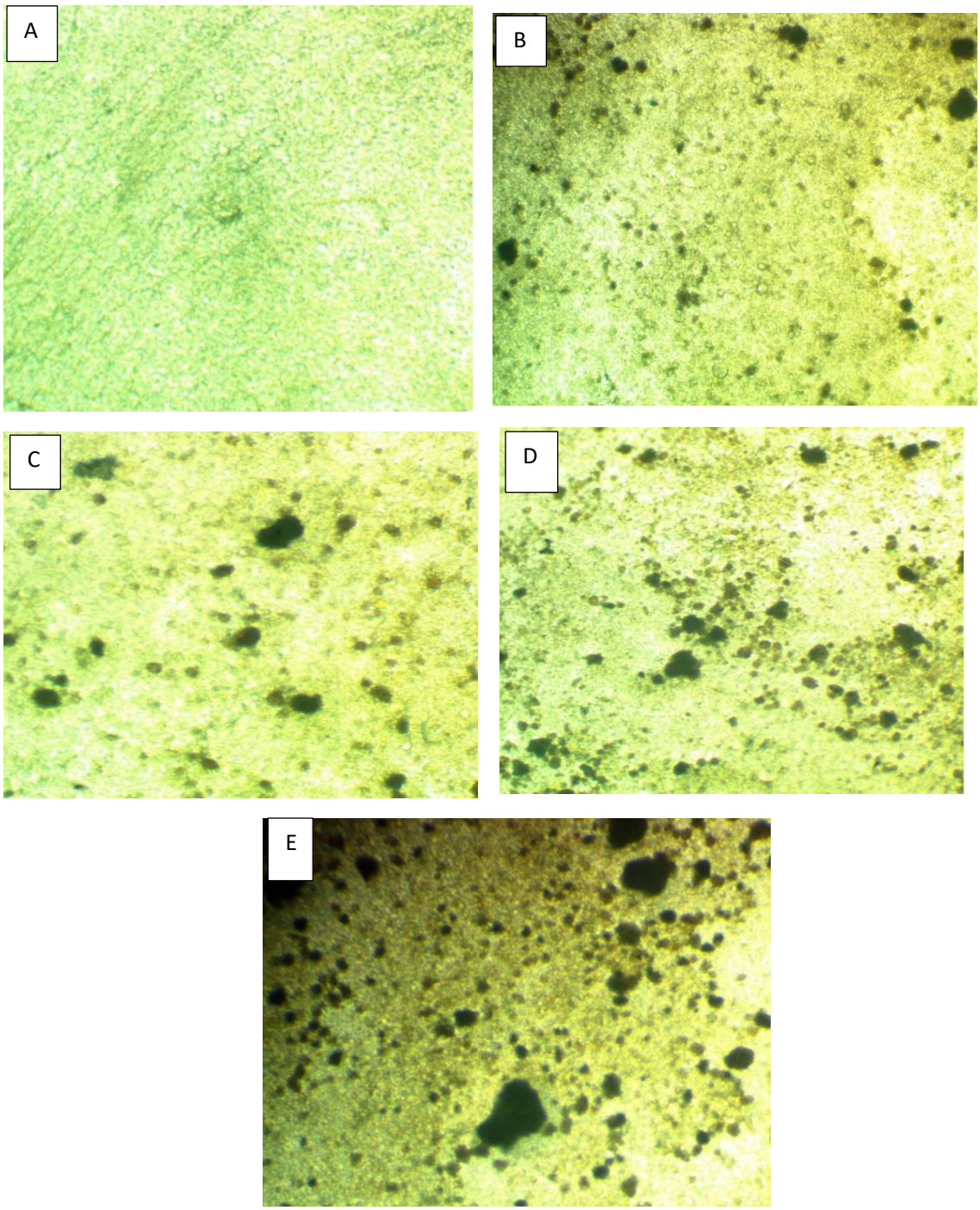

Figure (4.2): Images of OM (10x) for (PMMA-PS/Al_2O_3) nanocomposites films after exposed Ar plasma films: (A) for pure (B) for 2 wt.% Al_2O_3 NPs, (C) for 4 wt.% Al_2O_3 NPs, (D) for 6 wt.% Al_2O_3 NPs and (E) for 8 wt.% Al_2O_3NPs

4.2.2 Fourier Transform Infrared Rays (FTIR) Measurements

FTIR spectra of (PMMA-PS/Al_2O_3) nanocomposites films are shown in figure (4.3) at wavenumber range (500-4000) cm^{-1}. FTIR studies of nanocomposites show the interactions in nanocomposites. FTIR spectra of (PMMA-PS) polymer are reveals absorption band at 2984.45 cm^{-1} corresponding to the CH_3 bending vibration and the band 1723.34 cm^{-1} owing to the C=O stretching vibration. Band at 1435.14 cm^{-1} corresponding to the CH_3 stretching vibration. The absorption band at 1143.71 cm^{-1} attribute to the symmetric stretching vibration of C-O. The bands 984.77 cm^{-1}, 697.33 cm^{-1} and 749.08 cm^{-1} matching to the C–C bending and stretching vibration respectively [67].

After adding Al_2O_3 nanoparticles to the polymers (PMMA-PS) as shown in image (from B to E) from fig. (4.3) leads to the displacement of some of the bonds and not emergence of new peaks therefore, there is no interaction between Al_2O_3 nanoparticle and the PMMa-PS polymer matrix. these results agree with the researchers [68,69].

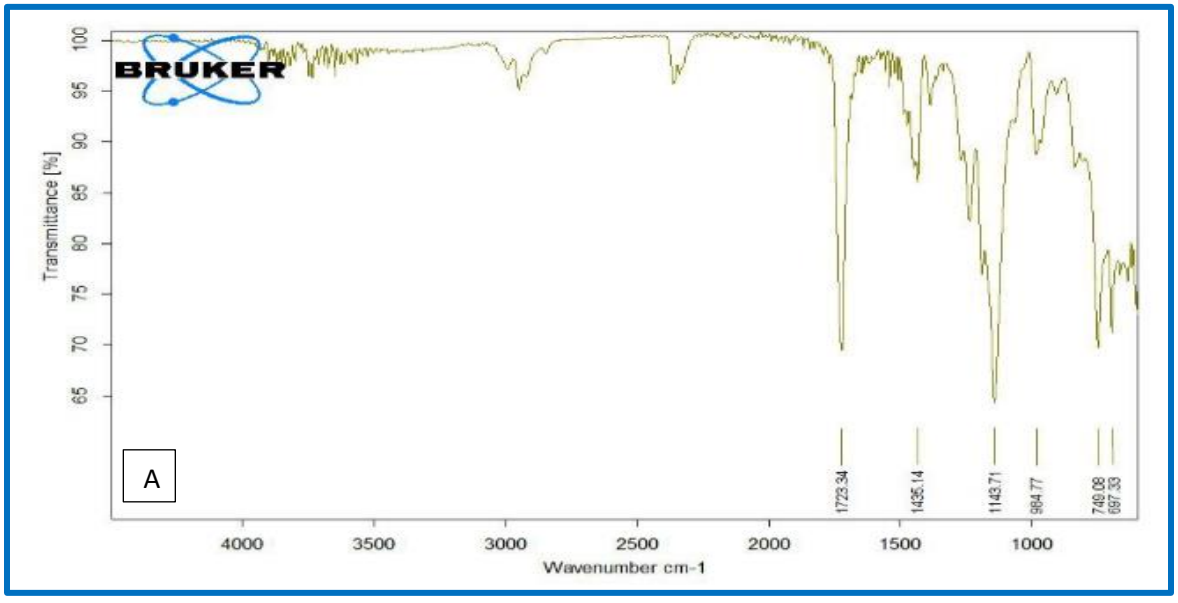

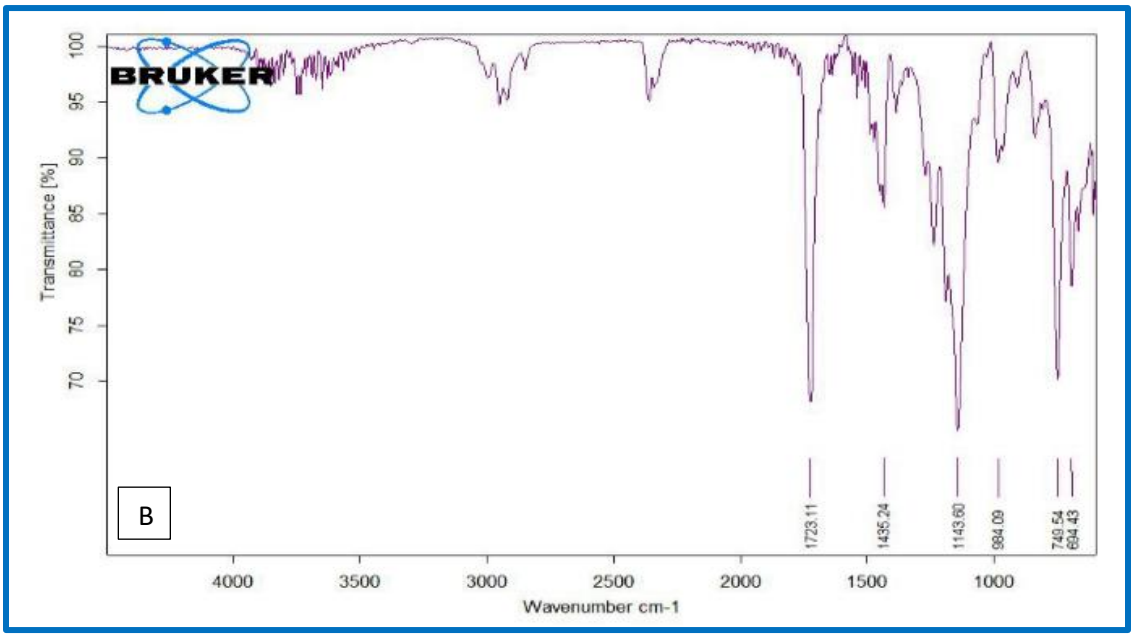
BRUKER
Transmittance [%]
100
95
90
85
80
75
70
B
1723.11
1435.24
1143.60
984.09
749.54
694.43
4000
3500
3000
2500
2000
1500
1000
Wavenumber cm-1

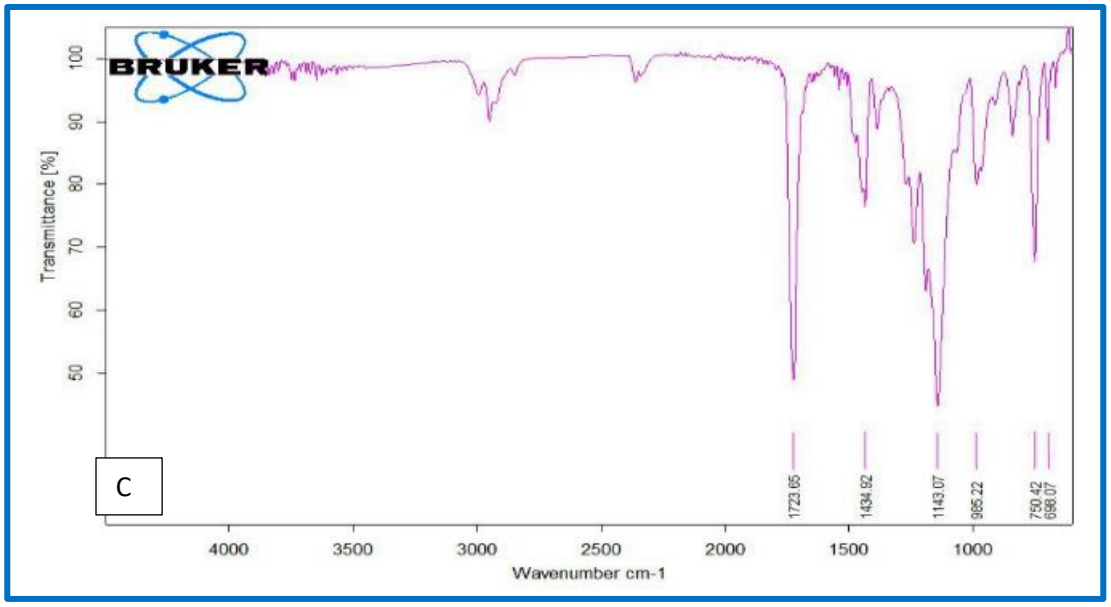
BRUKER
Transmittance [%]
100
90
80
70
60
50
C
1723.65
1434.92
1143.07
985.22
750.42
698.07
4000
3500
3000
2500
2000
1500
1000
Wavenumber cm-1

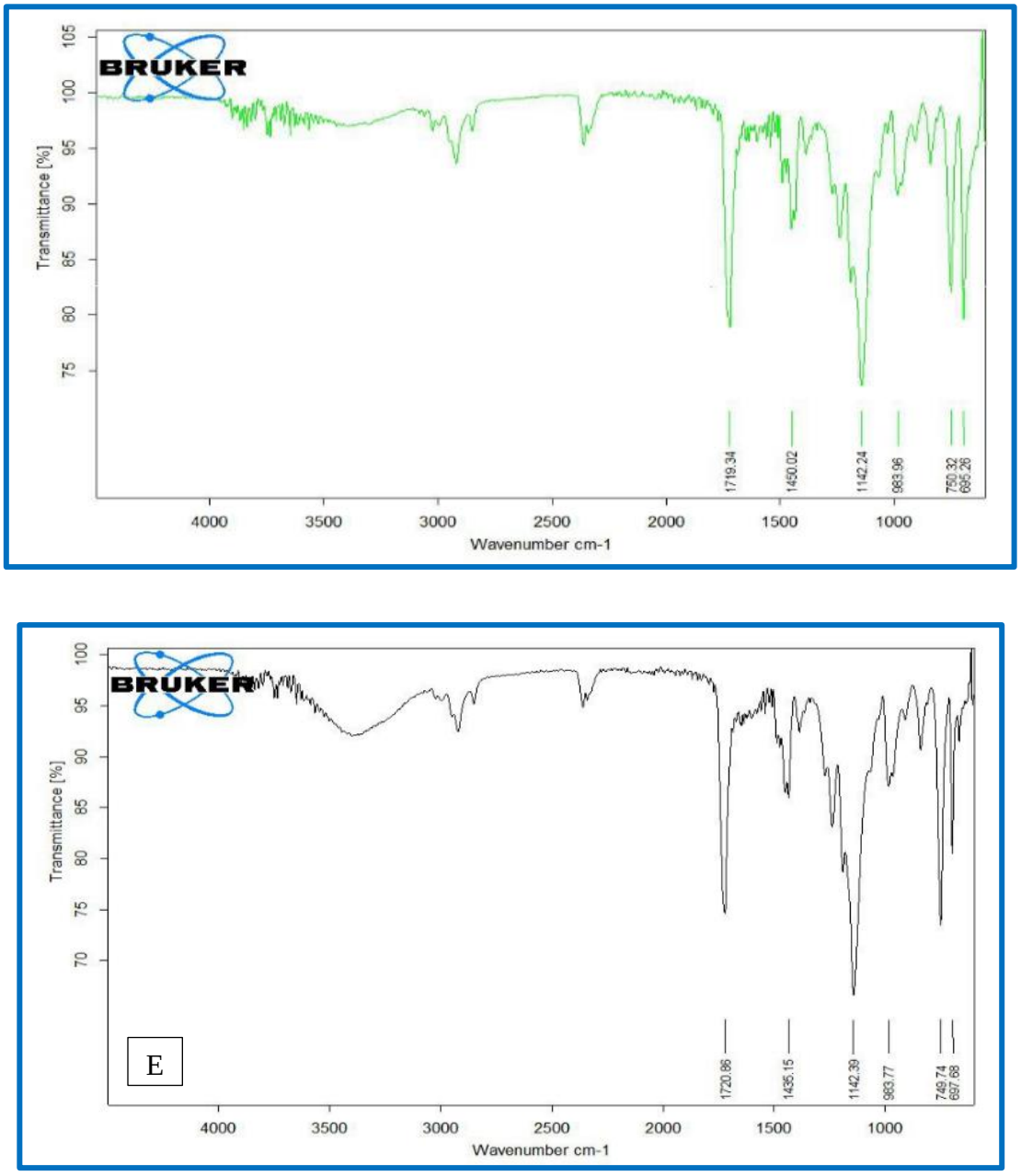

Figure (4.3) FTIR spectra of (PMMA-PS/Al2O3) nanocomposites films A. pure polymer, B. 2 wt.% of (Al_2O_3) NPs, C. 4 wt.% of (Al2O3) NPs, D. 6 wt.% of (Al2O3) NPs and E. 8 wt.% of (Al_2O_3) NPs.

4.2.3 Field Emission Scanning Electron Microscopy (FESEM) Measurements

Field Emission Scanning Electron Microscopy (FESEM) is tested to study the compatibility between vary components of the polymer and nanomaterials. The morphology of the surface of samples PMMa-PS/Al_2O_3 nanocomposite films is examined using an FESEM as shown in the figures (4.4) (4.5) at different scale before and after exposed Ar plasma.

Figure (4.4A) reveales the sample pure has a homogenous and smooth surface. When adding the concentrations of nanoparticles (Al_2O_3) to (PMMA-PS) polymer in image B, C, D and E, the results show that the nanoparticles inclined to create collections and good dispersed PMMA-PS/Al_2O_3 nanocomposites films as shown in images presented a uniform and revealed homogeneous films with a homogeneous surface. With the contribution of nanoparticles in the polymer, the nanocomposites displayed good spreading without accumulation. Most of the nanoparticles were well-scattered and densely dispersed on the surface of the nanocomposite films with well-distributed that showed variations in surface form.

From figure (4.5), it can be noted that the formation of craters results from surface exposure to the argon plasma gas, and when we reach a concentration of 8 wt.% Al_2O_3 NPs, the formation of grooves [70]. Treatments using reactive gases like argon are known to produce this effect. These processes involve the chemical interaction of energetic plasma particles with the sample species, which removes them and creates volatile byproducts including water vapor, carbon monoxide, and carbon dioxide that are subsequently pumped out of the reactor. Moreover, polar groups, which, if not removed from the system, may persist in the discharge and be reincorporated into the sample, may be created when the removed species recombine. This result agrees with [70,71].

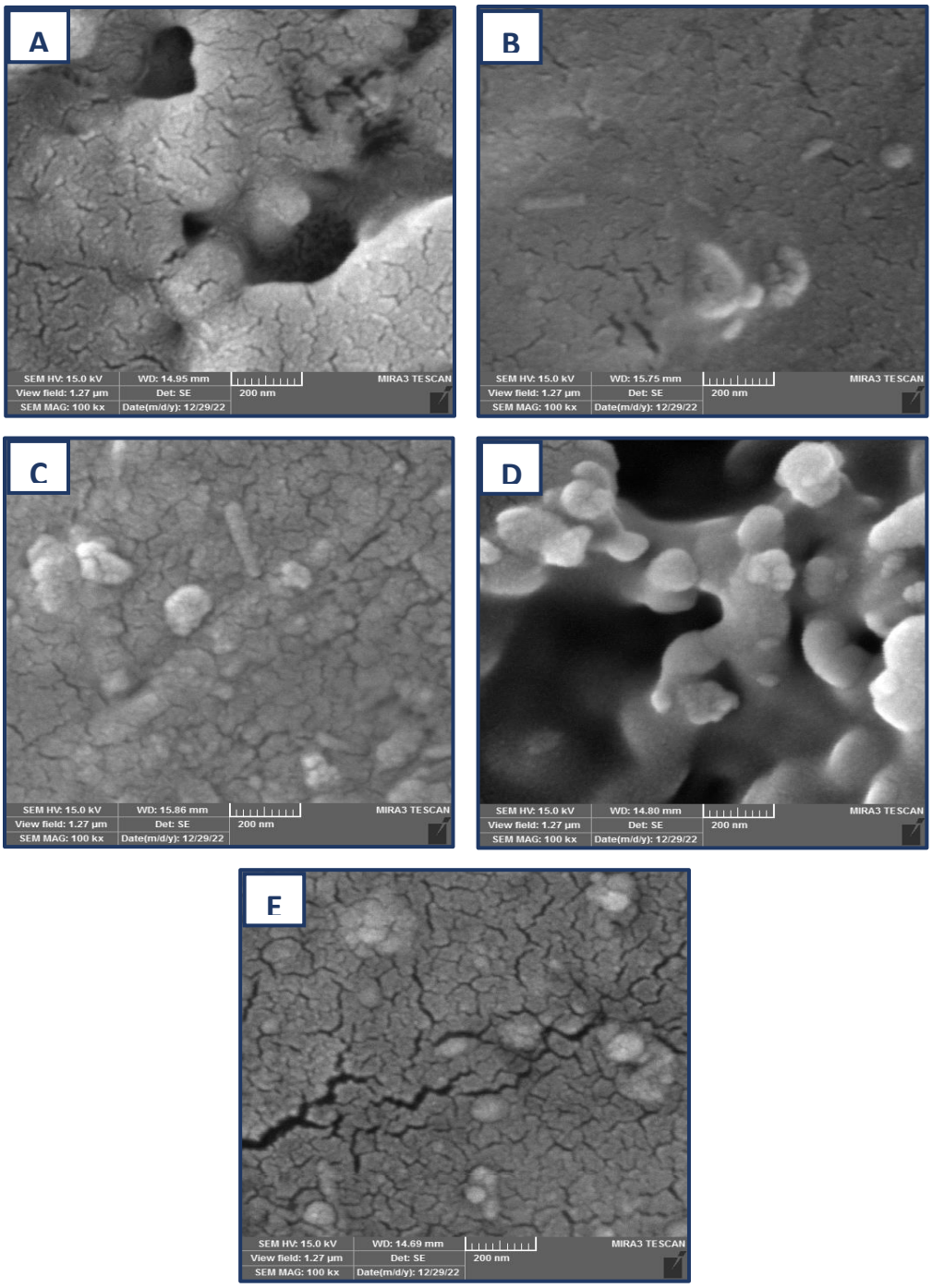

Figure (4.4) FE-SEM images of (PMMA-PS/Al_2O_3) nanocomposites films :(A) for (PMMa-PS/Al_2O_3), (B) 2 wt.% Al_2O_3 NPs, (C) 4 wt.% Al_2O_3 NPs, (D) 6 wt.% Al_2O_3 NPs, (E) 8 wt.% Al_2O_3 NPs

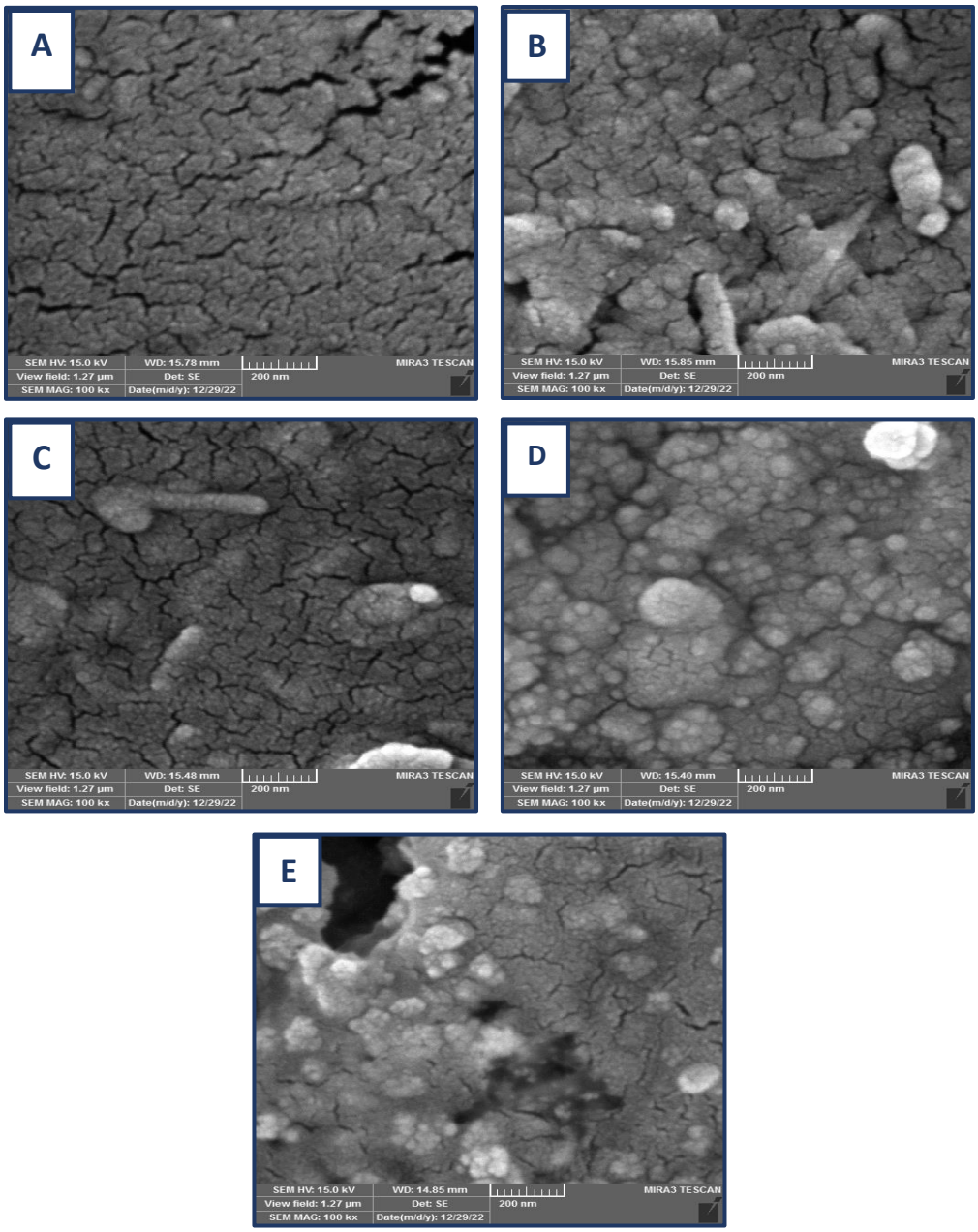

Figure (4.5): FE-SEM images of (PMMA-PS/Al_2O_3) nanocomposites films after exposed Ar plasma :(A) for (PMMA/PS/Al_2O_3), (B) 2 wt.% Al_2O_3 NPs, (C) 4 wt.% Al_2O_3 NPs, (D) 6 wt.% Al_2O_3 NPs, (E) 8 wt.% Al_2O_3 NPs

4.3 Optical Properties of (PMMA-PS/AL2O3) nanocomposites films:

The main purpose of studying the optical properties of the (PMMA-PS/Al_2O_3) nanocomposites films is to identify the effect of adding (Al_2O_3) nanoparticles on the optical properties of (PMMA-PS) films. The research covers the recording of the spectrum of absorbance for the (PMMA-PS/Al_2O_3) films at room temperature and calculating the absorption coefficient, extinction coefficient, and other optical constants, as well as identifying the types of electronic transitions and calculating energy gaps before and after exposed Ar plasma.

4.3.1 The Absorbance spectra

Figures (4.6) (4.7) demonstrations the influence of Al_2O_3 NPs on the absorbance of a PMMA/PS nanocomposite throughout a wavelength range of 200-1100 nm before and after exposed Ar plasma. Since free electrons absorb incident light, the absorbance of PMMA-PS/Al_2O_3 nanocomposite film rises as the Al_2O_3 ratio rises. Also, it notes that the absorbance has higher value at visible regions which attributed to the to the increased charge carriers and the occurrence of some bonds breaking. The results are agreed with [72,73,74].

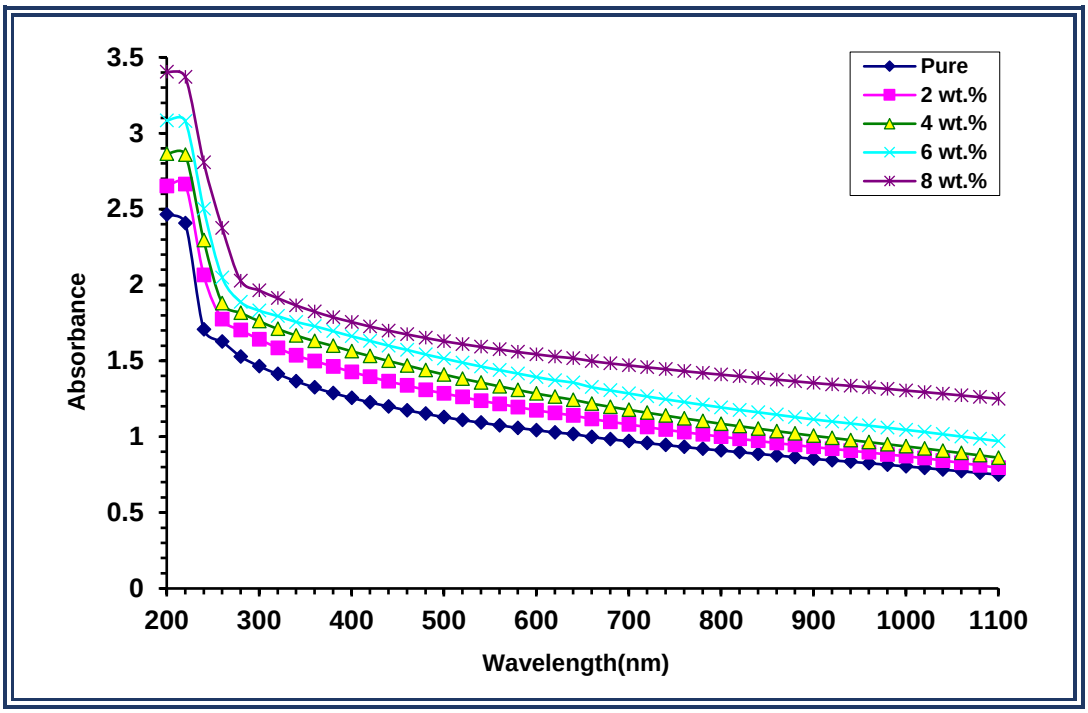

Figure (4.6): Absorbance of the PMMA-PS/Al_2O_3 nanocomposites films with wavelength before exposed Ar plasma.

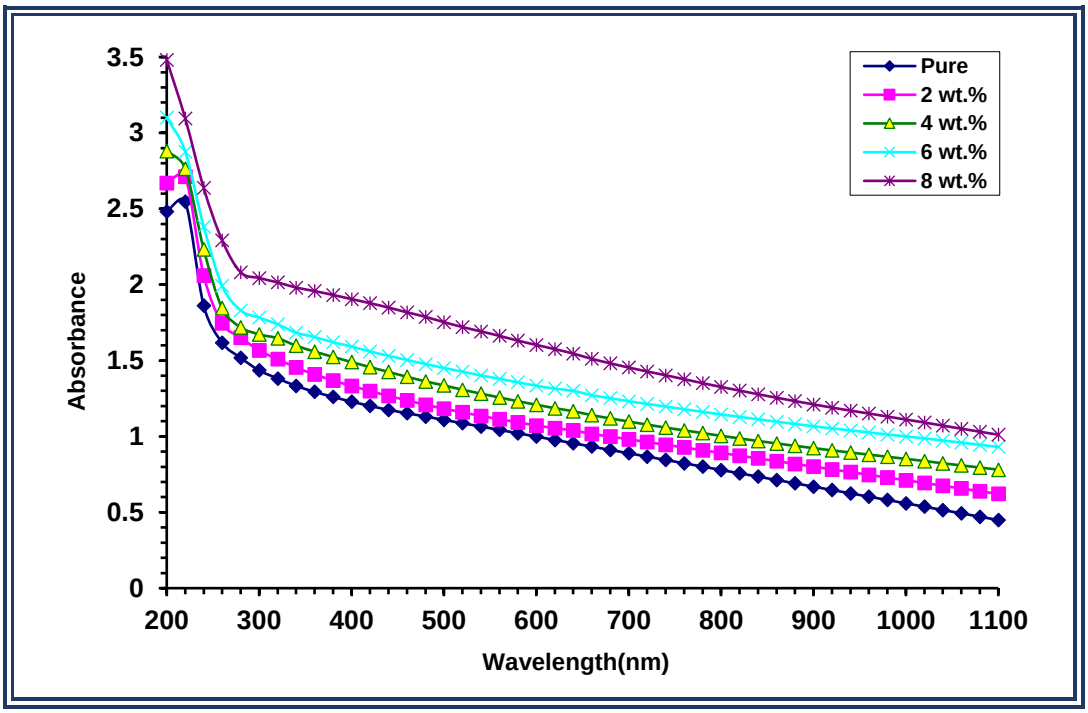

Figure (4.7): Absorbance of the PMMA-PS/Al_2O_3 nanocomposites films with wavelength after exposed Ar plasma.

4.3.2 The Transmittance spectra

Figure (4.8) (4.9) illustrates the optical transmittance of PMMA-PS/Al_2O_3 nanocomposites films before and after exposed to the Ar plasma. From these figures, it can be obtained that the transmittance decreased with increasing concentration of Al_2O_3, which attributed to increase of absorbance. The transmittance after irradiation has high values compared before irradiation which attributed to the increased charge carriers and the occurrence of some bonds breaking. This result is agreed with researchers [73,74].

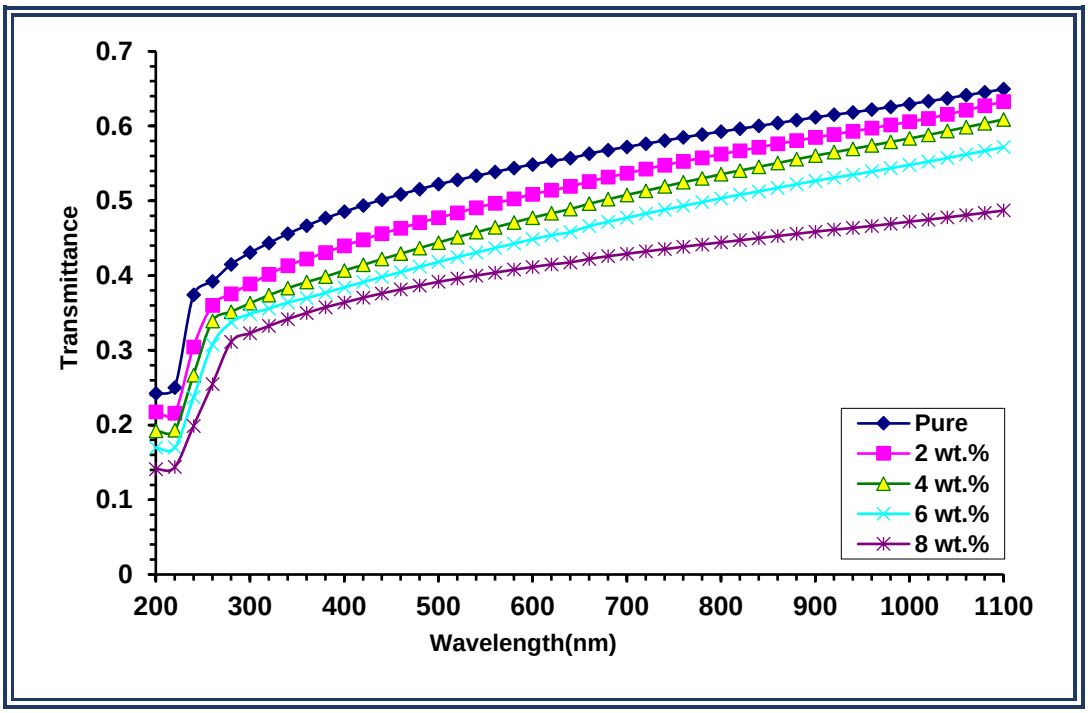

Figure (4.8): Optical transmittance spectra of PMMA-PS/Al_2O_3 nanocomposites films before exposed Ar plasma.

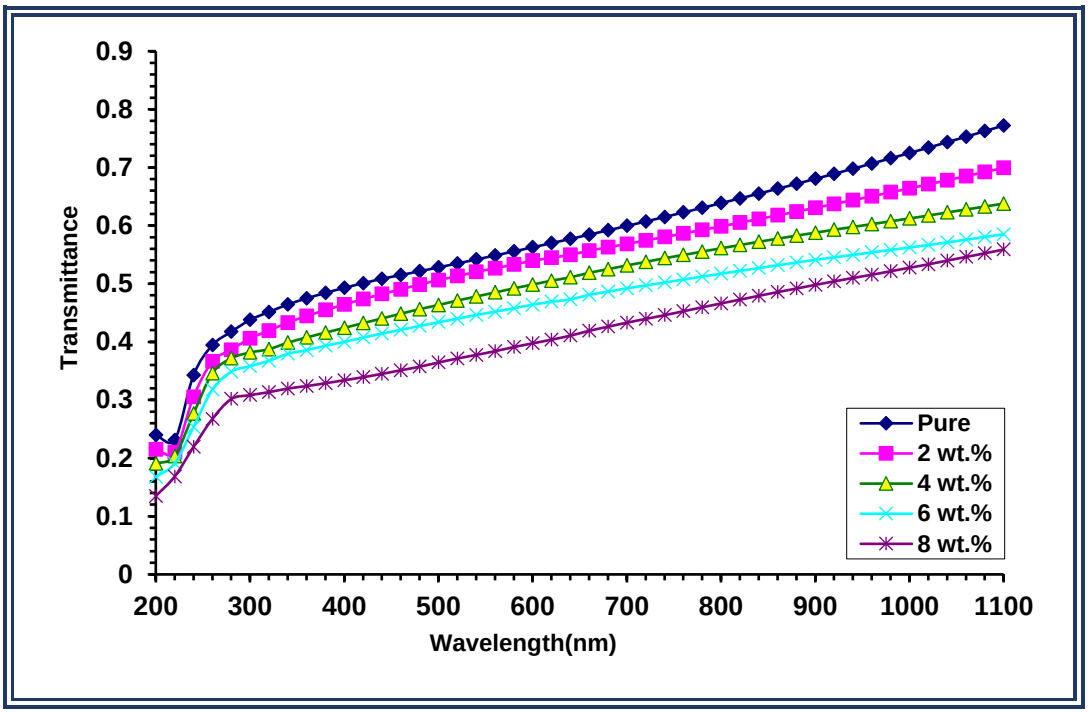

Figure (4.9): Optical transmittance spectra of PMMA-PS/Al_2O_3 nanocomposites films after exposed Ar plasma.

3.3.3 The absorption coefficient

The absorption coefficient was calculated from equation (2.7). Figures (4.10) (4.11) displays the absorption coefficient of the (PMMA-PS/Al_2O_3) nanocomposites films with the photon energy before and after exposed Ar plasma. The absorption coefficient might help you figure out what kind of electron transition you're dealing with. It is assumed that direct electron transitions occur when the material's absorption coefficient is large 10^4 cm^{-1}. When the absorption coefficient is low 10^4 cm^{-1}, an indirect transition of electrons is assumed. The values of absorption coefficient of (PMMA-PS/Al_2O_3) nanocomposite films is less than 10^4 cm^{-1}, the transition of electron is indirect. From these figures, the absorption coefficient of nanocomposites rises with the rises of the content of Al_2O_3 NPs, this is due to the rise of various charge carriers and therefore rising the absorption and absorption

coefficient for (PMMA-PS/Al_2O_3) nanocomposites films. The absorption coefficient after irradiation has high values compared before irradiation in visible and near infrared region which attributed to the increased charge carriers and the occurrence of some bonds breaking. This result agrees with [73,74,75].

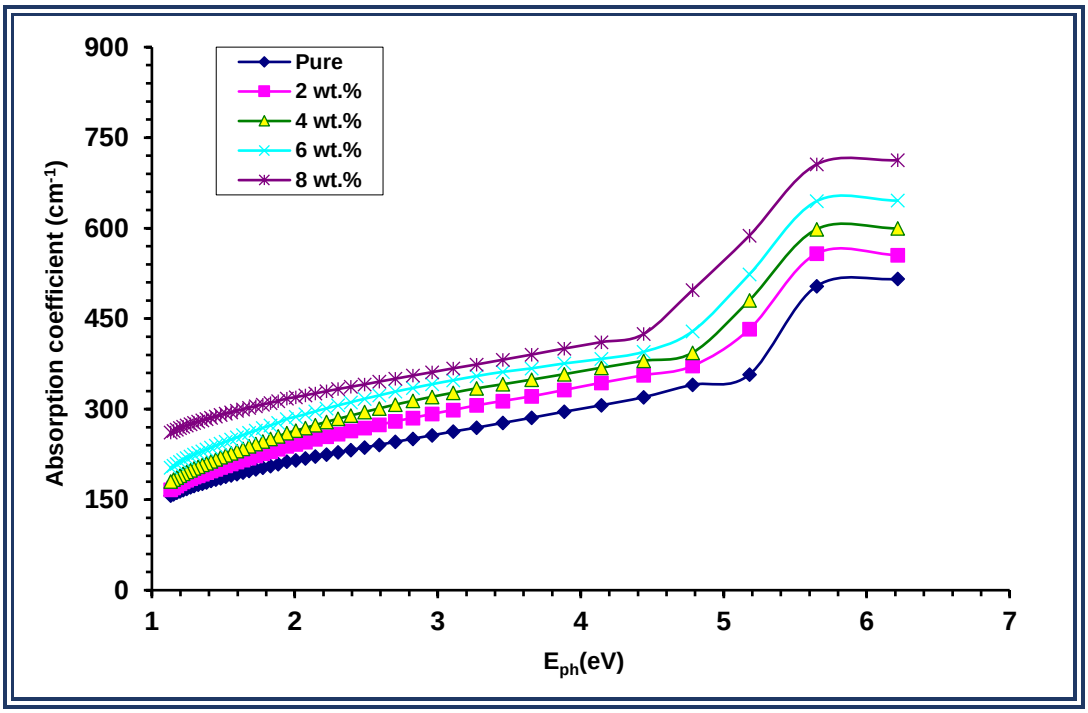

Figure (4.10): The variation absorption coefficient of (PMMA-PS/Al_2O_3) nanocomposite films with the photon energies.

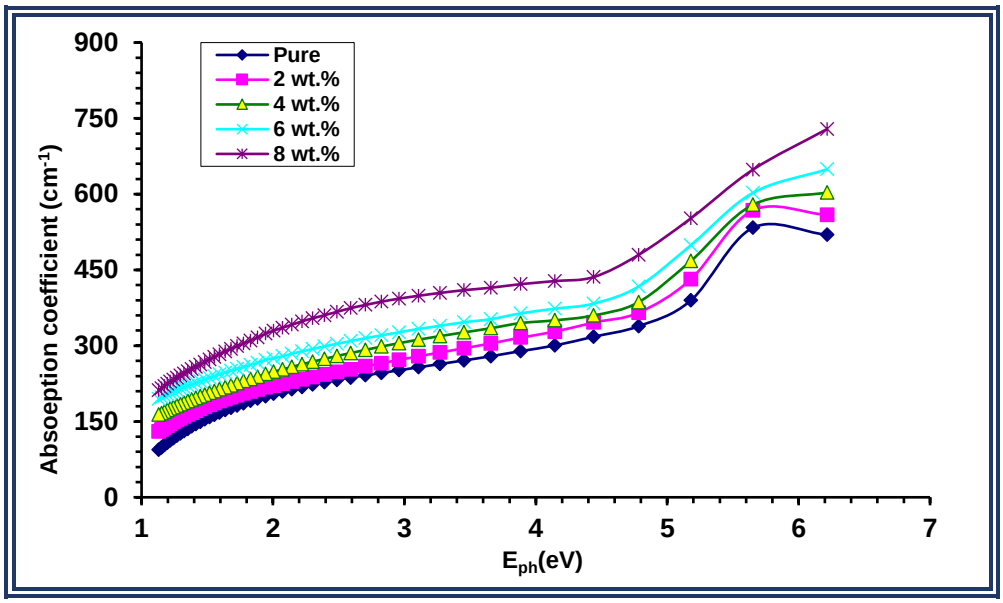

Figure (4.11): The variation absorption coefficient of (PMMA-PS/Al_2O_3) nanocomposite films with the photon energies after exposed Ar plasma.

4.3.4 The Energy Gap

The gap of energy was calculated from relation (2-5). The energy gap for allowed and forbidden indirect transitions of PMMA-PS/Al_2O_3 nanocomposites films are explain in figures (4.12) (4.13) (4.14) (4.15) before and after exposed Ar plasma. We may find the energy gap for the indirect transition by plotting the data or tang cut from the top of the curve to the (x axis) at (hv). From this figure, the energy gap is decreased with the increasing concentration of the Al_2O_3 NPs. This action is due to the formation of levels in the energy gap and therefore, these local levels decrease the energy gap with increase of the PMMA-PS/Al_2O_3 nanocomposite films. Also, from this figures, The indirect band gap for allowed and forbidden after irradiation have reduce values compared before irradiation which attributed to the increased charge carriers and the occurrence of some bonds breaking. Table (4-1) (4-2) obtained the values of allowed and forbidden energy gap before and after exposed Ar plasma. This result agree with researchers [73,74].

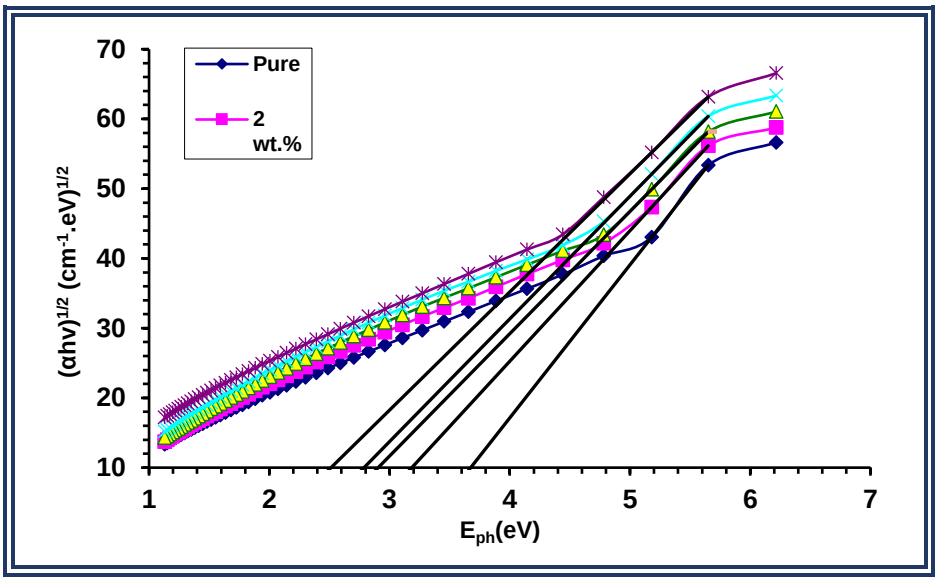

Figure (4.12): The Eg for the allowed indirect transition $(\alpha hv)^{1/2}$ $(cm^{-1}.eV)^{1/2}$ of (PMMA-PS/Al_2O_3) nanocomposite films before exposed Ar plasma.

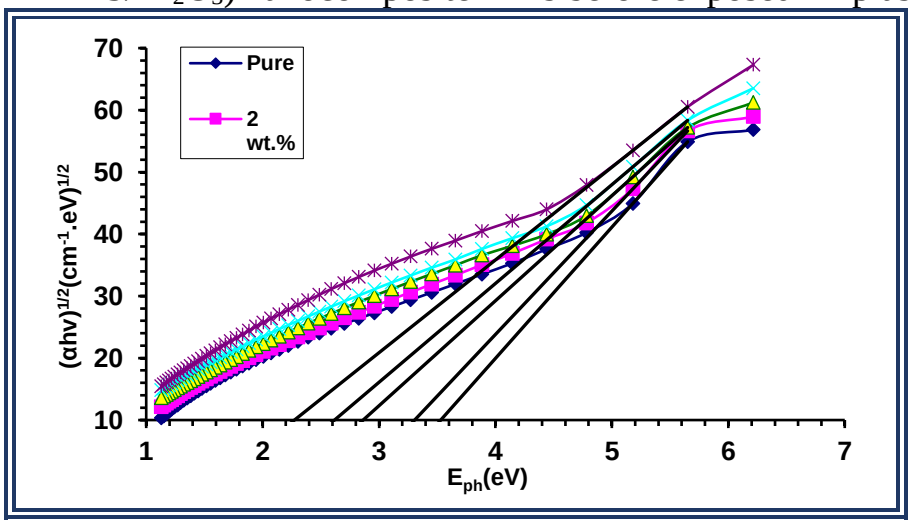

Figure (4.13): The Eg for the allowed indirect transition $(\alpha hv)^{1/2}$ $(cm^{-1}.eV)^{1/2}$ of (PMMA-PS/Al_2O_3) nanocomposite films after exposed Ar plasma.

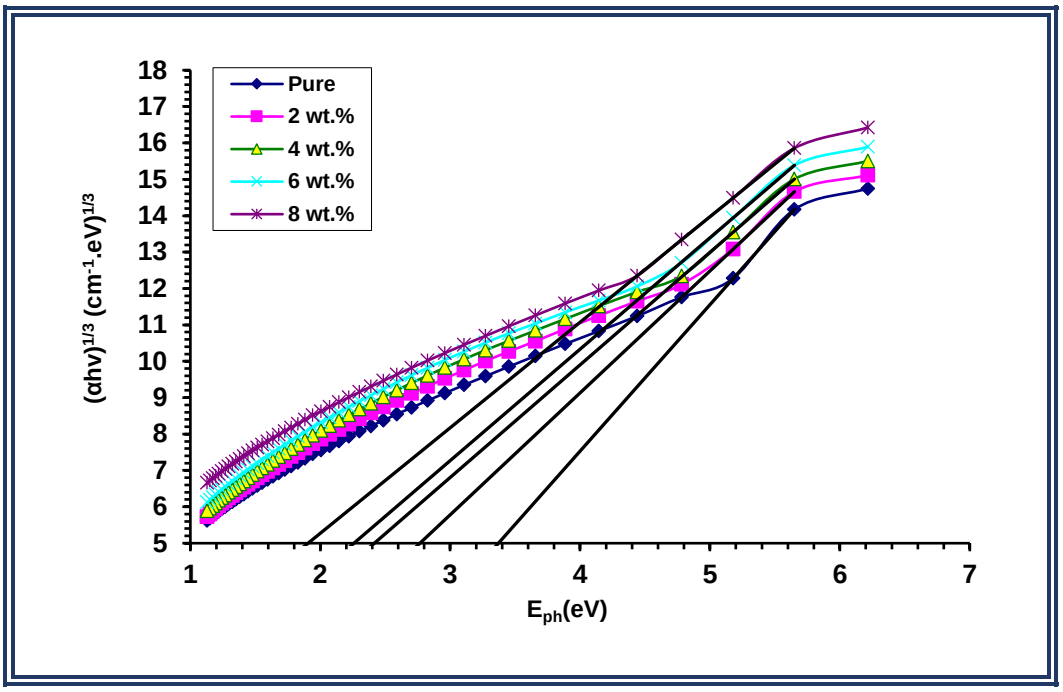

Figure (4.14): The E_g for the forbidden indirect transition $(\alpha h\nu)^{1/3}(cm^{-1}.eV)^{1/3}$ of (PMMA-PS/Al_2O_3) nanocomposite films before exposed Ar plasma.

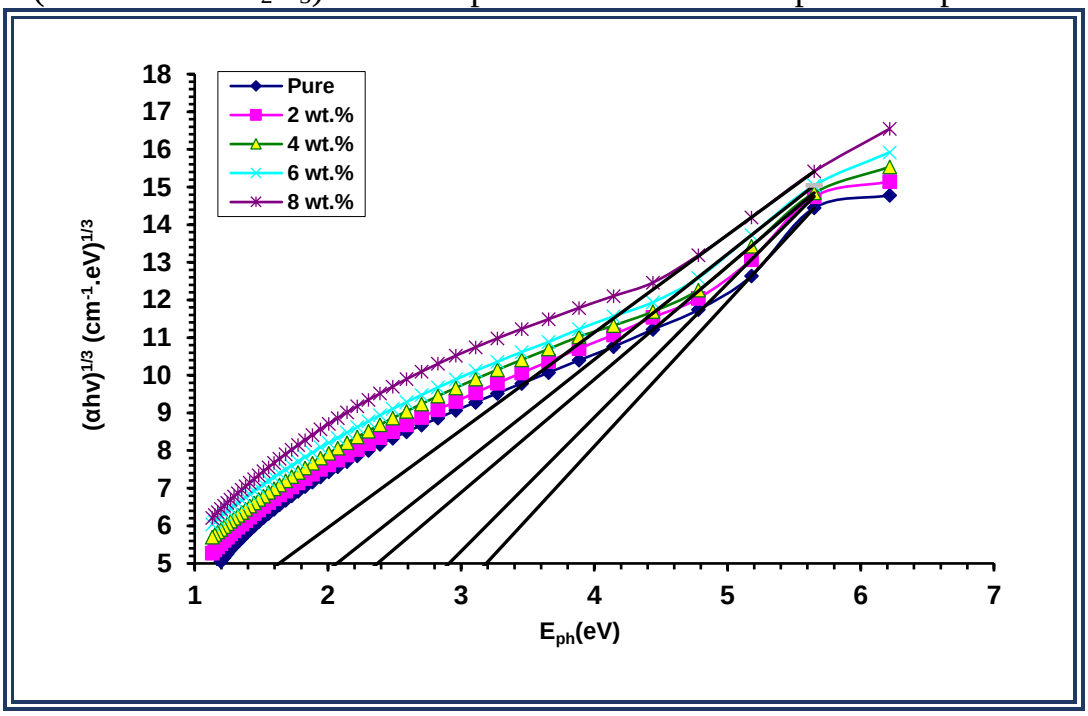

Figure (4.15). The E_g for the forbidden indirect transition $(\alpha h\nu)^{1/3}(cm^{-1}.eV)^{1/3}$ of (PMMA-PS/Al_2O_3) nanocomposite after exposed Ar plasma.

Table (4-1) The values of energy gap of(PMMA-PS/Al_2O_3)nanocomposites films befor exposed Ar plasma

Al_2O_3 NPs wt% content	Allowed of indirect energy gap (eV)	Forbidden of indirect energy gap (eV)
0	3.678	3.386
2	3.197	2.789
4	2.902	2.429
6	2.799	2.283
8	2.523	1.923

Table (4-2) The values gap of energy of (PMMA-PS/Al_2O_3) nanocomposites films after exposed Ar plasma

Al_2O_3 NPs wt% content	Allowed of indirect energy gap (eV)	Forbidden of indirect energy gap (eV)
0	3.535	3.206
2	3.312	2.936
4	2.873	2.396
6	2.629	2.092
8	2.293	1.664

4.3.5 The extinction coefficient

The extinction coefficient (K) was calculated (2-8). Figures (4.16) and (4.17) displays the extinction coefficient for (PMMA-PS/Al_2O_3) nanocomposites films with wavelength before and after exposed Ar plasma. It is important to note that extinction coefficient increased when Al_2O_3 NPs concentration increasing. This explanation relates to the increased the absorption coefficient with increasing Al_2O_3 NPs. Also from these figures, the extinction coefficient after irradiation has high values compared before irradiation in visible region, which attributed to the

increased charge carriers and the occurrence of some bonds breaking. The results are agreed with [72,73,76]

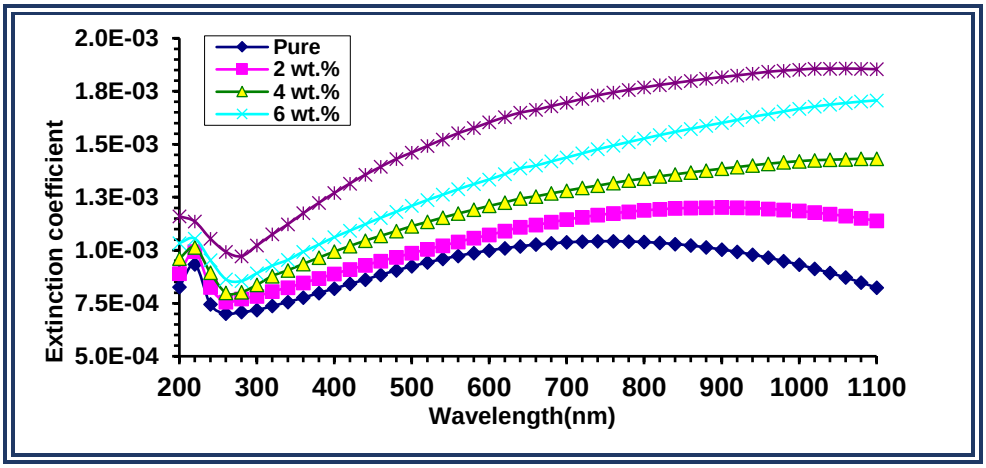

Figure (4.16). Extinction coefficient for (PMMA-PS/Al_2O_3) nanocomposites films before exposed Ar plasma.

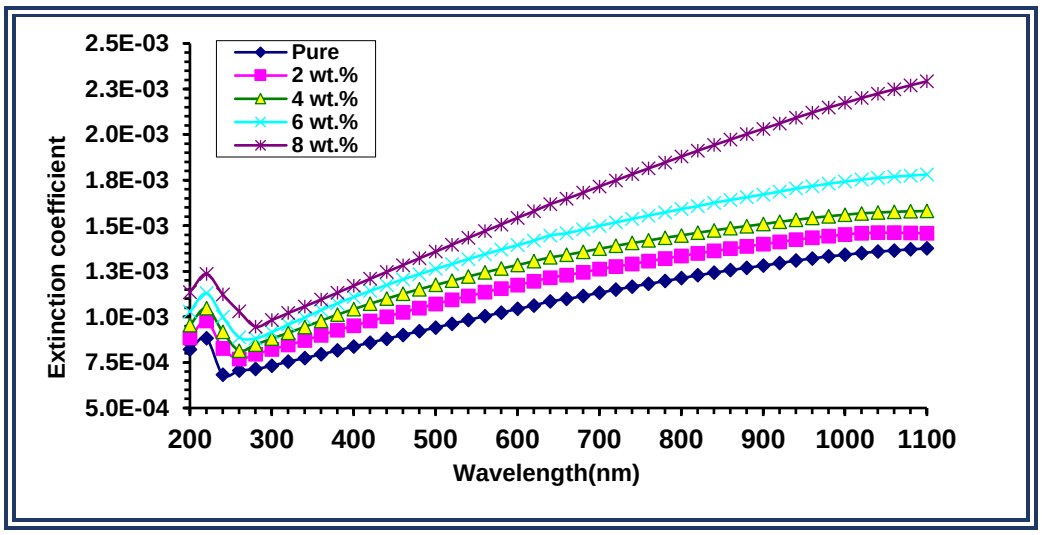

Figure (4.17). Extinction coefficient for (PMMA-PS/Al_2O_3) nanocomposites films after exposed Ar plasma.

4.3.6 The refractive index (n)

The refractive index (n) of (PMMA-PS/Al_2O_3) nanocomposites films was calculated from the equation (2-10). The refractive index of (PMMA-PS/Al_2O_3) nanocomposites films with wavelength as shown in figures (4.18) (4.19) before and after exposed Ar plasma. From these figures, the refractive index inclines to increase as the increasing concentration of Al_2O_3 NPs. The cause for this is that as the rise of Al_2O_3 content, the density of the nanocomposites rises as well. Also from these figures, the refractive index after irradiation has high values compared before irradiation in visible and near infrared region, which attributed to the increased charge carriers and the occurrence of some bonds breaking. This result are agree with researchers [73,74,77].

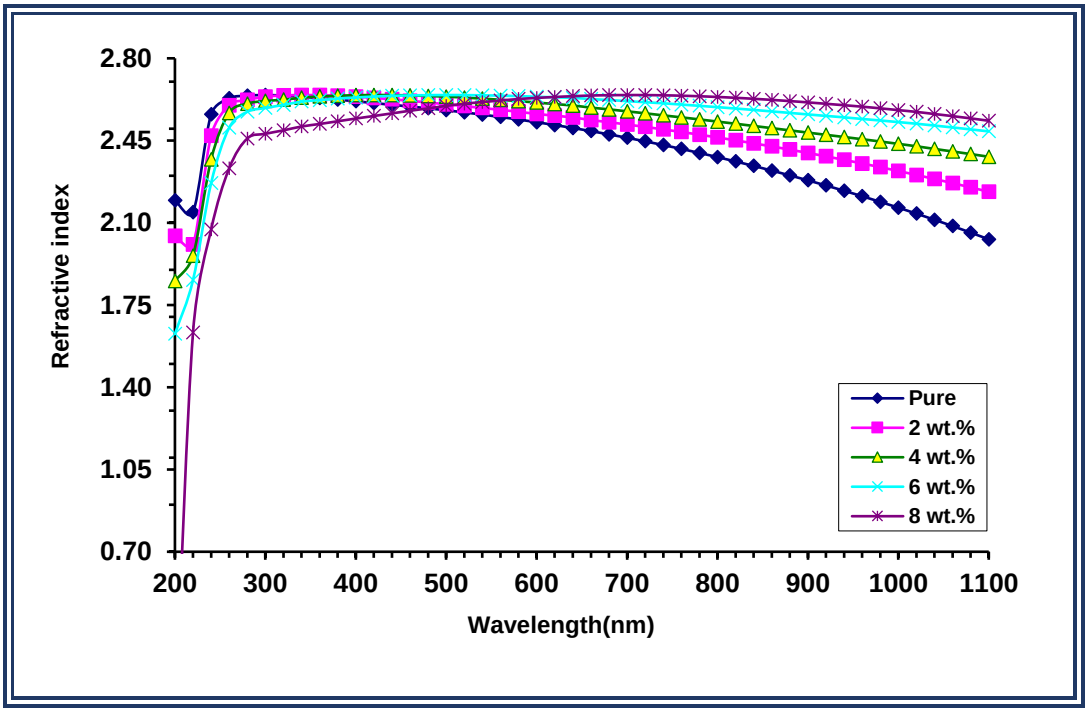

Figure (4.18) Refraction index of (PMMA-PS/Al_2O_3) nanocomposites films versus wavelength before exposed Ar plasma.

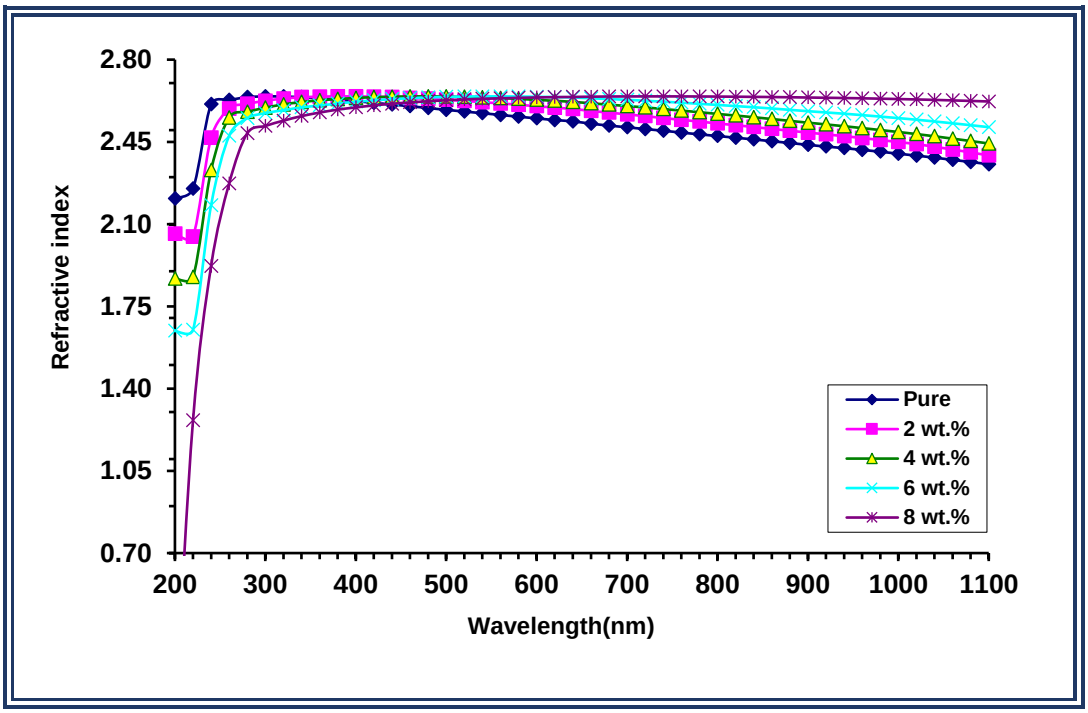

Figure (4.19) Refraction index of (PMMA-PS/Al_2O_3) nanocomposites films versus wavelength after exposed Ar plasma.

4.3.7 The real and imaginary dielectric constant (ε_1 and ε_2)

The real and imaginary (ε_1 and ε_2) components of the dielectric constant were calculated from the following equations (2-12) (2-13). The variation of ε_1 and ε_2 of (PMMA-PS/Al_2O_3) nanocomposites films with wavelength are explain in figures (4.20) (4.21) (4.22) (4.23) before and after exposed Ar plasma. From this figure, the real and imaginary of the dielectric constant of the (PMMA-PS/Al_2O_3) nanocomposite film are increased with the increasing of Al_2O_3 NPs content. The increase in electrical polarization related to the influence of nanoparticles content in the sample caused this finding [78]. The real and imaginary of the dielectric constant of nanocomposite change with wavelength. This is due to the ε_1 depends on refractive index since the outcome of extinction coefficient is minor, whereas the ε_2 depends on extinction coefficient. Also from these figures, the real and imaginary

after irradiation has high values compared before irradiation in visible and near infrared region, which attributed to the increased charge carriers and the occurrence of some bonds breaking. This result agrees with researchers [73,74,79].

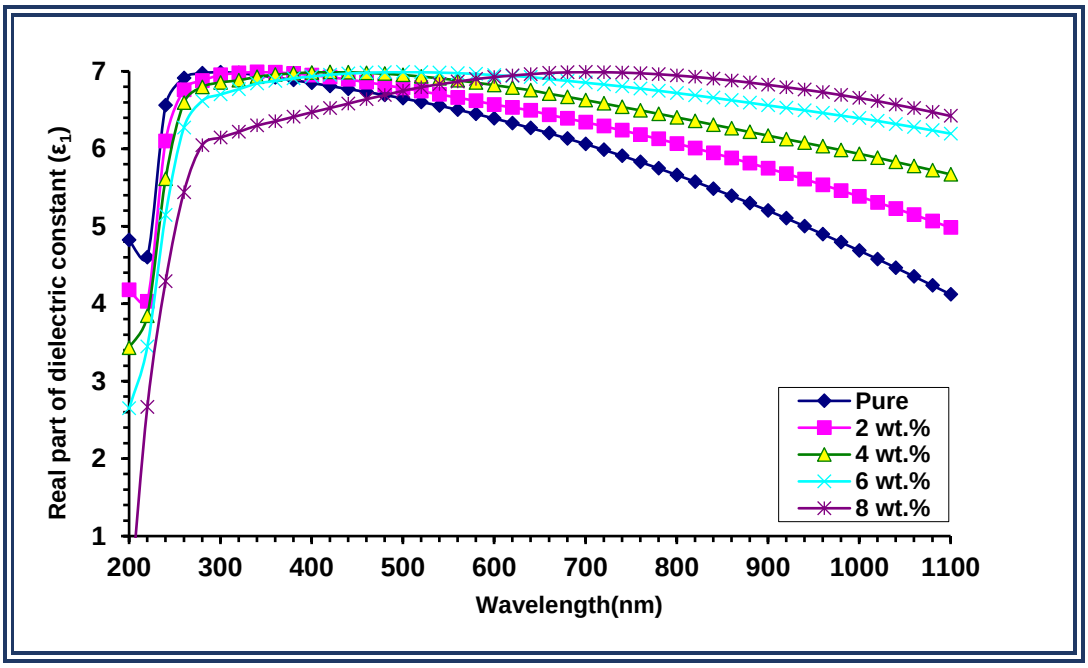

Figure (4.20) Variation of (ε_1) for PMMA-PS/Al_2O_3 nanocomposite films versus wavelength before exposed Ar plasma.

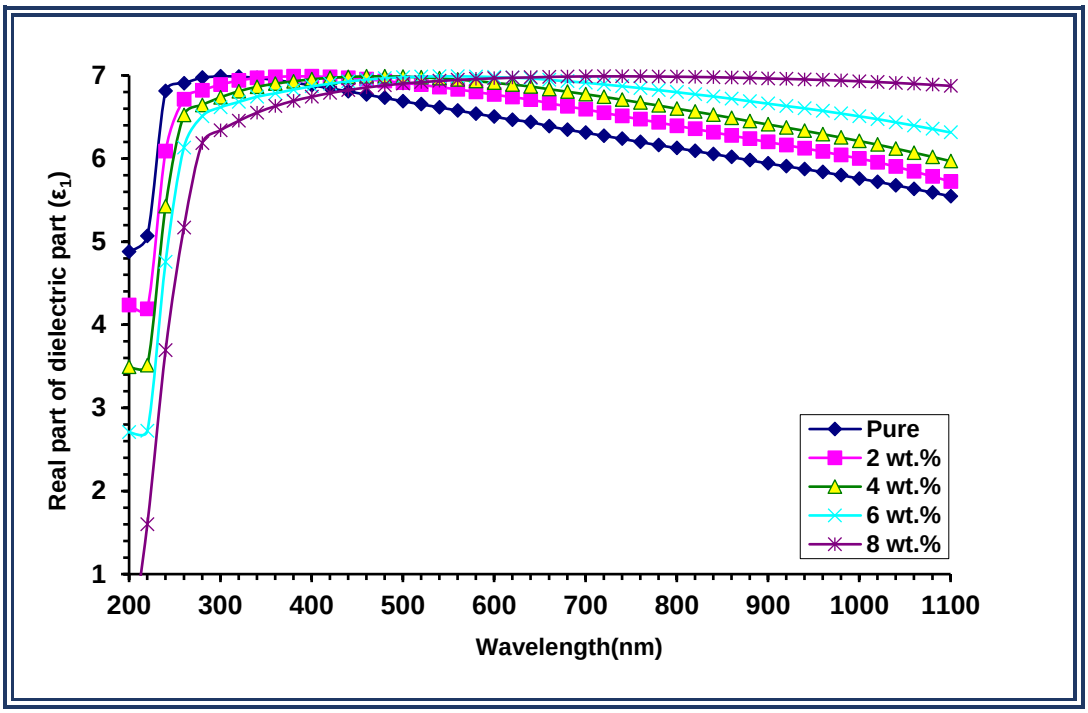

Figure (4.21) Variation of (ε_1) for PMMA-PS/Al_2O_3 nanocomposites films versus wavelength after exposed Ar plasma.

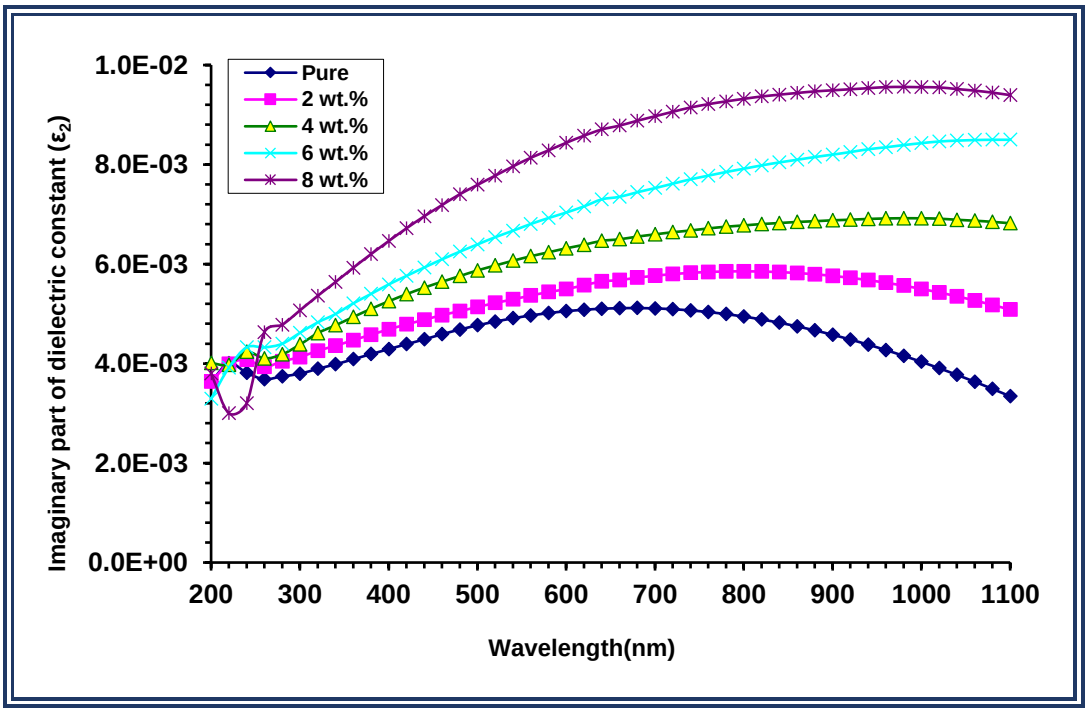

Figure (4.22) Variation of (ε_2) PMMA-PS/Al_2O_3 nanocomposite films versus wavelength before exposed Ar plasma.

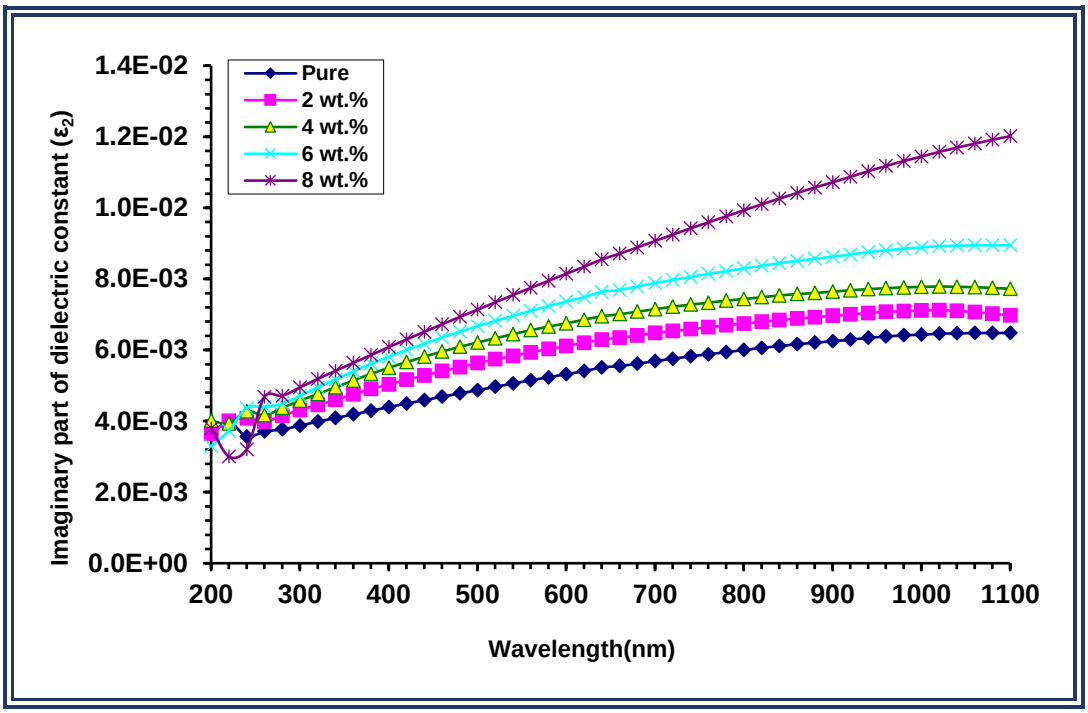

Figure (4.23) Variation of (ε_2) (PMMA-PS/Al_2O_3)nanocomposite films versus wavelength after exposed Ar plasma.

4.3.8 The optical conductivity ($\sigma_{op.}$)

The optical conductivity ($\sigma_{op.}$) was determined by the relation (2-14). Figures (4.24) (4.25) shows the optical conductivity of PMMA-PS/Al_2O_3 nanocomposites films with wavelength before and after exposed Ar plasma. The optical conductivity of the PMMa-PS/Al_2O_3 nanocomposite films increases as the Al_2O_3 content increases, which is related to the formation of local stages in the energy gap, rising nanoparticle content induced a rise in the density of local phases in the band structure therefore, a rise in the absorption coefficient suggests an increase in σ_{op} of the nanocomposites. Also from these figures, the optical conductivity after irradiation has high values compared before irradiation in UV region, which attributed to the increased charge carriers and the occurrence of some bonds breaking. The results are agreed with [73,74,80].

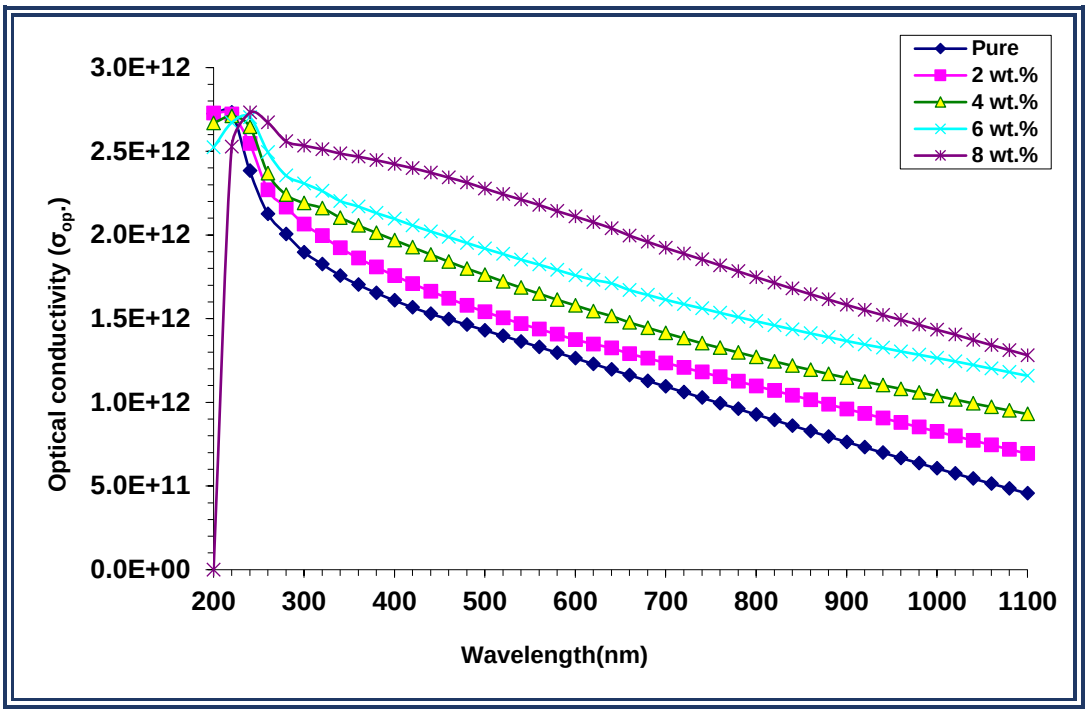

Figure (4.24) Variation of optical conductivity of (PMMA-PS/Al_2O_3) nanocomposite films versus wavelength.

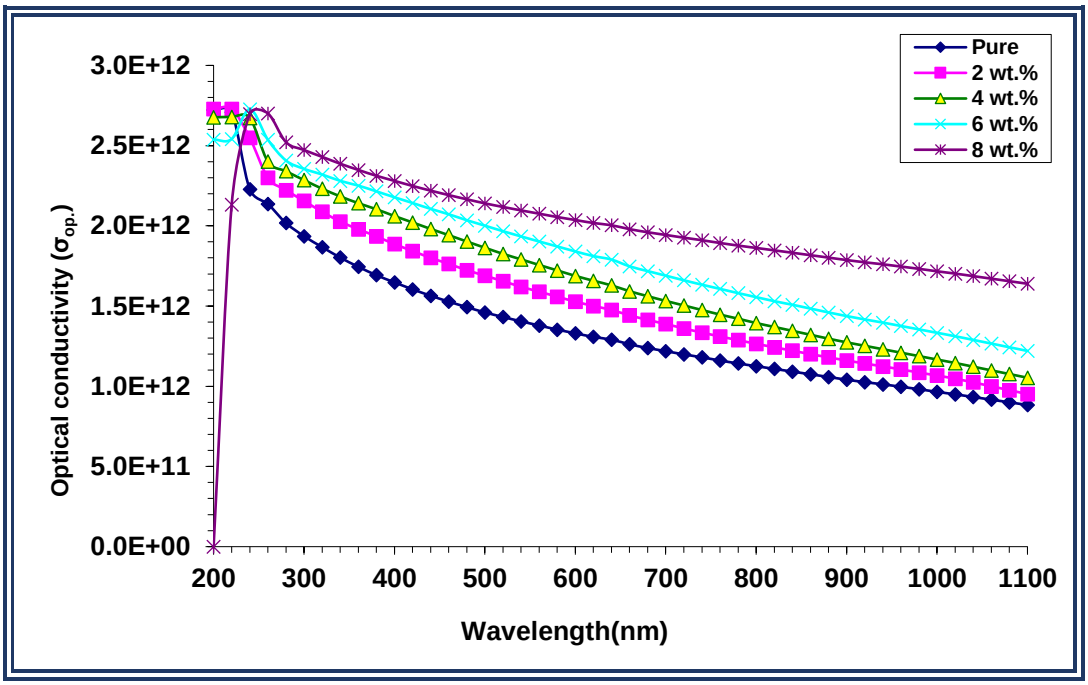

Figure (4.25) Variation of optical conductivity of (PMMA-PS/Al_2O_3) nanocomposite films versus wavelength after exposed Ar plasma.

4.4 The A.C Electrical Properties of (PMMA-PS/Al_2O_3) nanocomposites

The (PMMA-PS/Al_2O_3) nanocomposites films were investigated for their alternating current (A.C) electrical properties between 100Hz and 5MHz at room temperature. In order to identify the dielectric constant, that is the most essential of A.C characteristic, we used the equation (2-18). The dielectric loss can be calculated by the dielectric constant and (tanδ), using the equation (2-19), while A.C electrical conductivity (σ_{AC}) can be calculated by equation (2-20) by substituting the values of (ε'').

4.4.1 The dielectric constant for (PMMA-PS/Al_2O_3) nanocomposites films

The dielectric constant (έ) of (PMMA-PS/Al_2O_3) nanocomposites films with frequency before and after irradiation plasma are shown in figures (4.26) and (4.27). It is obvious that the dielectric constant decreases as the electric field frequency rises. This could be as a result of the samples' dipoles' propensity to align themselves with the directions of the applied electrical fields and with respect to total polarization, space charge polarization is decreasing. Space charge polarization is the most significant form of polarization at low frequencies, and as frequency rises, it becomes fewer significant, while the έ increasing with increasing concentration of Al_2O_3 NPs are shown in figures (4.28) and (4.29). Both an increase in the charge carriers of the (PMMA-PS/Al_2O_3) nanocomposites films and interfacial polarization within the nanocomposites in the applied field's alternating electric field might be used to explain these characteristics [81]. Also, it notes that the dielectric constant has high value after irradiation compare before irradiation which, may be due to interaction plasma with molecules which give more energy that effect on the dielectric constant of this nanocomposites. This result agrees with researcher [82].

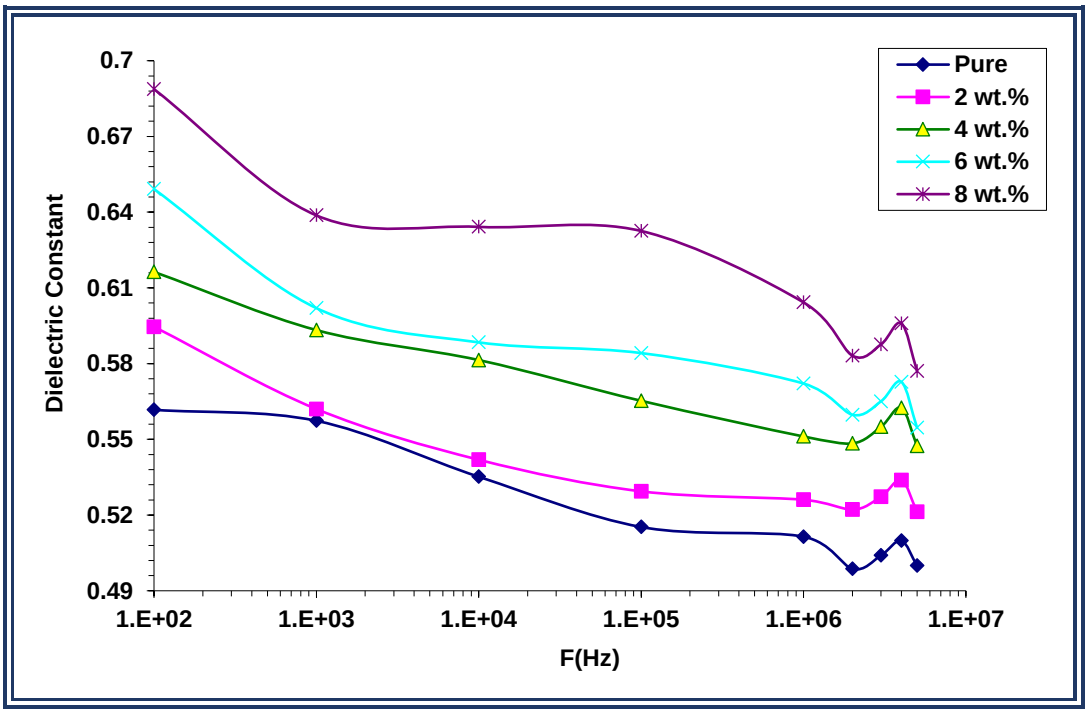

Figure (4.26): Variation of dielectric constant with the frequency of (PMMA-PS/Al_2O_3) nanocomposites films before exposed Ar plasma

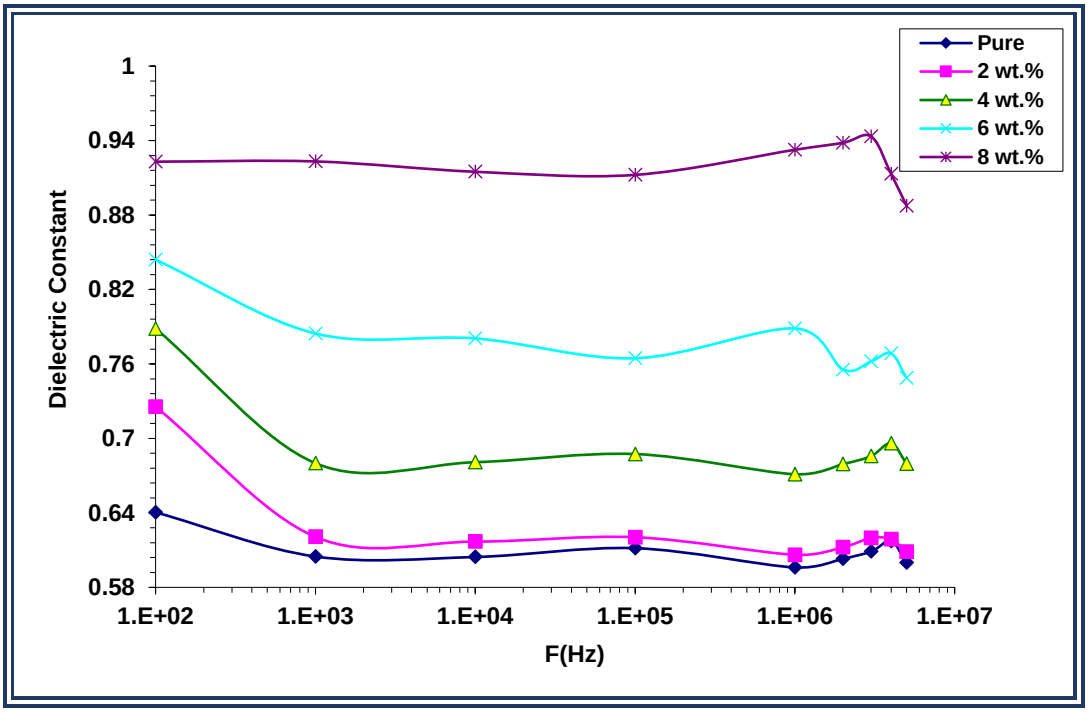

Figure (4.27): Variation of dielectric constant with the frequency of (PMMA-PS/Al_2O_3) nanocomposites films after exposed Ar plasma.

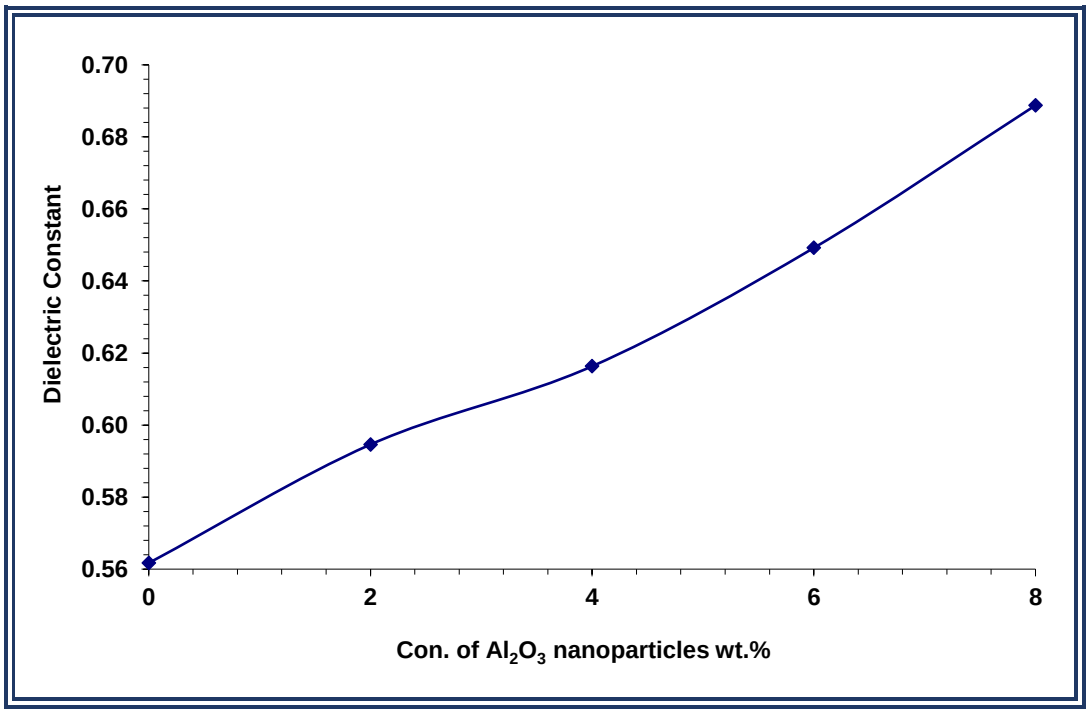

Figure (4.28): Influence of Al_2O_3 nanoparticles concentration on dielectric constant of (PMMA-PS/Al_2O_3) nanocomposites films before irradiation Ar plasma at 100 Hz.

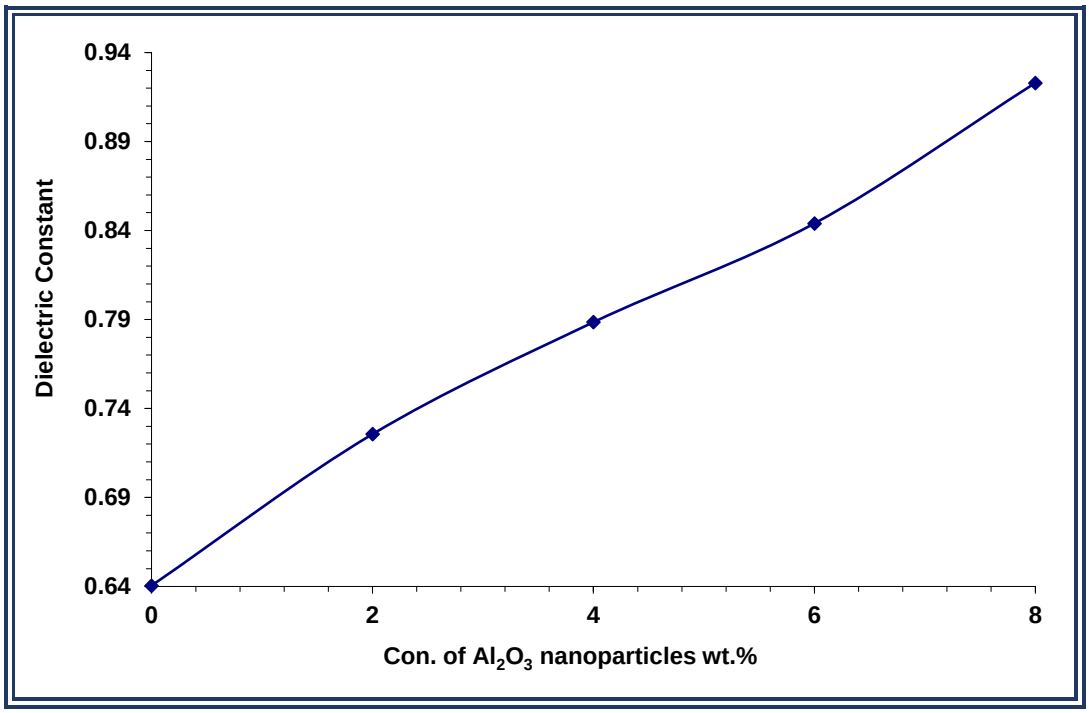

Figure (4.29): Influence of Al_2O_3 nanoparticles concentration on dielectric constant of (PMMA-PS/Al_2O_3) nanocomposites films after irradiation Ar plasma at 100 Hz.

4.4.2 The dielectric loss for (PMMA-PS/Al_2O_3) nanocomposites films

The variation of dielectric loss (ε″) (PMMA-PS/Al_2O_3) with electric field frequency before and after irradiation plasma are shown in figures (4.30)(4.31). The ε″ decreases with increasing frequency. This is due to a decline in the contribution of space charge polarization. With rise content of Al_2O_3 NPs, the ε″ of (PMMA-PS/Al_2O_3) nanocomposites films rises before and after irradiation plasma are explain in figures (4.32)(4.33), which ascribed to the rise of the number of charge carriers. At small contented of NPs, it creates as a cluster and at high contented reach to 8%, its formation a network inside the nanocomposites [83]. Also, it can be noted that the dielectric loss has value larger after irradiation plasma compared before irradiation plasma, which attributed to that the plasma give energy to this molecule that effect to the dielectric loss of this nanocomposites. This result is deal with scientists [84].

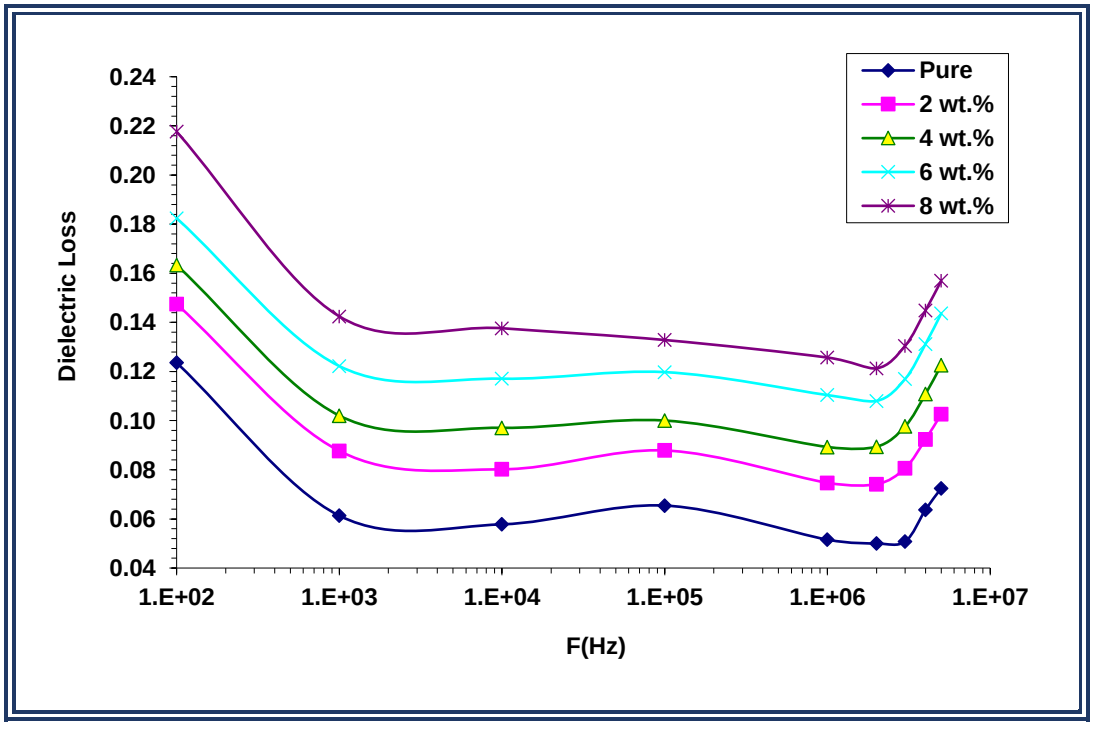

Figure (4.30): Variation of dielectric loss with the frequency of (PMMA-PS/Al_2O_3) nanocomposites films before exposed Ar plasma.

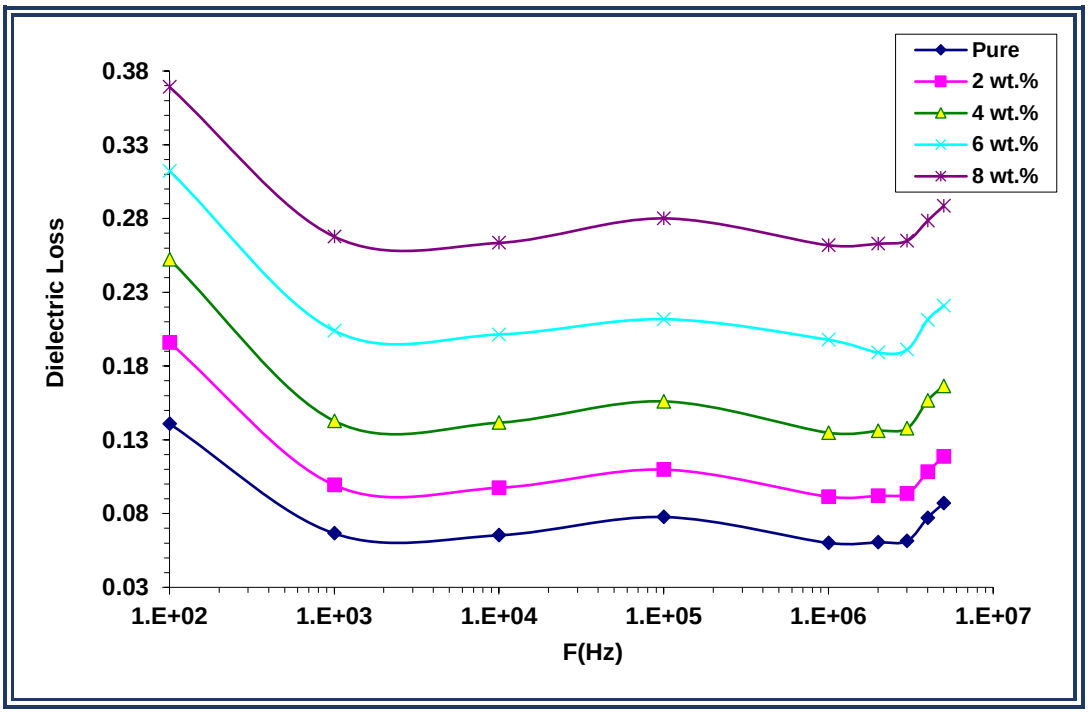

Figure (4.31): Variation of dielectric loss with the frequency of (PMMA-PS/Al_2O_3) nanocomposites films after exposed Ar plasma.

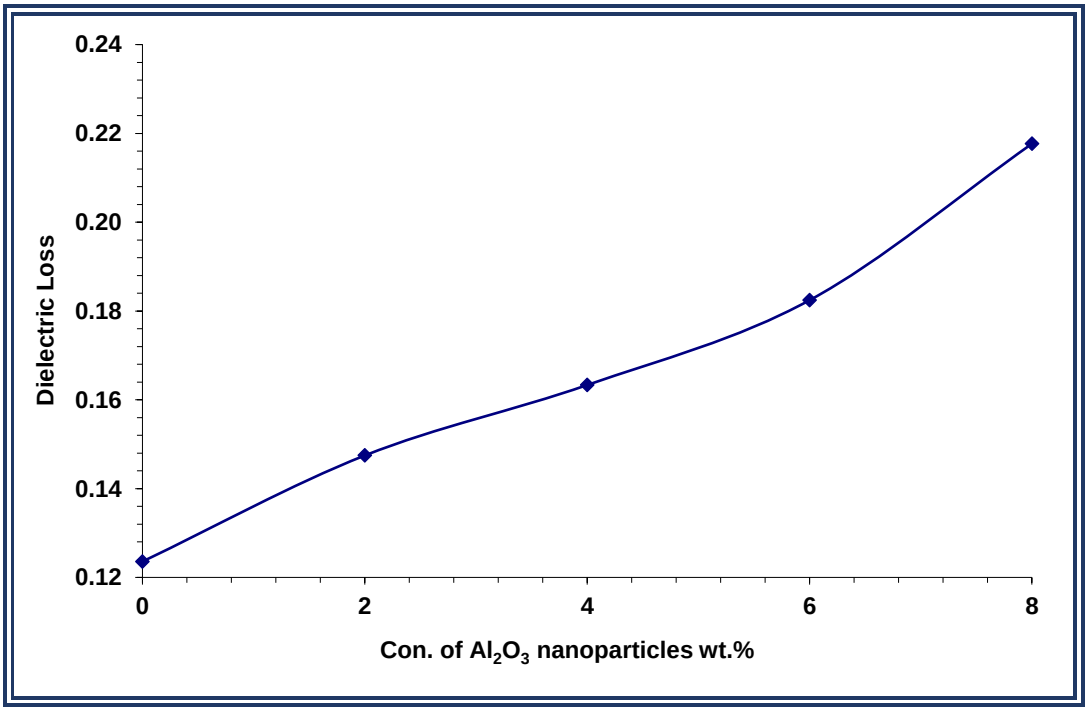

Figure (4.32): Influence of Al_2O_3 nanoparticles concentration on dielectric loss of (PMMA-PS/Al_2O_3) nanocomposites films before irradiation Ar plasma at 100 Hz.

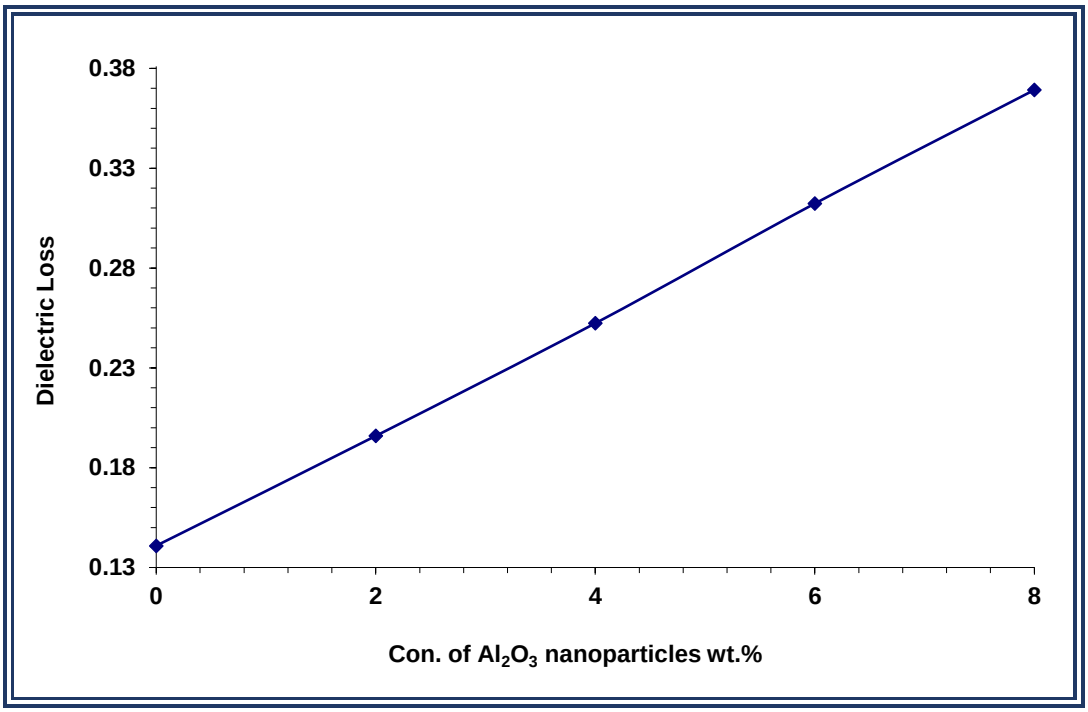

Figure (4.33): Influence of Al_2O_3 nanoparticles concentration on dielectric loss of (PMMA-PS/Al_2O_3) nanocomposites films after irradiation Ar plasma at 100 Hz.

4.4.3 The A.C electrical conductivity for (PMMA-PS/Al_2O_3) nanocomposites films.

The variation of A.C electrical conductivity with electric field frequency for (PMMA-PS/Al_2O_3) nanocomposites films before and after irradiation plasma are shown in figures (4.34) (4.35). The A.C electrical conductivity increased with increasing electric field frequency for all samples. This results from both the hopping motion of charge carriers and space charge polarization, which takes place at low frequencies [85]. Also, the figures (4.36) and (4.37) demonstrate how the conductivity rises with a rise in the weight percentage of Al_2O_3 NPs in the plasma before and after irradiation Ar plasma. Because of the regular arrangement of charge carriers in the polymer matrix and the action of the space charge, this phenomenon

is caused. Also, it should be noted that the A.C conductivity increased after plasma irradiation compared to before plasma irradiation, indicating that the plasma had an impact on the conductivity of these nanocomposites. This is agree with the researchers [86].

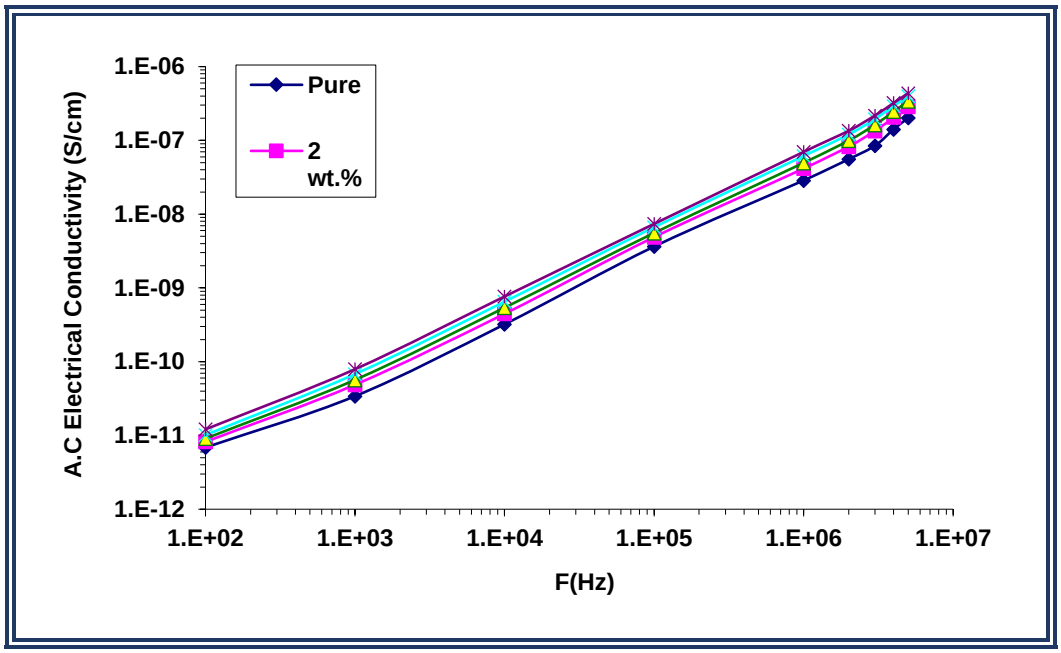

Figure (4.34): Variation of AC electrical conductivity with the frequency of (PMMA-PS/Al_2O_3) nanocomposites films before exposed Ar plasma.

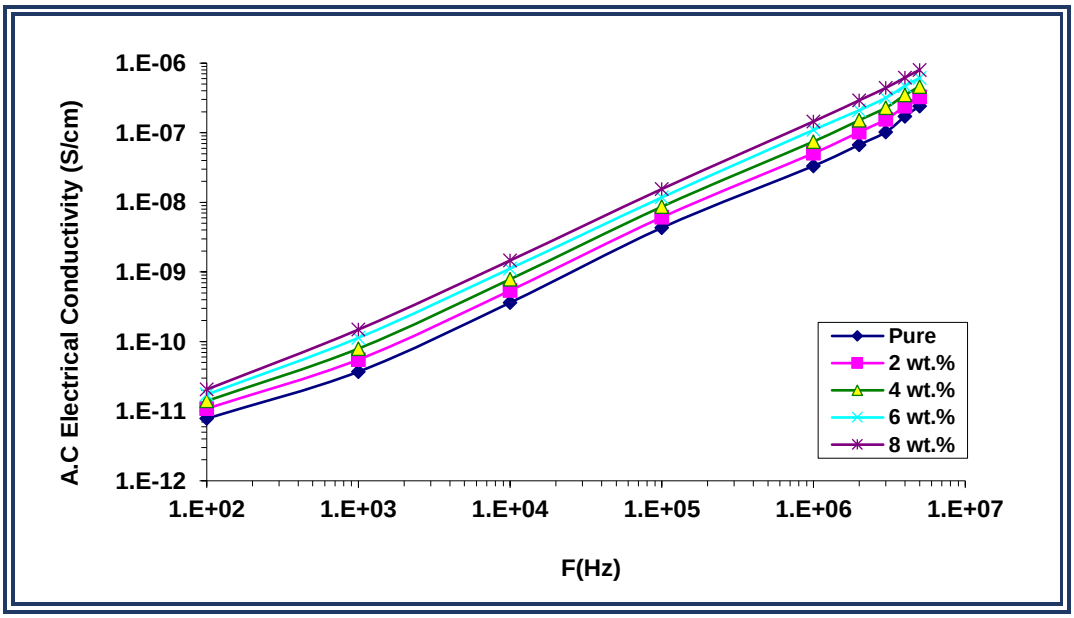

Figure (4.35): Variation of AC electrical conductivity with the frequency of (PMMA-PS/Al_2O_3) nanocomposites films after exposed Ar plasma.

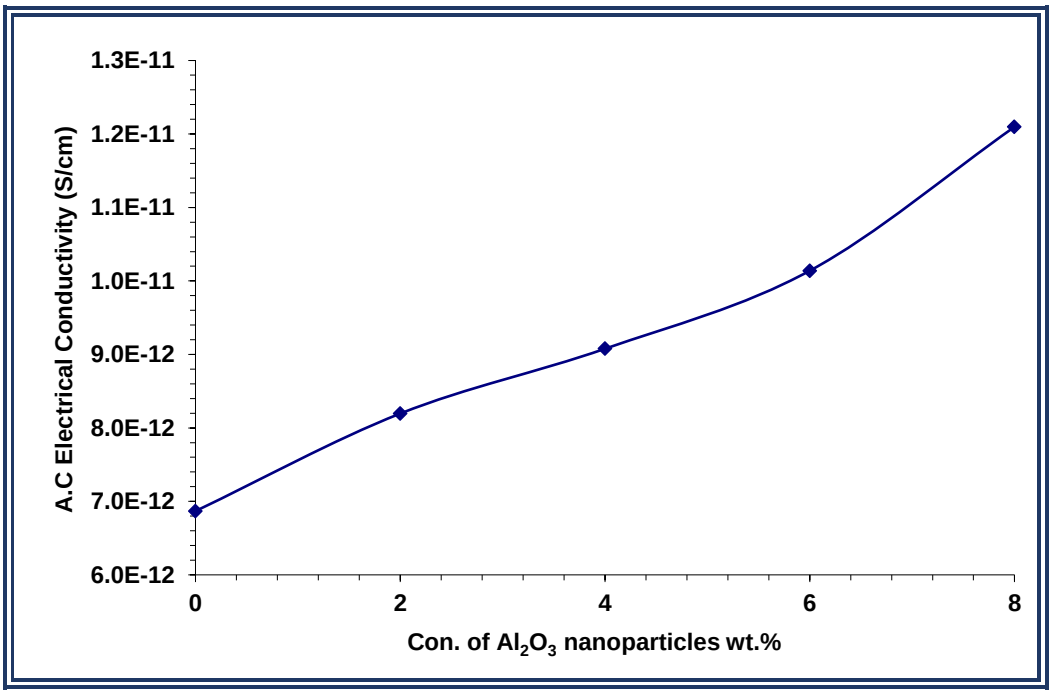

Figure (4.36): Influence of Al_2O_3 nanoparticles concentration on AC electrical conductivity of (PMMA-PS/Al_2O_3) nanocomposites films before irradiation Ar plasma at 100 Hz.

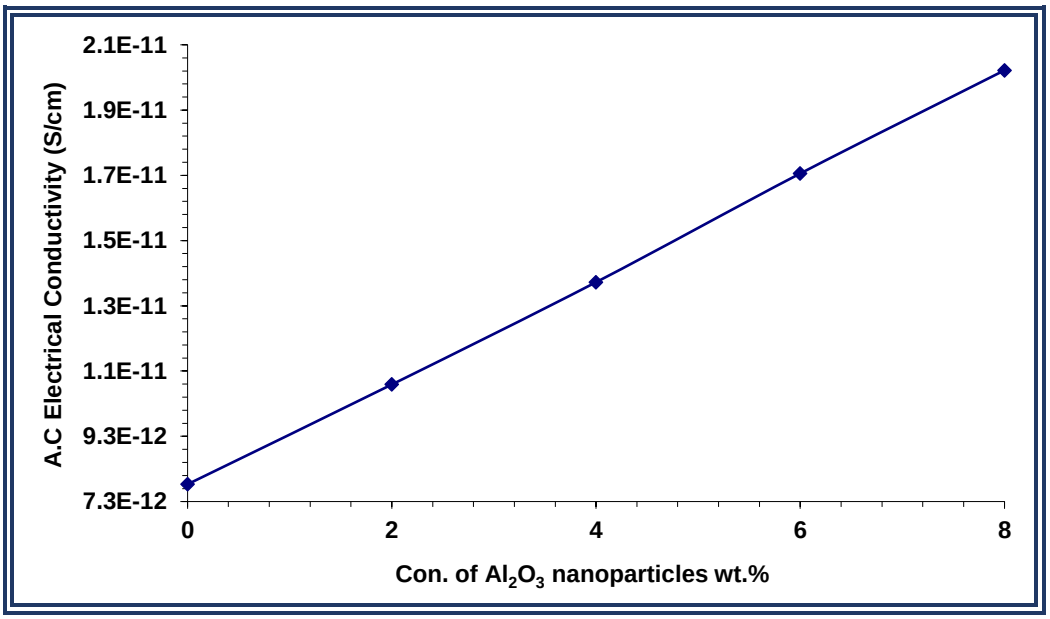

Figure (4.37): Influence of Al_2O_3 nanoparticles concentration on AC electrical conductivity of (PMMA-PS/Al_2O_3) nanocomposites films after irradiation Ar plasma at 100 Hz.

4.5 Application of (PMMA-PS/Al_2O_3) nanocomposites films for antibacterial activity.

Figure (4.38) shows the inhibition zone for PMMA-PS/Al_2O_3 nanocomposites films was greater in Gram-positive (Staphylococcus aureus) compounds than in Gram-negative (Escherichia coli). The width of the inhibition zone rises with increasing Al_2O_3 concentration and reaches its maxim μ_m value (21mm) for Gram-negative (S. aureus) compounds with the greatest Al_2O_3 content (8 wt.%) are shown in Figures (4.39) and (4.40). This result suggests that nanocomposite films suppress the development of Escherichia coli and Staphylococcus aureus [87]. Oxidative stress caused by reactive oxygen species (ROS) may be the primary mechanism behind the antibacterial activity of nanoparticle-based nanocomposites films. ROS contains radicals such as super oxide radicals (O^{-2}), hydroxyl radicals (-OH), and hydrogen peroxide (H_2O_2); and vest oxygen may be responsible for causing damage to the bacteria's proteins and DNA ($^1O_2$). The current (PMMA-PS/Al_2O_3) nanocomposites films exhibit the greatest antibacterial action against Suphylococcus aureus and Escherichia coli, which is attributed to the high antibacterial activity of Al_2O_3 nanoparticles [88].

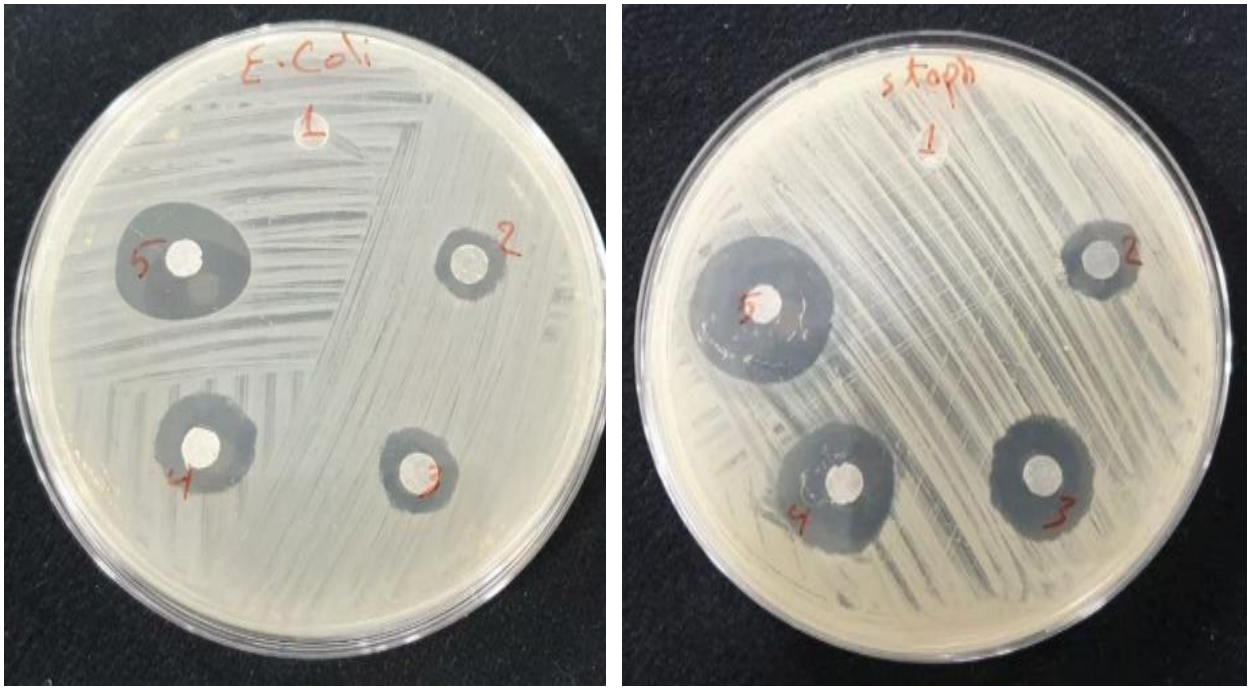

Figure (4.38): Images for inhibition zones of (PMMA-PS/Al_2O_3) nanocomposite films on S.aureus and E. coli.

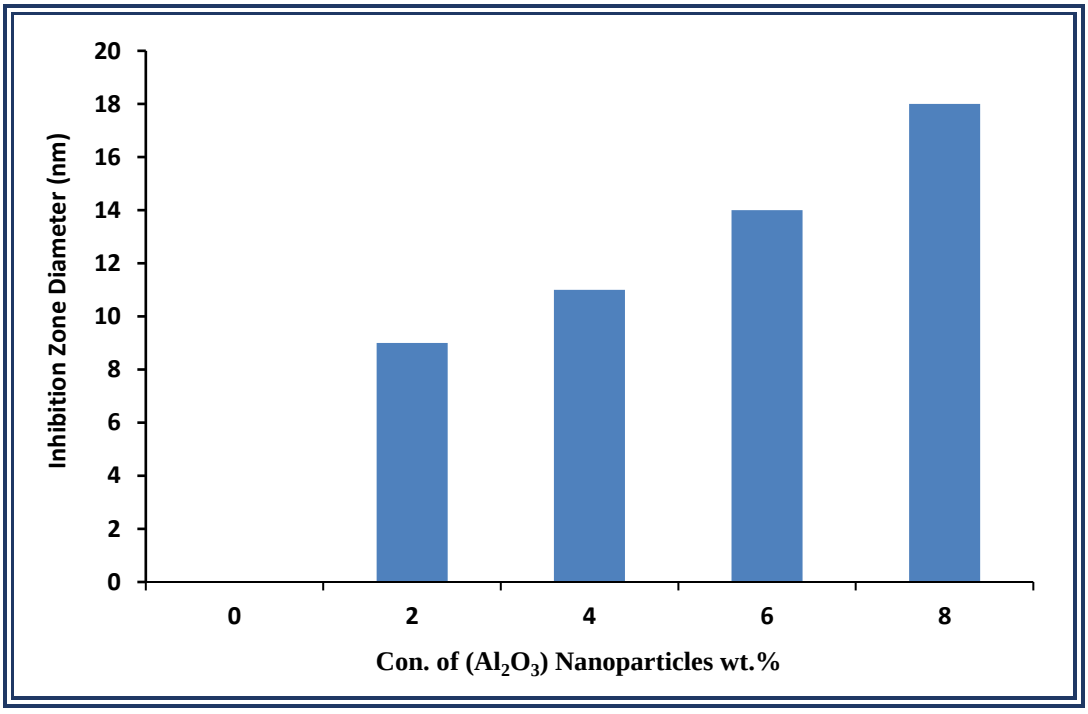

Figure (4.39): Variation of inhibition zone diameter for (PMMA-PS/Al_2O_3) nanocomposite films for E. coli with concentration of (Al_2O_3) nanoparticles

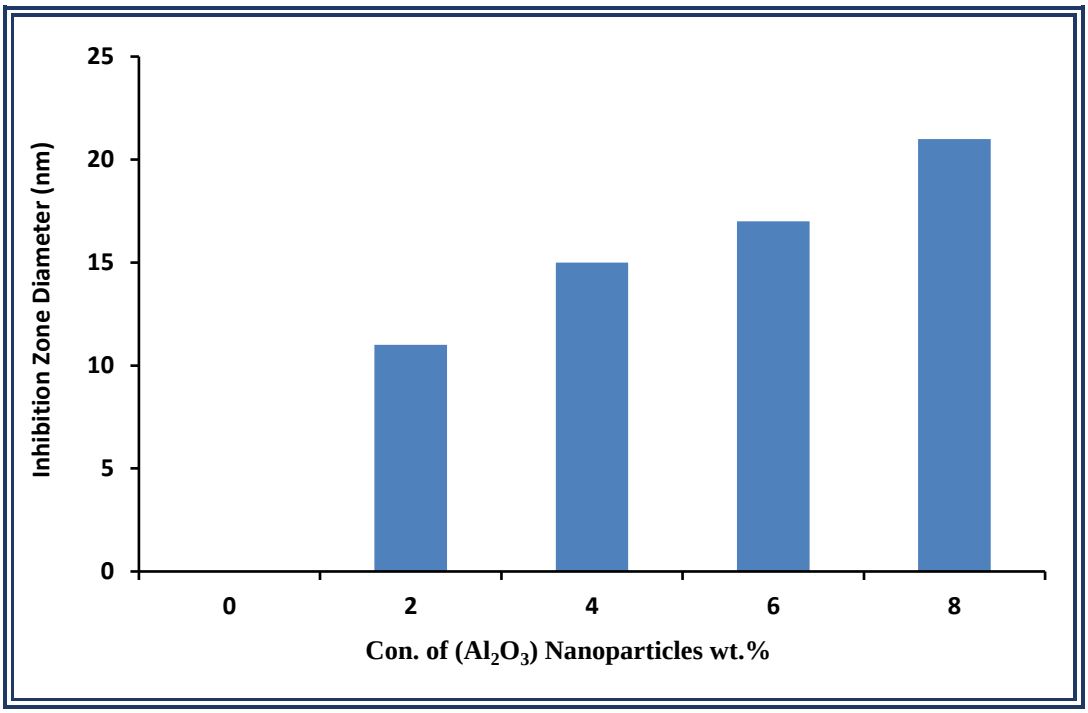

Figure (4.40). Variation inhibition zone diameter of (PMMA-PS/Al_2O_3) nanocomposites films for S. aureus with concentration of (Al_2O_3) nanoparticles.

4.6 Conclusions

From the obtained results and discussions, the following points are concluded:

1- The optical microscope images show that Al_2O_3 nanoparticles form a continuous network inside the polymers when the ratio of (8) wt.% before and after exposed Ar plasma. FTIR spectra show a shift in some bands and change in the intensities of other bands comparing with pure (PMMA-PS) films, this indicates there is no interaction between the polymers and the added nanoparticles. FESEM measurements reveal the surface morphology of the (PMMA-PS/Al_2O_3) nanocomposites films, which are homogeneous and coherent with aggregates or chunks scattered at random on the top surface. The variation in the morphology before exposed Ar plasma is the outcome of the impression progression encouraged by argon plasma species on the (PMMA-PS) surface.

2- The absorbance, absorption coefficient, refractive index, extinction coefficient, dielectric constant (real, imaginary) and optical conductivity of (PMMA-PS/Al_2O_3) nanocomposites films before and after exposed Ar plasma increased with the increasing of the concentrations of the Al_2O_3 nanoparticles. The transmittance and the energy gap for indirect transition (allowed, forbidden) decreased with the increasing of the concentrations of Al_2O_3 nanoparticles. This result can be used for optoelectronic device.

3- The dielectric constant and dielectric loss for (PMMA-PS/Al_2O_3) nanocomposites films are increased with the increasing of Al_2O_3 nanoparticles concentration and decreasing with the increase of frequency of the applied electric field while the A.C electrical conductivity increased with the increasing of nanoparticles concentration and frequency of the applied electric field before and after exposed Ar plasma. The dielectric constant, dielectric loss and A.C

electrical conductivity after irradiation have high values compared before irradiation which attributed to the plasma interact with the molecular of these nanocomposites. This result can be used for electronic device such as transistors.

4- The inhibition zone diameter increases with the increase in (Al_2O_3) nanoparticles concentrations. These materials can be used as antibacterial coating materials

4.7 Future works

1- Studying the thermal and magnetic properties of (PMMA-PS/Al_2O_3) nanocomposites films.

2- Studying the effect of radiation on some physical properties of (PMMA-PS/Al_2O_3) nanocomposites films.

3- Apply of (PMMA-PS/Al_2O_3) nanocomposites films as photodetector and gas sensor.

References

References

[1] G. Cao, "Nanostructures and Nanomaterials, Synthesis, Properties and Applications", Imperial College Press, (2004).

[2] A.T. Bell, "The Impact of Nanoscience on Heterogeneous Catalysis" Sci, Vol.299, pp.1688-1691, (2003).

[3] K. A. Shenoy, "Effects Of Multi-Wall Carbon Nanotubes On The Mechanical Properties Of Polymeric Nanocomposites", M.Sc. Thesis, Department of Mechanical Engineering and the faculty of the Graduate School of Wichita State University, (2008).

[4] G. Aziz, D. N. Geyter and R. Morent, R.,"Incorporation of primary amines via plasma technology on biomaterials" Advances in bioengineering, pp.21-48, (2015).

[5] A. Felten, C. Bittencourt, J. Pireaux, G. L. Van, J. C. Charlier, "Radio-frequency plasma functionalization of carbon nanotubes surface O2, NH3, and CF4 treatments" Journal of applied physics, Vol. 98, No. 7, p.074308, (2005).

[6] H. Conrads, M. Schmidt, "Plasma generation and plasma sources. Plasma sources" Science and Technology, Vol.9, No.4, pp.441-454, (2000).

[7] J. Furer "Growth of Single-Wall Carbon Nanotubes by Chemical Vapor Deposition for Electrical Devices" Ph.D thesis, Basel University (2006).

[8] Z. Miao, D. Xu, J. Ouyang, G. Guo, X. Zhao and Y. Tang. "Electrochemically induced sol–gel preparation of single-crystalline TiO_2 nanowires", Nano Lett. Vol.2, No.7, pp. 717–20, (2002).

[9] G. Mor, O. Varghese and M. Paulose "A review on highly ordered, vertically oriented TiO_2 nanotube arrays: Fabrication, material properties, and solar energy applications" J. Sol. Energy Mater. Sol. Cells, Vol. 90, pp.2011–2075, (2006).

[10] P. Avouris, B. Bhushan, K. V. Klitzing, H. SAkaki and R. Wiesendanger. "Nanosciencs and Technology" .Verlage Barlin Heidelberg, (2005).

[11] S. Mustafa ,"Engineering Chemistry", Library of Arab society for pub. and dis., Jordan, (2008).

[12] T. Beraada , G. al- Adam, " The Updated Chemistry of Large Molecules", University of Basrah , College of Sci., (1989).

[13] A. Muheisin, "Study of Electrical Conductivity for Amorphous and Semi crystalline Polymers Filled with Lithium Fluoride Additive", M.Sc. Thesis, University of Mustansiriah ,College of Sci.(2009).

[14] R. M. Paroli , K. lin , T. R. Simmons "Archived- thermoplastic polyolefin roofing membranes" National Ressarch council of Canada", Vol. 30, pp. 1206-1220, (1999).

[15] A. Mohammed, " Chemistry of Plastics", University of Mousl, (1993).

[16] G. Akovali , "Hand Book of Composites Fabrication" , Ankara , (2001).

[17] G. Al - Adam and H. Ali , "Technology and Polymer Chemistry", University of Basrah, College of Sci., (1983).

[18] C. Uzunpinar, "Effect of Dispersion of Swcntson the Viscoelastic and Final Properties ofEpoxy Based Nanocomposites", M. Sc. Thesis,Graduate Faculty of Auburn University, (2010).

[19] J. Robertson, "Realistic applications of CNTs", Materials Today, Vol.7, pp.46-52, (2004).

[20] L. Bokobza, "Multiwall carbon nanotube elastomeric composites: a review",Poly, Vol.48, pp. 4907-4920, (2007).

[21] S. Belkoff, J. Mathis, L. Jasper and H. Deramond, "The biomechanics of vertebroplasty. "The effect of cement volume on mechanical behavior" , Spine (Phila Pa 1976), Vol. 26, No.14, pp.1537–1541, (2001).

[22] H. Kaczmarek and H. Chaberska, " Effects of Oxygen RF Plasma on Properties of Poly Methyl Methacrylate Polymer ", Appl. Surf. Sci., Vol. 252, p. 8185, (2006).

[23] A. Tawansi and H. M. Zidan, " Influence of $AlCl_3$ on the optical properties of new synthesized 3-armed poly(methyl methacrylate) films", Int. J. Polym, Vol. 15, pp.77-83, (1991).

[24] S. Nandi, P. Mukherjee, R. Subbasis, B. Kundu, D. Kumar and D. Basu, "Local antibiotic delivery systems for the treatment of osteomyelitis: A review", Mater Sci. Eng. C, Vol. 29, No. 24, pp. 78–85, (2009).

[25] F. W. J. Billmeyer,"Textbook of Polymer Science". John Wiley and Sons, New York

[26] J. Scheirs, D. Priddy "Modern Styrenic Polymers: Polystyrenes and Styrenic Copolymers" John Wiley and Sons, (2003).

[27] M. Mihai, M. A. Huneault, and B. D. Favis, Foaming of polystyrene/thermoplastic starch blends, Journal of cellular plastics, Vol. 43, No.3, pp. 215-236, (2007).

[28] K. A. Evans, "Properties and uses of aluminium oxides and aluminium hydroxides". In Downs, A. J. (ed.). The Chemistry of Aluminium, Indium and Gallium. Blackie Academic. ISBN 978-0751401035, (1993).

[29] L. Hudson, K. Misra, C. Perrotta, J. Anthony, W. Karl and F. S. Williams, "Aluminum Oxide" in Ullmann's Encyclopedia of Industrial Chemistry, Wiley-VCH, Weinheim.

[30] C. Mandolfino, E. Lertora, C. Gambaro, "Effect of cold plasma treatment on surface roughness and bonding strength of polymeric substrates,"Key engineering materials", Vol. 611, pp. 1484-1493, (2014).

[31] L. M. Wallenhorst, S. Dahle, M. Vovk, L. Wurlitzer, L. Loewenthal, , N. Mainusch and W. Viöl,"Characterisation of PMMA/ATH layers realised by means of atmospheric pressure plasma powder deposition", Advances in Condensed Matter Physics, (2015).

[32] A. M. Shehap, and D. S.Akil," Structural and optical properties of TiO2 nanoparticles/PVA for different composites thin films, . Nanoelectronics and Materials, Vol.9, No. 1, pp. 17-36, (2016).

[33] R. G. Kadhim, M. A. Habeeb and Q. M. Jebur, "Dielectric and optical properties for (Poly vinyl alcohol-Carboxymethyl Cellulose –Copper Oxide) Nanocomposites and their Applications", Journal of Chemical and Pharmaceutical Sciences, Vol.10, (2017).

[34] M. Vovk, L. Wallenhorst, C. Kaldun, J. N. Meuthen, A. L. Arendt, M. Sernek, and S. Dahle, S., "Air plasma treatment of aluminium trihydrate filled poly (methyl methacrylate)", Journal of adhesion science and Technology, Vol. 32, No. 12, pp.1369-1391, (2018).

[35] N. M. El-Sayed, "Optical and electrical properties of plasma surface treated polymethylmethacrylate films. Arab" Journal of Nuclear Sciences and Applications, Vol. 52, No. 4, pp. 83-92, (2019).

[36] Y. Al-Mahweet, "Physicochemical properties of prepared ZnO/polystyrene nanocomposites: structure, mechanical and optical", Journal of Ovonic Research, Vol, 16, No. 1, pp. 71-81, (2020).

[37] J. Meza-Arroyo, M. S. Rao and K. C. S. Reddy, A. Sánchez-Martinez, O. Rodríguez-López, M. Quevedo-López and R. Ramírez-Bon, "Ultra-dry air plasma treatment for enhancing the dielectric properties of Al2O3-GPTMS-PMMA hybrid dielectric gate layers in a-IGZO TFT applications" Nanotechnology, Vol. 32, No.13, p. 135203. (2021).

[38] Q. A. Alsulami, and A. Rajeh, "Structural, thermal, optical characterizations of polyaniline/polymethyl methacrylate composite doped by titanium dioxide

nanoparticles as an application in optoelectronic devices" Optical Materials, Vol. 23, (2022).

[39] A. Hashim, M. H. Abbas, N. A. Al-Aaraji, and A. Hadi, A. "Controlling the morphological, optical and dielectric characteristics of PS/SiC/CeO_2 nanostructures for nanoelectronics and optics fields" Journal of Inorganic and Organometallic Polymers and Materials, Vol. 33, No. 1, pp. 1-9, (2023).

[40] K. Mathes and J. I. Kroschwitz, "Electrical and Electronic Properties of Polymers: A State-of-the-Art Compendum." NY: John Wiley & Sons, Inc, (1988).

[41] J. Pattar, H.Singh, T. Singh, J. Sharma, "Structural optical and electrical properties of vacuum evaporated indium doped zinc telluride thin films," Int. J. Electrochem. Sci, Vol. 4, pp. 369–376, (2009).

[42] M. A. Omar, Elementary solid state physics: principles and applications. Pearson Education India, (1975).

[43] J. I. Pankove, "Optical processes in semiconductors Prentice-Hall," New Jersey, Vol. 92, (1971).

[44] H. Abbas, "Study Structural and Optical Properties0T of0T CdSe: Al Thin Films as a Function of Doping Ratio and Annealing Temperature." Msc Thesis. Baghdad University. Ibn Al-Haytham collage, (2015).

[45] W. D. Callister, Fundamentals of materials science and engineering, vol. 471660817. Wiley London, (2000).

[46] W. A. Morais, B. de Barros, I. M. F. Cavalcanti, F. H. Xavier, N. S. Santos-Magalhães, and M. A. M. Maciel, "Coencapsulation of trans-Dehydrocrotonin and trans-Dehydrocrotonin: hydroxypropyl-β-cyclodextrin into Microparticles," J. Braz. Chem. Soc., Vol. 28, pp. 1494–1505, (2017).

[47] C. Kittel, "Introduction to solid state physics Eighth edition," (2021).

[48] S. M. Sze, "Semiconductor devices: physics and technology" John wiley & sons, (2008).

[49] S. M. Sze and K. K. Ng, "Tunnel devices," Phys. Semicond. Devices, pp. 415–465, (1981).

[50] D. A. Neamen, "Semiconductor Physics and Devices, University of New Mexico, Richard D. Irwin." Inc, (1992).

[51] J. H. Nahida, "Spectrophotometric analysis for the UV-irradiated (PMMA)," Int. J. Basic Appl. Sci., Vol. 12, No. 2, pp. 58–67, (2012).

[52] J. I. Pankove, "Optical processes on semiconductors Dover publication," Inc. New york, (1971).

[53] S. A. Salman, M. H. Abdu-allah, and N. A. Bakr, "Optical characterization of red methyl doped poly (vinyl alcohol) films," Int. J. Eng. Tech. Res., Vol. 2, No. 4, (2014).

[54] A. Hashim, M. Habeeb, and Q. Jebur, "Structural, Dielectric and Optical properties for (Polyvinyl Alcohol–Polyethylene Oxide-Manganese Oxide) Nanocomposites," Egypt. J. Chem., Vol. 62, pp. 735–749, (2019).

[55] D. M. Bigg, "Mechanical, thermal, and electrical properties of metal fiber-filled polymer composites," Polym. Eng. Sci., Vol. 19, No. 16, pp. 1188–1192, (1979).

[56] P. Barber, S. Balasubramanian, Y. Anguchamy, S. Gong, A. Wibowo, H. Gao, H. J. Ploehn, and C.Z. Loye," Polymer composite and nanocomposite dielectric materials for pulse power energy storage," Materials (Basel)., Vol. 2, No. 4, pp. 1697–1733, (2009).

[57] T. Putjuso and P. Sangarun, "Influence of annealing on the giant dielectric properties of cuo ceramics prepared by a simple pva sol-gel," Asia-Pacific J. Sci. Technol., Vol. 17, No. 2, pp. 203–210, (2012).

[58] M. Akram, A. Javed, and T. Z. Rizvi, “Dielectric properties of industrial polymer composite materials,” Turkish J. Phys., Vol. 29, No. 6, pp. 355–362, (2006).

[59] S. Kitouni, “Dielectric properties of triaxial porcelain prepared using raw native materials without any additions,” Balk. J. Electr. Comput. Eng., Vol. 2, No. 3, (2014).

[60] S. Prasher, M. Kumar, and S. Singh, “Analysis of electrical properties of Li3+ ion beam irradiated lexan polycarbonate,” Asian J. Chem, Vol. 21, No. 10, pp. 43–46, (2009).

[61] P. R. Hsueh, “New Delhi metallo-β-lactamase-1 (NDM-1): an emerging threat among Enterobacteriaceae,” J. Formos. Med. Assoc., Vol. 109, No. 10, pp. 685–687, (2010).

[62] G. M. Rossolini, F. Arena, P. Pecile, and S. Pollini, “Update on the antibiotic resistance crisis,” Curr. Opin. Pharmacol., Vol. 18, pp. 56–60, (2014).

[63] X. Li, S. M. Robinson, A. Gupta, K. Saha, Z. Jiang, D. F. Moyano, A.Sahar, M. A. Riley, and V. M. Rotello,“Functional gold nanoparticles as potent antimicrobial agents against multi-drug-resistant bacteria,” ACS Nano, Vol. 8, No. 10, pp. 10682–10686, (2014).

[64] C. K. Birdsall and A. B. Langdon, " Plasma physics via computer simulation" CRC press. (2004).

[65] F. F. Chen,"Introduction to plasma physics" Springer Science & Business Media., (2012)

[66] J. E. Drummond, "Plasma physics" Courier Corporation, (2013).

[67] A. Paydayesh, A. A. Azar and A. J. Arani, "Investigation the effect of Graphene on The Morphology, Mechanical and Thermal properties of PLA/PMMA Blends, " Ciência Natura, Vol. 37, pp. 15-22, (2015)

[68] T. S. Praveenkumar, J. S. Ashwajeet and R. Ramanna, “Dielectric and AC Conductivity Studies in PPy-Ag Nanocomposites” Journal of Polymers, Vol.2015, (2015).

[69] M. Rezvanpour, M. Hasanzadeh, D. Azizi, A. Rezvanpour and M. Alizadeh, “Synthesis and characterization of micro-nanoencapsulated n-eicosane with PMMA shell as novel phase change materials for thermal energy storage” Mater. Chem. Phys., Vol. 215, pp. 299–304, (2018).

[70] A. A. Mohaimeed, B. H. Rabee, "Influence of Berry dye on some properties of nanocomposite (PVA/TiO2) films". Opt Quant Electron, Vol. 55, p.254, (2023).

[71] H. Shivashankar, K. A. Mathias, P. R. Sondar, M. H. Shrishail, and S. M. Kulkarni, "Study on low-frequency dielectric behavior of the carbon black/polymer nanocomposites", J Mater Sci: Mater Electron, Vol.32, (2021).

[72] C. Srikanth, B. C. Sridhar, M. V. N. Prasad and R. D. Mathad, "Characterization and DC conductivity of novel ZnO doped polyvinyl alcohol (PVA) nano-composite films" Journal of Advanced Physics, Vol. 5, No.2, pp.105-109, (2016).

[73] N. K. Abdalameer, "Effects of cold atmospheric plasma on the optical properties of SnO2 thin film" Advances in Natural and Applied Sciences, Vol.11, No. 9, pp.357-364, (2017).

[74] E. K. Jebur,"Effect of the Dielectric Barrier Discharge Plasma on the Optical Properties of CDS Thin Film", Baghdad Science Journal, Vol.16, No.4, (2019).

[75] A. Hashim, "Fabrication and characteristics of flexible, lightweight, and low-cost pressure sensors based on PVA/SiO2/SiC nanostructures", J Mater Sci: Mater Electron, (2021).

[76] D. Kumar, S. K. Jat, P. K. Khanna, N. Vijayan and S. Banerjee , "Synthesis, characterization, and studies of PVA/Co-Doped ZnO nanocomposite films" International Journal of Green Nanotechnology, Vol. 4, No.3, pp. 408-416, (2012).

[77] O. B. Fadil and A. Hashim, "Fabrication and tailored optical characteristics of CeO2/SiO2 nanostructures doped PMMA for electronics and optics fields" Silicon, Vol. 14, No. 15, pp. 9845-9852, (2022)

[78] M. K. Mohammed, G. Al-Dahash and A. Al-Nafiey, "Synthesis and characterization of PVA-Graphene-Ag nanocomposite by using laser ablation technique" In Journal of Physics: Conference Series, Vol. 1591, No. 1, p. 012012. (2020).

[79] A. Mohammad, K. Hooshyari, M. Javanbakht, and M. Enhessari, "Fabrication and Characterization of Poly Vinyl Alcohol/ Poly Vinyl Pyrrolidone/MnTiO Nanocomposite Membranes for PEM Fuel Cells", Iranica Journal of Energy & Environment, Vol. 4, No. 2, PP. 86-90, (2013).

[80] S. S. Mirtalebi, H. Almasi and M. A. Khaledabad, M. A. ,"Physical, morphological, antimicrobial and release properties of novel MgO-bacterial cellulose nanohybrids prepared by in-situ and ex-situ methods" International journal of biological macromolecules, Vol. 128, pp. 848-857, (2019).

[81] K. Praveenkumar, T. Sankarappa, J. S. Ashwajeet, and R. Ramanna, Dielectric and AC Conductivity Studies in PPy-Ag Nanocomposites, Journal of Polymers, Vol.2015, (2020).

[82] J. S.G. D. Camargo, A. J. D. Menezes, N. C. D., E. C. Rangel and A. D. O. Delgado-Silva," Morphological and chemical effects of plasma treatment with

oxygen (O2) and sulfur hexafluoride (SF6) on cellulose surface" Materials Research, Vol.20, pp. 842-850, (2018)

[83] S. Ju1, M. Chen1, H. Zhang and Z. Zhang" Dielectric properties of nanosilica/low-density polyethylene composites: The surface chemistry of nanoparticles and deep traps induced nanoparticles", Journal of express Polymer Letters Vol.8, No.9, PP. 682–691, (2014).

[84] G. Chakraborty, K. Gupta, D. Rana and A. Kumar Meikap, "Dielectric relaxation in polyvinyl alcohol- polypyrrole–multiwall carbon nanotube composites below room temperature", Advances in Natural Sciences, Vol. Vol.4, PP. 1-4, (2014).

[85] S. Ju1, M. Chen1, H. Zhang and Z. Zhang" Dielectric characteristics of nanosilica/low-density polyethylene composites: The surface chemistry of nanoparticles and deep traps induced nanoparticles", Journal of express Polymer Letters Vol.8, No.9, PP. 682–691, (2014).

[86] M. Habeeb, A. Hashim, N. Hayder, "Fabrication of (PS-Cr2O3/ ZnCoFe2O4) Nanocomposites and Studying their Dielectric and Fluorescence Properties for IR Sensors", Egypt.J.Chem. Vol. 62, pp.709- 717, (2019).

[87] S. M. Mahdi, M. A. Habeeb, "Synthesis and augmented optical characteristics of PEO–PVA–SrTiO3–NiO hybrid nanocomposites for optoelectronics and antibacterial applications"Optical and Quantum Electronics, Vol. 54, No. 12, pp. 1-17, (2022).

[88] M. Abdul Nabi, R. M. Yusop, E. Yousif, B. M. Abdullah, J. Salimon, N. Salih, and S. I. Zubairi, "Effect of nano ZnO on the optical properties of poly (vinyl chloride) films. International journal of polymer science", (2014).

الخلاصة

في هذه الدراسة، تم تحضير المتراكب النانوي ($PMMA/PS/Al_2O_3$) باستخدام طريقة الصب مع نسب وزنية مختلفة من Al_2O_3 النانوية (2, 4, 6 و 8). wt% . تم تشخيص الخصائص التركيبية والسطحية والبصرية والكهربائية للمتراكب النانوي ($PMMA/PS/Al_2O_3$). تتضمن الخصائص التركيبية المجهر الضوئي والتحليل الطيفي للأشعة تحت الحمراء (FTIR) وصور المجهر الإلكتروني الماسح (SEM). أظهرت صور المجهر الضوئي توزيع الجسيمات النانوية Al_2O_3 بشكل شبكة مستمرة داخل البوليمر عند النسبة (8 wt.%) . اظهر طيف (FTIR) زحف في بعض القمم وزيادة في شدة لقمم اخرى مقارنة مع الغشاء (PMMA/PS) وهذا يشير بانه لا يوجد تفاعل بين البوليمر والمواد النانوية المضافة. اظهرت صور (FESEM) لسطح الأغشية للمتراكب النانوي ($PMMA/PS/Al_2O_3$) والتي تكون متجانسة ومتماسكة مع الركام أو القطع المنتشرة بشكل عشوائي على السطح العلوي. الاختلاف في سطح الغشاء بعد التعرض لغاز الاركون بلازما هو نتيجة لتطور الانطباع الذي تشجعه أنواع بلازما الأرجون على سطح (PMMA/PS) . أظهرت نتائج الخصائص البصرية للمتراكب النانوي قبل وبعد التعرض لغاز اركون بلازما بأن الامتصاصية، معامل الامتصاص، معامل الانكسار, معامل الخمود, ثابت العزل الحقيقي والخيالي ,التوصيلية البصرية تزداد مع زيادة تركيز جسيمات النانوية Al_2O_3. النفاذية وفجوة الطاقة للانتقال غير مباشر المسموح والممنوع تقل مع زيادة تركيز جسيمات النانوية Al_2O_3 . اظهرت نتائج الخصائص الكهربائية المتناوبة (A.C) تزداد مع زيادة تركيز جسيمات النانوية Al_2O_3 وتتناقص مع زيادة تردد المجال الكهربائي المسلط بينما التوصيلية الكهربائية المتناوبة (AC) تزداد مع زيادة تركيز جسيمات النانوية Al_2O_3 و التردد. ثابت العزل, الفقدان العزلي والتوصيلية الكهربائية المتناوبة بعد التشعيع لها قيم عالية مقارنة قبل التشعيع الذي يعزى إلى زيادة حاملات الشحنة وتكسر بعض الاواصر. اختبرت المتراكبات النانوية ($PMMA/PS/Al_2O_3$) كمضادات لبكتريا موجبة غرام (المكورات العنقودية الذهبية) وسالبة غرام (الشريطية القولونية) و بينت النتائج أن منطقة التثبيط ازدادت بزيادة تراكيز الجسيمات النانوية Al_2O_3.

جمهورية العراق
وزارة التعليم العالي والبحث العلمي
جامعة بابل
كلية التربية للعلوم الصرفة
قسم الفيزياء

المعالجة البصرية بالبلازما الباردة لخليط بوليمري مطعم بالنانو الومينا

رسالة مقدمة
الى مجلس كلية التربية للعلوم الصرفة في جامعة بابل
وهي جزء من متطلبات نيل درجة الماجستير
في التربية / فيزياء

من قبل الطالبة

فاطمة محمد نايف

بكالوريوس تربية فيزياء
جامعة بابل 2018 م

بأشراف

أ. د. بهاء حسين صالح ربيع

1445هـ **2023م**